August 2017

Observer Based Cylinder Charge Estimation for Spark-ignition Engines

Zhe Wang
Clemson University, zwang5@g.clemson.edu

OBSERVER BASED CYLINDER CHARGE ESTIMATION FOR SPARK-IGNITION ENGINES

A Dissertation
Presented to
the Graduate School of
Clemson University

In Partial Fulfillment
of the Requirements for the Degree
Doctor of Philosophy
Automotive Engineering

---

by
Zhe Wang
August 2017

Accepted by:
Dr. Robert Prucka, Committee Chair
Dr. Hussein Dourra
Dr. Zoran Filipi
Dr. Simona Onori

ABSTRACT

Internal combustion engines require accurate cylinder charge estimation for determining engine torque, controlling air-to-fuel ratio (AFR), and ensuring high after-treatment efficiency. This is challenging due to the highly transient operating conditions that are common in automobile engines. The problem is further complicated by spark ignition (SI) engine technologies such as variable valve timing (VVT) and exhaust gas recirculation (EGR) which are applied to improve fuel economy and reduce pollutant emissions. With manifold filling/emptying/mixing phenomenon and different actuator response times, these technologies significantly increase the complexity of cylinder charge estimation.

Current cylinder charge estimation methodologies require a combination of sensors and empirical models to deal with the high degrees of control freedom existent on the engine. But these methods have the drawbacks of great dependency on accurate calibration and poor transient performance. Most importantly, the current methods isolate feed-forward cylinder charge estimation and feedback AFR control. When there is discrepancy between target lambda value and sensed lambda value at exhaust side, the current control/estimation method will trim the fuel injection amount no matter where the error source is. As a matter of fact, the error might come from the throttle flow estimation, the fuel injection flow estimation, EGR flow estimation, or any combination of these error sources. Increased air-path complexity and drawbacks of traditional methods drive the need for cost effective solutions that produce high air/EGR/fuel charge

estimation accuracy with the ability to identify the error source while minimizing sensor cost, computational effort, and calibration time.

This research first evaluates the existing work on air charge estimation for SI engines with massive experimental tests covering various operating conditions, which are designed for the algorithm verification of this research. Then several estimation methods which utilize both Manifold Absolute Pressure (MAP) and Mass Air Flow (MAF) sensors are studied and analyzed. Reduction of calibration effort and improvement of accuracy are observed from the proposed cylinder air charge estimation methods. Following that, a model is built to study the engine gas path dynamics and characteristics and then simplified to provide system dynamic basis for the following estimation algorithm development. Using the developed model, a disturbance observer based cylinder charge estimation technique is developed based on a combination of sensors including MAF, MAP, and exhaust lambda sensors. This developed algorithm significantly improves engine states estimation accuracy compared to conventional Single-Input-Single-Output (SISO) methods. Also, the augmentation of disturbance observation is able to pin point the source of the estimation error. Through experimental validation, using the developed estimation method with proper parameters, the error source of estimation can be identified and rectified when disturbance is introduced to throttle flow model, EGR flow model, fuel injection flow model or any combination of these models. The structure of the proposed algorithm should adapt to most SI engine configurations. It can help the engine controller to mitigate modeling errors thus improve the performance of physics model based engine control especially AFR control.

ACKNOWLEDGMENTS

First of all, I would like to thank my advisor, Dr. Robert Prucka, for his continuous support, patient guidance and constant encouragement throughout my Ph.D. program. I am extremely fortunate and honored to have Dr. Prucka as my advisor. I believe this project wouldn't come so far without his inspiration and passion. He is and always will be my mentor not only for the research work but also my personal growth.

I would also like to express my gratitude to my committee members. I want to thank Dr. Zoran Filipi for introducing me to this group and providing me generous help. I also want to thank Dr. Simona Onori for the beneficial discussion about the estimation and control theory. I would like to thank Dr. Hussein Dourra, who gives me insights of the state-of-art technologies in the automotive industry and a lot of great suggestions which make my research work applicable in real world.

I gratefully appreciate the financial and technical support from FCA North America LLC. Specifically, I would like to thank Mr. Michael Prucka and Mr. Ethan Bayer for their valuable suggestions and comments. I learned a lot from them as they showed me the best way to carry out engineering work.

My teammates, my roommates and all other friends have given me great help, inspirations and a lot of fun during my Ph.D. life. Thank you all.

Last but not the least, I would like to thank my family. Without their continuous and unconditional understanding, support, encouragement and love, it is impossible for me to finish this study and dissertation. Thank you!

TABLE OF CONTENTS

LIST OF TABLES

LIST OF FIGURES

CHAPTER ONE

1. INTRODUCTION

1.1 Motivation

Energy usage and environmental issues are two major concerns regarding the sustainable development of our modern society. Many countries have established increasingly strict statutes to limit harmful emissions and improve energy efficiency of vehicles which are powered by internal combustion engines. For example, The National Highway Traffic Safety Administration (NHTSA), the U.S. Environmental Protection Agency (EPA) and the California Air Resources Board (CARB) are intended to reduce energy consumption by introducing Corporate Average Fuel Economy (CAFE), a regulation in United States, to increase the fuel economy of cars and light trucks produced for sale in the United States. On July 29, 2011, the Obama administration announced new CAFE standards to increase fuel efficiency levels rapidly over the next several years, reaching a combined efficiency of 54.5 miles per gallon by 2025 [1]. To achieve these standards, the automobile manufacturers have to improve the efficiency of today's vehicles significantly in the future (Figure 1.1).

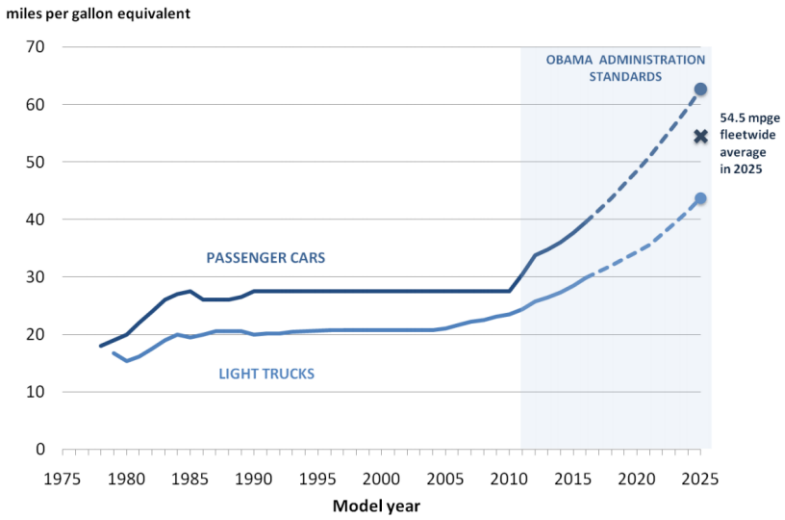

Figure 1.1 Corporate Average Fuel Economy (CAFE) standards [1]

There have been similar levels of regulation in internal combustion engine emissions regulations. Figure 1.2 shows regulations of various emission species for gasoline powered light-duty vehicles in both the United States and the European Union[2]. It can be observed that the limits for all the regulated emissions have been progressively lowered over the past years.

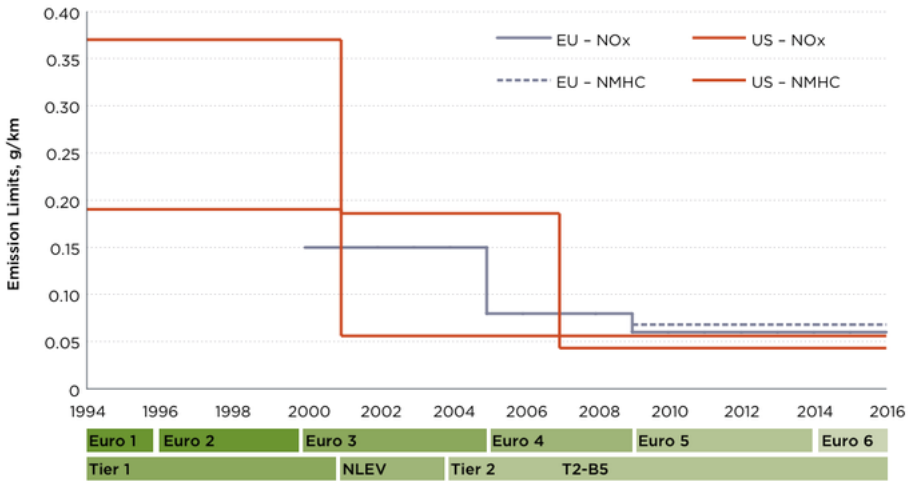

Figure 1.2 Emission limits for gasoline powered LDVs in the US and the EU [2]

To meet these unprecedented regulations, automobile manufacturers commonly use Three Way Catalysts (TWC) for reducing HC, CO and NOx from SI engines. TWCs are passive devices that rely on the engine to control their conversion efficiency. The engine controls catalyst efficiency by supplying heat to enable reactions and providing the proper mix of exhaust species at all times. Its conversion efficiency as function of normalized AFR is shown in Figure 1.3. In order to achieve maximum TWC emissions conversion efficiency, the AFR has to be controlled to very near stoichiometry.

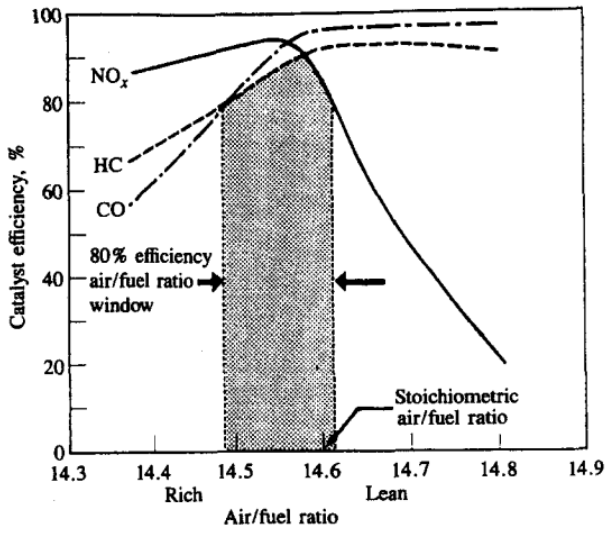

Figure 1.3 Three Way Catalyst conversion efficiency [20]

Traditional engine AFR control is based on both feed-forward control and feed-back control[3–7]. The fresh air mass is first estimated based on a combination of sensor inputs and calibration tables. And then the engine control module (ECM) decides the quantity of fuel to be injected to achieve the target AFR. This process requires accurate in-cylinder air charge estimation under all operating conditions so that the proper fuel mass can be delivered. The feed-forward system is accompanied by feedback control.

The feed-back loop uses an exhaust lambda sensor to determine if the engine is operating with fuel rich or lean. The ECM adjusts the fuel injection quantity according to the feedback signal. When the measured lambda value is larger than target lambda value, which indicates the cylinder mixed gas being too lean, the fuel injection amount will be tuned up to make the air-fuel mixture richer. Similarly, when the measured lambda value is smaller than targeted value, which suggests the cylinder mixed gas being too rich, the fuel injection amount will be trimmed to lean down the mixed gas. The schematic is shown in Figure 1.4. During steady state conditions feedback methods work well. Under transient conditions, the transport time required for the air-fuel mixture to travel from the engine cylinder and to be sensed by the exhaust lambda sensor (including sensor response time) can limit the usefulness of feedback controls without complex correction strategies. Extra sensors are not an acceptable solution due to the high pressure on the increased cost. Therefore feed-forward air charge estimation is very important to avoiding large AFR excursions during transient operation.

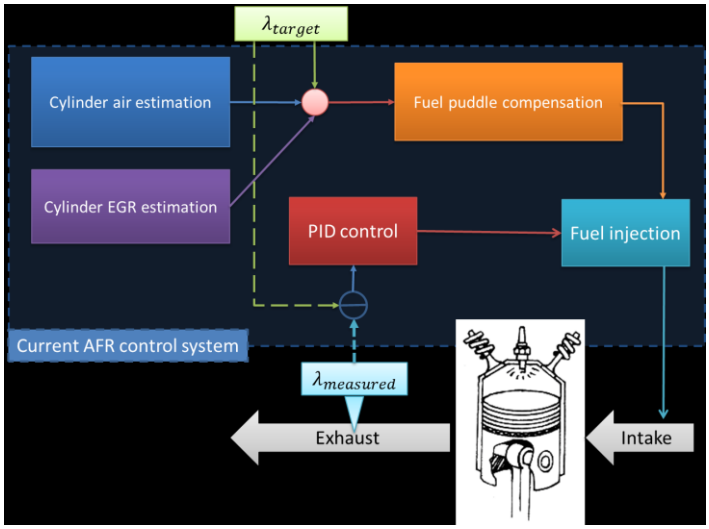

Figure 1.4 Traditional engine AFR control schematic diagram

Besides controlling AFR and ensuring high after-treatment efficiency, cylinder charge estimation is important for other aspects of engine control. Examples include estimation strategies for engine torque and physics-based combustion phasing control [8,9]. With more and more control actuators being added to SI engines to improve fuel economy and/or emissions, cylinder charge estimation becomes more complex and challenging. For example, the variable valve timing system can alter the timing/lifting of intake/exhaust camshaft and improve engine performance and emissions. These new technologies add degrees of freedom to the volumetric efficiency tables, which significantly increase the complexity and cost of volumetric efficiency mapping and calibration.

External EGR system is also introduced to SI engine. EGR could reduce pumping loss at part load range and reduce NOx emission levels by recirculating a portion of exhaust gas back to the engine cylinders[10,11]. For cylinder EGR charge estimation, the traditional orifice flow model is widely used. This model design needs to be calibrated accurately and may change gradually because of engine aging. Using this model, flow calculation can also be uncertain when pressure differential across the valve is low.

Increased air-path complexity and traditional methods' shortcomings drive the need for cost-effective solutions that produce the cylinder air/EGR/fuel charge estimation with high accuracy while minimizing sensor cost, computational effort, and calibration time. A large number of air charge estimation techniques have been developed by academic researchers and industrial engineers using a range of sensor sets combined with empirical and/or physics-based models. Some examples include speed-density algorithm

with physics-based volumetric efficiency (VE) model, high gain input estimation method, and closed-loop observer based methods. Although these methods work well for certain applications, there are some common defects. Firstly, most of these methods still require lots of experimental calibration and/or extra sensors such as the in-cylinder pressure sensor. Secondly, the performance of these methods in transient conditions is limited. Moreover, existing methods do not scale well when external EGR system is added. Last but not the least, the AFR feedback control trims only the fuel injection amount no matter where the error sources are. In summary, all these defects with existing estimation methods need to be addressed and solved in our study to enhance the cylinder charge estimation.

1.2 Research objective

To overcome the defects mentioned above, a cylinder charge estimation algorithm which is capable of real-time operations is needed. The primary objective of this research is to develop an estimation/control-oriented gas path model and a model-based observer utilizing MAP, MAF and exhaust lambda sensors to estimate cylinder air/fuel/EGR charge with significantly improvements of engine states estimation accuracy compared to conventional SISO methods and the potential to reduce calibration time and computational effort. And more importantly, the developed algorithm should be able to isolate the source of the estimation error and properly correct error source, which will be a major improvement to the current state of art.

1.3 Dissertation overview

Chapter 1 introduces the background and presents the motivation and objective of this research. Following the introduction, Chapter 2 reviews the relevant literature related to this research. First, Chapter 2 provides a technical review of a large number of air charge estimation techniques which have been developed using a range of sensors sets combined with empirical and/or physics-based models. Then several typical cylinder charge estimation methods are evaluated and compared through experimental test data. The purpose is to provide an overall understanding and reliable evaluation of current SI engine cylinder charge estimation techniques and to identify their advantages and disadvantages in key areas.

Chapter 3 describes the simulation and experimental environment setup for model testing, debugging and validation which includes the hardware and software, the data acquisition system and the rapid prototyping engine control system. Chapter 4 focuses on the construction and analysis of the gas path estimation/control-oriented engine models. Physics-based modeling of the engine gas path is divided into five models: air path, fuel path, EGR path, intake manifold, and exhaust lambda path models. These five parts are then analyzed, modeled and validated through experimental test. In addition, the proposed model is modified with certain system states chosen for estimation proposes. Also in this Chapter, the Padé approximation technique is discussed to solve time delay issues.

In Chapter 5, an observer based cylinder air charge estimation method, that combines both a mass air flow (MAF) sensor and a manifold absolute pressure (MAP)

sensor, is proposed. Current cylinder air charge estimation methodologies in existing researches, literatures and production applications generally depend upon either a MAF sensor or a MAP sensor individually. Methods based on either sensor have their own advantages and disadvantages respectively. Some production vehicles are equipped with both MAF and MAP sensors to offer air charge estimation and other benefits. In this Chapter, several observer-based cylinder air charge estimation methods are proposed. These new methods take advantage of both MAF and MAP sensors to potentially reduce calibration work while providing acceptable transient and steady-state accuracy with low computational load and low sensor cost.

Chapter 6 focuses on separating and correcting error sources regarding AFR control. Cylinder fuel and EGR charge estimation are also considered in the study. With the ensemble of throttle flow model, EGR valve flow model and fuel injection flow model as basis for the cylinder air/fuel/EGR charge estimation algorithm design, the problem comes along as several sources of errors are introduced with complexity to eject the model error and identify the error source. To deal with this issue, a disturbance observer technique is then integrated into the proposed engine cylinder charge estimation routine. This technique reconstructs the system dynamics with the assumption that these input models are not perfect and might contain disturbances. With such improvement, when there is (are) input modeling error(s), the EKF can quickly identify the source(s) of the error(s) in terms of system states, instead of lowering confidence in the sensors as how a conventional EKF would react. Therefore, the impact of the modeling errors can be mitigated within seconds with better quality. The proposed state estimation algorithm

is programmed into the prototyping controller and validated under various operating conditions. Finally, Chapter 7 summarizes the content and main contributions of this dissertation. Suggestions for future directions of the continuous work are given based on lessons learned from this research.

1.4 Contributions

Cylinder charge is highly complex and uncertain, making it difficult to estimate, especially when being incorporated with engine control strategies. To have a more accurate estimation of the cylinder air/fuel/EGR with controllable sensor cost and minimal request of computational power, a comprehensive understanding and analysis of observers, physical models and the combinations of sensors for cylinder charge estimation is needed for this research. The contribution of this dissertation on the cylinder charge estimation compared to the existing research in literatures and industrial applications can be categorized as below:

1) Engine dyno cell experimental tests and existing methods evaluation: In order to implement the experimental verification and ensure the feasibility of the developed algorithm, and to evaluate the existing estimation methods found in literatures, the engine experimental test dyno cell is setup with a 3.6-liter engine modified with an external EGR system and a ETAS ES910 prototyping engine control module. Great amount of steady-state and transient tests are specifically designed and conducted to validate the performance of the designed estimator under various engine operating conditions. To the author's knowledge, the comparative experimental evaluation of the existing methods

and validations of developed engine cylinder charge estimation using such amount of engine test data has not been done before in previous literatures.

2) Estimation-oriented physics-based engine gas path modeling: In order to have a comprehensive understanding of cylinder charge process in SI engines and to provide the basis for observer based cylinder charge estimation algorithm, the engine gas path dynamics is investigated and a nonlinear gas path model is developed. The nonlinear model is further simplified to an estimation-oriented model. This comprehensive model is consisted of the modelling of air path, fuel path, EGR path, lambda path and intake manifold dynamics. Though the individual subcomponents have been studied in previous literatures superlatively, the ensemble of all the sub-models built especially with lambda path model integrated to serve the estimation of the cylinder charge is introduced and studied in this research for the first time, which is another major contribution of this research.

3) Cylinder air charge estimation based on MAF and MAP sensors: Current cylinder air charge estimation methodologies generally depend upon either a MAF sensor or a MAP sensor. Methods based on either sensor have their own advantages and disadvantages. Some production vehicles are equipped with both MAF and MAP sensors to offer air charge estimation and other benefits. This research proposes several observer-based cylinder air charge estimation methods that take advantage of both MAF and MAP sensors to potentially reduce calibration work while providing acceptable transient and

steady-state accuracy with low computational load. More importantly, the fact that the proposed methods do not use VE as a model input significantly reduces calibration effort, possibly making it favorable during early engine development.

4) Disturbance observer based cylinder charge estimation: Besides the cylinder air charge estimation, the cylinder EGR and fuel charge estimation are also important for engine control system. However, most literatures are only focused on either aspect of them. Also, as mentioned before, the current AFR control is based on both feedforward and feedback controls. The feedback control trims fuel injection amount based on exhaust lambda sensor value no matter where the error source is. In this research, for the first time, a disturbance observer based cylinder charge estimation algorithm is developed and verified with the ability to estimate cylinder air, fuel and EGR charge, and most importantly, to identify the throttle flow, EGR valve flow and fuel injection flow model error with readings of the MAF sensor, the MAP sensor and the exhaust lambda sensor. The developed method enables more accurate AFR control, torque estimation and physical based combustion modeling. Moreover, the research achievements of this dissertation could be used for development of model based engine control strategy. It could help automobile manufacturers to build more fuel-efficient engines to meet the standards of government mandates for fuel economy and remit serious air-quality problems gradually.

CHAPTER TWO

2. LITERATURE REVIEW

As mentioned in previous chapter, along with the growing of other advanced engine technologies, a large number of cylinder charge estimation techniques have been developed using a range of sensor sets combined with empirical and/or physics-based models [12]. The estimation of the cylinder charge is with great significance and challenges due to the complexity of the modern engine physical system and multiple sources of uncertainties. The purpose of this chapter is, first to introduce the widely used air path model for the real-time control, then to review and evaluate the cylinder air charge estimation methods recently developed. Both the advantages and disadvantages of each method are discussed. And certain simulation/experimental tests are conducted by deploying various estimation methods with the results shown and analyzed afterwards for performance evaluation.

2.1 Engine Air Path Model

Instantaneous air mass flow through the intake valve(s) is difficult to measure directly. Many existing air charge estimation techniques require intake manifold and engine air-mass-flow models to utilize information gathered by other available sensors upstream in the air-path. This section briefly introduces the most commonly used air-path modeling methods.

For real time engine control applications, mean value engine models (MVEMs) are well accepted for their physics-based nature, high computational efficiency and

decent accuracy, although the reciprocating behavior is neglected [13–15]. Figure 2.1 depicts the naturally aspirated SI engine air intake system with modeling variables in a mean value approach.

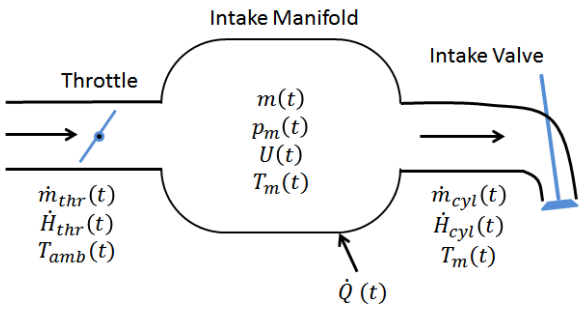

Figure 2.1 Intake system model for air mass estimation [16]

The intake manifold is assumed to be a lumped parameter reservoir with fixed volume [16]. Based on the assumption that no heat or mass is transferred through the walls and there are no substantial energy changes in the flow, the mass and energy balance of the intake manifold can be expressed as

$$\frac{d}{dt}m(t) = \dot{m}_{thr}(t) - \dot{m}_{cyl}(t) \tag{1}$$

$$\frac{d}{dt}U(t) = \dot{H}_{thr}(t) - \dot{H}_{cyl}(t) \tag{2}$$

where m is mass, H is enthalpy, and U represents internal energy. The subscripts thr and cyl represent flow into the system (through throttle) or out of the system (into cylinder) respectively.

Considering the ideal gas law and energy balance (after some algebraic manipulation), the engine intake manifold dynamics are shown in equation (3) and (4).

$$\dot{p}_m = \frac{\gamma R}{V_m}\left(\dot{m}_{thr} T_{amb} - \dot{m}_{cyl} T_m\right) \tag{3}$$

$$\dot{T}_{\mathrm{m}} = \frac{\mathrm{RT_m}}{p_m V_m}\left[\dot{m}_{thr}(\gamma T_{thr} - T_m) - \dot{m}_{cyl}(\gamma - 1) T_m\right] \tag{4}$$

where p_m is intake manifold pressure, V_m is effective volume of manifold, T_m is intake manifold temperature, T_{amb} is ambient temperature, R is the ideal gas constant, γ is ratio of specific heats, $\dot{m}_{thr}$ is air mass flow through throttle, and $\dot{m}_{cyl}$ is air mass flow through intake valve.

The adiabatic assumption is reasonable for reservoirs with small surface-to-volume ratio. If there is a large surface-to-volume ratio then the isothermal assumption is a better approximation [16]. In this case, the temperature in the reservoir is considered to be constant. Therefore, the manifold model can be simplified as

$$\dot{p}_m = \frac{R T_m}{V_m}\left(\dot{m}_{thr} - \dot{m}_{cyl}\right) \tag{5}$$

$$T(t) = T_{amb}(t) = T_m(t) \tag{6}$$

The adiabatic intake manifold model considers the effects of temperature change under transient conditions. The isothermal intake manifold model proposed by Hendricks et al. [13] is widely used for engine applications and includes cylinder air charge due to its simple characteristic and accuracy. Furthermore, the adiabatic intake manifold model does not provide substantial accuracy improvements over the isothermal manifold models for air charge estimation [17–19].

The isenthalpic orifice model is widely used to compute the valve mass flow. Examples include air mass flow through the throttle and exhaust gas through the EGR valve [16,20]

$$m(t) = c_d A(t) \frac{p_i(t)}{\sqrt{RT_i(t)}} \Psi\left[\frac{p_i(t)}{p_o(t)}\right] \tag{7}$$

$$where, \Psi\left(\frac{p_i}{p_o}\right) = \sqrt{\gamma\left(\frac{2}{\gamma+1}\right)^{\frac{\gamma+1}{\gamma-1}}}, \qquad p_o < p_{cr}$$

$$= \left(\frac{p_o}{p_i}\right)^{\frac{1}{\gamma}} \sqrt{\frac{2\gamma}{\gamma-1}\left[1-\left(\frac{p_o}{p_i}\right)^{\frac{\gamma-1}{\gamma}}\right]}, \qquad p_o \geq p_{cr}$$

$$with\ p_{cr} = \left(\frac{2}{\gamma+1}\right)^{\frac{\gamma}{\gamma-1}} \cdot p_i\ , critical\ pressure$$

where c_d is discharge coefficient, A is the effective flow area of valve, p_i is pressure of the intake side, p_o is pressure of the output side, and T_i is intake temperature.

The air mass flow into the cylinder can modelled as [16,20]

$$\dot{m}_{cyl} = \frac{p_m V_d \eta_{VE} N}{120 R T_m} \tag{8}$$

where N is engine speed, and η_{VE} is the volumetric efficiency. This engine flow model is based on the speed-density approach. Details of the speed-density approach will be described later.

2.2 Mass Air Flow Sensor Methods

If only a throttle position sensor is available the air charge can be estimated by throttle opening position and engine speed using look-up tables. This solution requires no extra sensors (e.g. MAP and MAF sensors), making it the most cost-effective option. However, this method cannot guarantee accuracy even at steady state. Therefore, this method usually is a backup solution in case of malfunctioning of the primary method.

Mass air flow (MAF) based approaches are one of the most widely used primary methods for in-cylinder air charge estimation. These methods rely on a MAF sensor positioned before the throttle to compute the air mass flow entering the intake system. Under steady state conditions the MAF sensor directly measures the cylinder air charge regardless of most of other factors which change the volumetric efficiency such as engine aging [21][22]. This is the most important advantage of the MAF air charge estimation approach. The main drawbacks of MAF sensor methods are the high cost and their sensitivity to debris. Additionally, during transient engine operation the MAF sensor measurement does not necessarily equal the air mass flow going into the cylinder due to the manifold filling and empty dynamics [17]. Finding the optimal manifold dynamics compensation routine is a core problem for MAF based methods.

A nonlinear open-loop air charge observer based on MAF sensor was proposed in [23], where an isothermal intake manifold was used and the MAF sensor dynamics was considered as a first order system delay

$$\frac{d}{dt}\hat{p}_m = \frac{RT_m}{V_m}\left(\dot{m}_{thr} - f(N, \hat{p}_m)\right) \tag{9}$$

$$\tau\frac{d}{dt}\dot{m}_{thr} + \dot{m}_{thr} = \dot{m}_{MAF} \tag{10}$$

where $f(N, p_m)$ is cylinder air charge with respect to engine speed, N, and intake manifold pressure, p_m, $\dot{m}_{MAF}$ is the sensor-measured mass flow rate, $\dot{m}_{thr}$ is the air mass flow rate through the throttle, and τ is the time constant of MAF sensor.

The intake manifold pressure is first estimated, the cylinder air charge is then computed from the function $f(N, p_m)$. Experimental results show that the proposed air charge observer can significantly improve AFR control compared with the stock AFR control.

For engines with VVT system cylinder air charge is more a function of engine speed, intake manifold pressure, along with intake and exhaust valve timing. In this case, the previously described open-loop observer can be utilized. For example, in [24] to determine cylinder air charge for a dual independent variable cam engine with MAF sensors the affine relationship between intake manifold pressure and cylinder air charge is defined as

$$\dot{m}_{cyl} = \hat{p}_m \cdot f_{slope}(N, IVO, EVC) + f_{offset}(N, IVO, EVC) \tag{11}$$

In equation 11, $\hat{p}_m$ is the estimated intake manifold pressure, and f_{slope} and f_{offset} are the coefficients for cylinder air charge as a function of engine speed and valve timing. The f_{slope} and f_{offset} coefficients can be stored in three-dimensional look-up tables, which require significant memory space in the ECM, and most importantly more calibration efforts. To overcome this issue the inverse distance interpolation method is proposed in [24], which use relatively fewer data points to produce equal results.

If the volumetric efficiency is known, another open-loop observer can be designed based on the isothermal intake manifold model and engine flow model from previous section. The cylinder air charge model for this derivation is shown as (neglecting MAF sensor dynamics)

$$\frac{d}{dt}\dot{m}_{cyl} = -\frac{V_d \eta_{VE} N}{120 V_m}\dot{m}_{cyl} + \frac{V_d \eta_{VE} N}{120 V_m}\dot{m}_{MAF} \tag{12}$$

The experimental verification (Figure 2.2) indicates that this MAF based air charge observer (green line) has acceptable performance compared with the reference (blue line) although the error increases during transient conditions. Possible sources of the error are from sensor dynamics, inaccurate effective manifold volume and errors in VE calibration. Although this method does not require the knowledge of intake manifold pressure, it still needs accurate volumetric efficiency calibration. Issues related to volumetric efficiency modeling will be discussed in later sections.

All the MAF based methods that consider manifold filling and emptying dynamics have better cylinder air charge estimation during transient operating conditions compared with those using MAF sensor measurement alone. Disadvantages of open-loop observers are that they all require cylinder air charge estimates as function of intake manifold pressure or volumetric efficiency. This information is generally stored in tables, which require significant calibration effort for high degree of freedom SI engines. Also, since they are open-loop observers it is difficult to compensate for modeling, measurement and/or calibration errors.

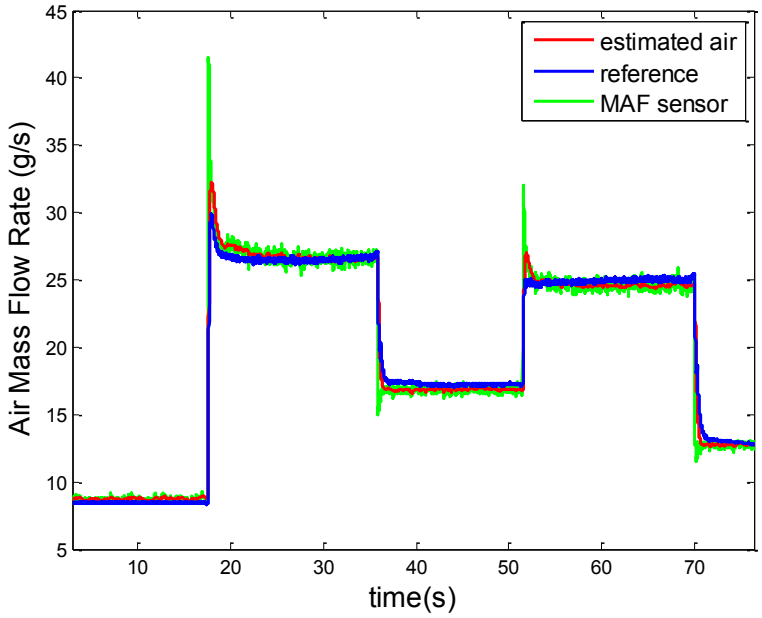

Figure 2.2 Experimental results for cylinder air charge estimation based on open-loop observers

2.3 Speed-Density Methods

Another popular cylinder air charge estimation method is the speed-density approach. This method first calculates the air density in the intake manifold based on ideal gas law (with MAP and temperature sensors). With the air density and the displacement of engine, the amount of air filling the engine cylinder can be computed with a known/modeling volumetric efficiency (VE). Traditionally, VE is calibrated as a function of engine speed and intake manifold pressure. With a calibrated VE table, the air mass flow into the engine can be computed using equation (8).

Compared to the MAF sensor, the MAP sensor costs less, and has faster response time. Figure 2.3 shows simulation results comparison among the MAF sensor measurement, MAF based estimation methods and speed-density approach with accurate volumetric efficiency and noise free model inputs. It can be observed that that speed

density method has better transient performance than the MAF based open-loop observer. The volumetric efficiency calibration is conducted during steady state engine operation. During transient conditions, the volumetric efficiency computation, which is based on a steady state calibration table might be inaccurate. This phenomenon was first investigated under wide open throttle operating condition by Smith et al.in [25]. Later Chevalier et al. made the conclusion that a conventional VE table calibrated in steady state operating condition is capable of describing the cylinder air charge performance with remarkable accuracy during transient operating conditions [19].

Another problem is that technologies like VVT and external EGR system increase the number of control actuators that influence engine air mass flow. For engines with external EGR, the air mass flow through the throttle and EGR valve can be computed using an orifice model (7). Then, the speed-density approach can be used to compute both cylinder air and EGR charge. For engines with VVT, the volumetric efficiency will no longer be a simple function of intake pressure and engine speed and cannot be stored as a simple two-dimensional look-up table. The calibration effort and storage space of the enhanced VE map will increase exponentially.

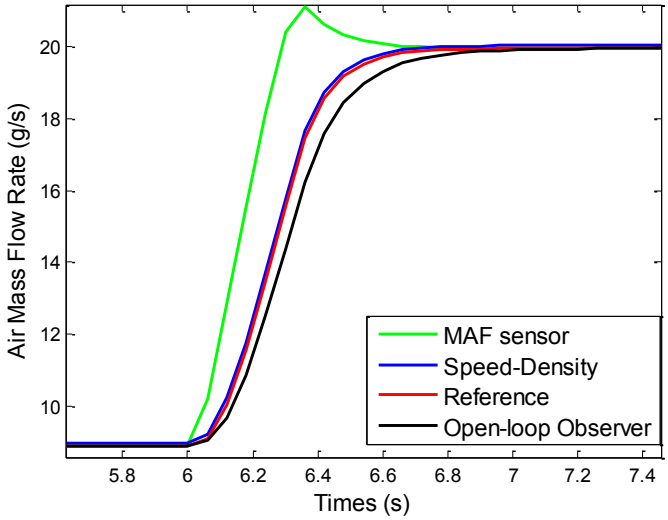

Figure 2.3 The Comparison for MAF sensor and Speed-Density Approach

Regarding this issue, researchers have proposed methods to reduce VE calibration work and the size of the VE tables. For instance, Artificial Neural Network (ANN) based VE models have been proposed to reduce the size of calibration maps [26–28]. The ANN can identify the underlying relationships between inputs and outputs by training samples even if when the studied system is very complex and highly non-linear. For example, an ANN was used to replace traditional volumetric efficiency look-up tables for SI engine with VVT in [27]. In this case, intake manifold pressure, p_m, engine speed N, intake valve timing and exhaust valve timing were used as inputs. The ANN model was successfully validated with both dynamometer and vehicle tests. However, ANN-based models might have extrapolation issues for engine operating conditions beyond the original training region.

An analytical volumetric efficiency model was proposed by Turin et al. to decrease the calibration work and increase the accuracy of volumetric efficiency[29]. The

model is derived from energy conservation rule over the period between intake valve opening (IVO) and intake valve closing (IVC) as

$$E_{IVC} = E_f + E_r + E_b - W_{piston} + Q_{heat} \quad (13)$$

In Equation (13), E_{IVC} is the internal energy of in cylinder gas at IVC, E_f is the internal energy of the charged air from TDC to IVC, E_r is residual exhaust gas energy at IVO, E_b is back flow gas energy from IVO to exhaust valve closing (EVC), W_{piston} is piston work from IVO to IVC, and Q_{heat} is heat transfer to cylinder gas from TDC to IVC. After derivation with energy relations and the ideal gas law, the volumetric efficiency is proposed as a physics-based regression model with 16 calibrated parameters. Experimental results show a good VE prediction for most engine operating conditions with the calibration of 16 parameters.

While the VE model proposed by [29] considers the energy balance of the gas exchange process with other effects captured empirically as regression functions, Kocher et al. [30] applied a similar concept to construct a physics-based VE model for diesel engines with VVT. This research work used cylinder pressure measurement to compute the internal energy of in cylinder gas. Effective compression ratio is also used as a model input to improve accuracy. There are few calibration factors in this physics based VE model. The experimental results show that the proposed model accurately predicts the volumetric efficiency with less than 5% error comparing to a calibrated table.

Due to transient performance and low cost, speed-density based approaches are widely researched for high degree of freedom SI engines. These methods (e.g. ANN based VE model) work well for engines with VVT, but calibration for all engine

operating conditions is still time and labor intensive. Meanwhile physics-based VE models are promising in that they have the potential to eliminate burdensome calibration, but these models either still required calibrated parameters or need more sensors (e.g. cylinder pressure). Moreover, all these methods suffer from the inaccuracy of calibrated/calculated volumetric efficiency [31]. To deal with these issues, previous researchers proposed some other methods.

2.4 Input Estimation Methods

If both MAF and MAP sensors are available, the cylinder air mass flow can be calculated from equation (14), which is derived from the model for an isothermal intake manifold using equation (5).

$$\dot{m}_{cyl} = \dot{m}_{thr} - \frac{V_m}{RT_m}\dot{p}_m \tag{14}$$

In this equation, $\dot{m}_{thr}$ is measured by the MAF sensor, $\dot{p}_m$ can be differentiated from the MAP sensor output, and T_m is measured by the intake temperature sensor. $\dot{m}_{cyl}$ is the cylinder air charge we want to know. Since all terms on the right hand side of equation (14) are known, the cylinder air charge can be calculated. The primary challenge of this approach is sensor noise suppression, especially since the MAP sensor signal is differentiated. To take an alternate view, the system dynamics can be represented as

$$\dot{z} = x + y \tag{15}$$

This derivation transfers the problem to estimating x while measuring y and z. The method for estimating $\dot{z}$ with noisy measurements of z is the core of this method.

Theoretically, it could be solved by Euler's difference formula. But this method may amplify the error from noisy signals because of differentiation. There are several numerical differentiation techniques, such as dirty differentiation, high gain input observers and sliding mode input observers, designed to help solve this issue, and thus help solve the cylinder air mass charge estimation problem [17,32–34]. However, these methods could limit transient performance. If calibrated a VE table is available then a better estimation can be obtained by, for example, a high gain input observer[17]. It is defined as

$$\hat{x} = \alpha z - \varepsilon \tag{16}$$

$$\dot{\varepsilon} = -\alpha\varepsilon + \alpha y + \alpha^2 z \tag{17}$$

where α is a positive observer gain and ε is an auxiliary variable.

A system model can also be derived based on the speed-density approach with an isothermal intake manifold assumption and known VE table. In this case the VE table is assumed to contain some error because of engine aging and/or ambient conditions. The actual volumetric efficiency, η_{VE}, is assumed to be the summation of the pre-calibrated volumetric efficiency η_{SS} and the volumetric efficiency uncertainty $\Delta\eta$.

$$\eta_{VE} = \eta_{\mathrm{ss}} + \Delta\eta \tag{18}$$

The speed-density equation can be rewritten as follows

$$\dot{m}_{cyl} = \eta_{ss}\frac{p_m N V_d}{120 R T_m} + \Delta\eta\frac{p_m N V_d}{120 R T_m} \tag{19}$$

Then, the manifold model is transferred into Equation (19)

$$\frac{d}{dt}p_m = \frac{RT_m}{V_m}\left(\dot{m}_{MAF} - \eta_{ss}\frac{p_m N V_d}{120RT_m} - \Delta\eta\frac{p_m N V_d}{120RT_m}\right) \tag{20}$$

The manifold dynamics described by (20) share a similar structure to equation (15). By measuring p_m and $\dot{m}_{MAF}$, one can estimate $\Delta\eta$. The high gain input observer then applied. The cylinder air charge can then be estimated based on the calibrated η_{ss} and estimated $\Delta\eta$ using equations (21) and (22).

$$\hat{\dot{m}}_{CAC} = \eta_{ss}\frac{p_m N V_d}{120RT_m} + (\varepsilon - \alpha p_m)\frac{V_m}{RT_m} \tag{21}$$

$$\dot{\varepsilon} = -\alpha\varepsilon - \alpha\eta_{ss}\frac{p_m N V_d}{120V_m} + \alpha\frac{RT}{V_m}\dot{m}_{MAF} + \alpha^2 p_m \tag{22}$$

The experimental results of this air charge estimation method are shown in Figure 2.4 (base VE in this figure refers to η_{ss}). The convergence and stability proof of the high gain input observer can be found in [17].

Equation (21) and (22) imply that at steady state conditions the estimated cylinder air charge is equal to the MAF sensor output, and they correct the nominal speed-density approach by estimating the volumetric efficiency uncertainty $\Delta\eta$. Under transient operating conditions, this approach is equal to the speed-density method with corrected volumetric efficiency ($\eta_{ss} + \Delta\eta$). However, this method still requires calibrated VE and the performance can deteriorate at very fast transients scenarios [35].

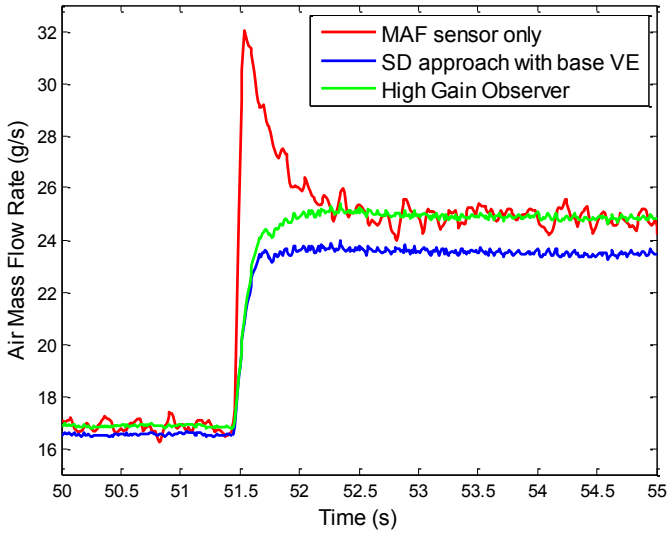

Figure 2.4 The performance of a High Gain Input Observer for air charge estimation

2.5 Close-loop Observer Based Methods

Although the observer concept is mentioned in the previous section, it is only for numerical differentiation without considering cylinder air charge. This section will introduce some close-loop state observer based cylinder air charge estimation methods.

System state observers are an important class of estimation techniques. Different from open-loop observers, the state observers can estimate unmeasurable system states with output measurement and system models. Two Luenberger-like observers were proposed in [18] for turbocharged SI engines with VVT. The first observer is based on an isothermal intake manifold model with the consideration of volumetric efficiency uncertainty. The following equation represents the intake manifold dynamics for this approach

$$\frac{d}{dt}p_m = \frac{RT_m}{V_m}\left[\dot{m}_{MAF}(t) - (\eta_{ss} + \Delta\eta)\frac{p_m N V_d}{120 R T_m}\right] \tag{23}$$

Let the intake manifold pressure p_m and the small variation of volumetric efficiency $\Delta\eta$ be the states. Assuming $\Delta\eta$ does not change much for a short period of time, the system state space model can be written as

$$\begin{cases} \dfrac{d}{dt}p_m = \dfrac{RT_m}{V_m}\left[\dot{m}_{MAF} - (\eta_{ss} + \Delta\eta)\dfrac{p_m N V_d}{120RT_m}\right] \\ \dfrac{\mathrm{d}}{\mathrm{dt}}\Delta\eta = 0 \\ y = p_m \end{cases} \tag{24}$$

Where η_{ss} is the calibrated volumetric efficiency as a function of engine speed N and intake manifold pressure p_m. Notice that the uncertainty of volumetric efficiency, $\Delta\eta$, includes the variance made by valve time changes with the VVT system. Based on this model, a nonlinear states observer is constructed in Equation (25).

$$\begin{cases} \dfrac{d}{dt}\hat{p}_m = \dfrac{RT_m}{V_m}\left[\dot{m}_{MAF} - \left(\eta_{ss} + \widehat{\Delta\eta}\right)\dfrac{p_m N V_d}{120RT_m}\right] + L_1((\hat{p}_m - y)) \\ \dfrac{\mathrm{d}}{\mathrm{dt}}\widehat{\Delta\eta} = L_2(\hat{p}_m - y) \end{cases} \tag{25}$$

In Equation (25) L_1 and L_2 are the observer gains. The observer gains are selected based on estimation error convergence rate [18]. Experimental tests show good cylinder air charge estimation. A second observer presented in [18] is based on the adiabatic intake manifold model instead of isothermal model. The manifold temperature T_m and the ambient temperature T_a are added as system states. Both observer designs generated similar results. The Luenberger-like observers have also been applied to engines with external EGR in [36] [37]. The performances of these air charge estimation routines were verified using simulation with high-fidelity engine models.

Kalman Filters (KF) can be used to estimate system states with process and measurement noise, so they are widely used for automotive control applications, including cylinder air charge estimation [38–43]. A nonlinear air charge observer base on an Extended Kalman Filter (EKF) was proposed by Hendricks et al. [43]. The intake manifold pressure p_m and the engine speed N are the two states based on the isothermal intake manifold model and crank shaft speed model. The air path model is augmented with nonlinear fuel film dynamics. The observer gain is computed offline for different engine operating conditions, and stored in a table with respect of engine speed and intake manifold pressure. This research work investigated the advantages of EKF based cylinder air charge estimation against conventional methods. Chevalier et al. [44] also applied EKF to cylinder air charge estimation, with detailed analysis of sensors, actuators and EKF performance. The system model is based on isentropic intake manifold dynamics. Uncertainty of cylinder air charge (instead of volumetric efficiency) is considered as a system state. The proposed EKF observer was validated on a dynamometer over the entire engine operating range. However, the complex air path model needs to be simplified for real time operation considering the computational capacity of engine ECUs. The isothermal intake manifold model is simpler than the isentropic model, and is capable of capturing the dynamics of manifold pressure. Therefore, it is widely used for most Kalman Filter based air charge estimation research [45][46][47]. Air flow through the throttle is measured by a MAF sensor or computed by an orifice model, as in Equation (7). The cylinder air charge can be modeled by a speed-density approach, and its uncertainty can be modeled directly as its variance $\dot{m}_{cyl}$. It can also be accounted for

with volumetric efficiency variation $\Delta\eta$ (like Equation 18). If the MAF senor is used to measure throttle air flow and $\Delta\eta$ is applied to account for air charge uncertainty, the air path dynamics model can be established as

$$\begin{cases} \dot{p}_m = \dfrac{RT_m}{V_m}\left[\dot{m}_{MAF} - (\eta_{ss} + \Delta\eta)\dfrac{p_m N V_d}{120 R T_m}\right] = f(p_m, \Delta\eta, \dot{m}_{MAF}) + w_1 \\ \dot{\Delta\eta} = w_2 \\ y = p_m + v \end{cases} \tag{26}$$

Where w_1 and w_2 are assumed as model error. In Equation (26), v is MAP sensor measurement noise. This model is similar to Equation (24) with explicitly modeled process/measurement noise. If the process and measurement noise are normally distributed without bias, Extended Kalman Filter can be used to compute the optimal states. Experimental results of the EKF air charge estimation are shown in Figure 2.5.

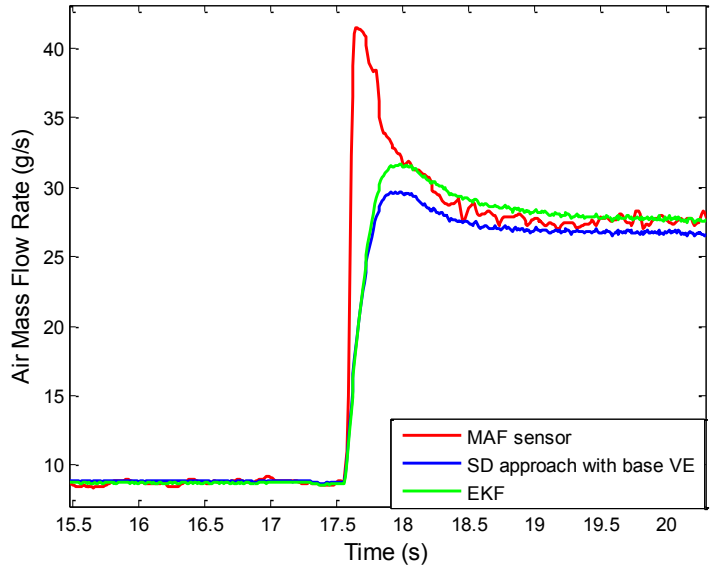

Figure 2.5 The Performance of Extended Kalman Filter for Air Charge Estimation

For EKF based estimation, better performance can be expected by adding the MAP and MAF sensor dynamics into system model[48] [49]. For engines with an

external low pressure EGR systems, Castillo et al. [40] proposed a estimation strategy for EGR mass flow rate and cylinder air charge of diesel engines. Exhaust lambda sensor feedback was also utilized in this research work.

Besides EKF estimation, some other observer based methods, like sliding model observers, can also be used for the cylinder air charge estimation. For example, the sliding model techniques for identifying unmeasured critical parameters like volumetric efficiency are proposed in [50][51]. Nonlinear adaptive observers were also used to improve air charge observers in [48,52–55]. For example, an adaptive observer that is able to correct volumetric efficiency offset was proposed by Tseng et al. [54]. The adaptive air charge estimation in [52] related VE to engine speed N and an adaptive parameter θ

$$\eta_{VE}(t) = f(N(t)) \cdot \theta(t) \tag{27}$$

The time varying parameter $\theta(t)$, which accounts for all the factors affecting volumetric efficiency, needs to be identified in real time. The identification of $\theta(t)$ is based on the difference between the estimated $\hat{p}_m$ and measured $\bar{p}_m$. The same algorithm was adopted by Stefanopoulou [53]. Instead of using expensive MAF sensors, MAP sensors were utilized for that research work. Another adaptive air charge estimation technique was realized with a composite adaptation law, adjustable σ-modification, and feed forward learning which have good performance during fast transients [56].

2.6 Other Methods

Modeling and/or storing volumetric efficiency is considered insufficient to describe the cylinder air charge as the number of control degrees of freedom increases on SI engines. Some researchers proposed to directly model the intake valve flow rate, the integral of which is the cylinder air charge. Qu et al. [57] developed a dynamic quasi-steady flow model that is capable to predict instantaneous intake valve flow rate for an SI engines with VVT. The quasi-steady flow model requires intake\exhaust manifold dynamics models, cylinder pressure sensor and intake\exhaust pressure sensors to generate crank angle resolved valve flow and cylinder mixture prediction.

Xu et al. [58] proposed a 0-D orifice model with crank angle resolution for air charge prediction. This algorithm calculates cylinder pressure during the intake period (from IVO to IVC) based on open thermodynamics, eliminating the need for cylinder pressure sensors. Pressure upstream the intake valves can be either calculated from manifold pressure model or mapped from experimental calibration. This method greatly improves the robustness of orifice flow model against pressure errors. Most importantly, it eliminates calibration for volumetric efficiency. This model was validated with GT-Power simulations and real vehicle tests with a rapid-prototype engine controller. The model produced less than 5% error in terms of air charge prediction for most engine operating conditions.

In [59–63], cylinder pressure sensors were used for air mass flow estimation in naturally aspirated SI engines and turbocharged diesel engines. For example, a cylinder air charge estimation based on cylinder pressure without MAF and MAP sensors is proposed in [21]. It employed a neural network to compute cylinder air charge as a

function of engine speed, throttle position and cylinder pressure. Experimental results showed good performance under steady state conditions. However, the performance was limited during transient engine operation.

2.7 Conclusions

This chapter reviews research work on cylinder air charge estimation for spark ignition engines. Particular focus is given to methods utilizing MAF sensors, speed-density algorithms, input estimation, and closed-loop observers. Although they work well for some applications, there are some common defects.

Firstly, most of these methods still require lots of experimental calibration. For MAF sensor based methods, the open-loop observer needs either the cylinder air charge or volumetric efficiency as function of engine speed and intake manifold pressure. For speed-density based methods, the volumetric efficiency is needed. Some physical based volumetric efficiency model is used for eliminating the calibration work but more information is needed such as cylinder pressure.

Secondly, the performance of these methods in transient condition is limited. For example, the transient performance of MAF sensor based method is barely satisfactory because of the open-loop observer characteristic. Speed-density approach shows good performance at both steady-state and transient operating condition only if all inputs are very accurate which is impossible. The volumetric efficiency, as one of its inputs, is pre-calibrated thus speed-density approach cannot guarantee even the steady-state performance because of engine aging. Input estimation methods and close-loop observer

based methods may have potential to improve the transient performance but need further research.

Moreover, existing methods do not scale well when external EGR system is added. The widely used method to deal with external EGR system is using orifice model and transport delay model to estimate the EGR mass flow rate. Then this EGR estimation method will cooperate with the air charge estimation to determine the cylinder charge amount and charge composition. But the drag coefficient in the orifice equation is pre-calibrated and cannot deal with engine aging problem such as EGR valve deposit. And when the differential pressure of the two side of EGR valve is small, this method will give a large error.

Last but not the least, the feedback control is used only for trimming fuel injection amount no matter where the error source is. As mentioned before, the AFR control strategy includes feedforward control and feedback control. The feedforward part controls the fuel injection amount according to the cylinder air charge estimation. The feedback part adjusts fuel injection amount according to the exhaust lambda sensor signal without considering where the feed forward AFR control error is from. The error might from air estimation error, fuel puddle model error or even the fuel injector issue and will influence other engine control system such as torque estimation although.

To overcome these defects, a cylinder charge estimation algorithm which is capable of real time engine control with accuracy for both air and EGR is needed. Compared with the other cylinder charge estimation, the proposed method should be better for all aspects (Table 2.1).

In conclusion, the objective of this research work is to solve these key issues for existing cylinder charge estimation.

Table 2.1 The comparison of cylinder charge estimation methods

	Open loop observer	**Semi empirical**	**Neural network**	**Physical based**	**Input estimation**	**State observer**	**Proposed approach**
Steady-state accuracy	Good	Bad	Bad	Good	Good	Good	Good
Transient performance	Bad	Good	Good	Good	Good	Good	Good
Sensor needed	MAF	MAP	MAP	P_cyl P_port	MAF MAP	MAF MAP	MAF, MAP, λ_{ex}
Calibration needed	More	More	More	Less	More	More	Less
Computation power	Less	Less	Less	More	Less	Less	Less
Adaptation	Fuel only	Fuel only	Fuel only	Fuel only	Fuel only	Fuel only	Air/Fuel/EGR

CHAPTER THREE

3. SIMULATION AND EXPERIMENTAL SETUP

Regarding the model development, a high-fidelity simulation model is needed as a test bed for the algorithm design because of its cost and time efficiency. After development of model and the estimation algorithm, the experimental environment is needed for the validation of these models. This chapter will elaborate the simulation environment and experimental environment setup designed for this research.

3.1 Simulation Setup

GT-POWER is a powerful commercial software package based on one-dimensional dynamics of vehicle especially for engine system modeling and simulation. The GT-POWER model created in this work will effectively serve as a virtual engine, and allow fast and economical exploration of the design, and creation of large data sets for tuning or testing proposed models and estimation algorithms.

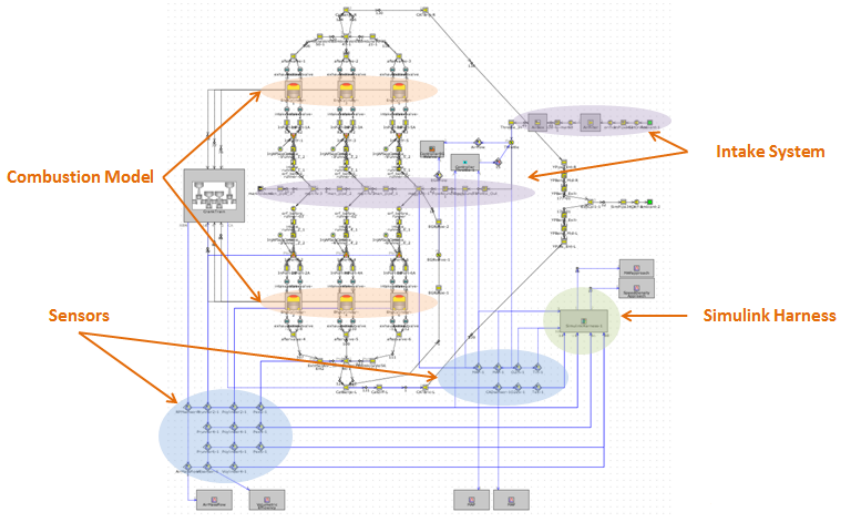

Figure 3.1 The GT-POWER model used in this research

The GT-POWER model was developed based on test engine geometry and configurations (Table 3.1) as shown in Figure 3.1. The intake and exhaust environment parameters are set as same as the real test cell ambient environment. The widely used SI engine Wiebe model is implemented for cylinder combustion process. The air path, EGR path and exhaust path are modeled based on the actual size of the pipes and volumes.

Since the objective of this work is cylinder charge estimation, intake runner pressure wave and pumping loop are chosen for model validation. In Figure 3.2, the modeled intake runner pressure of bank 2 (cylinder 2, 4, and 6) is compared with the experimental intake runner pressure at the same operating condition. In Figure 3.3, the modeled pumping loop is compared with the experimental cylinder pressure at the same operating condition. It can be concluded that the built GT-POWER model has solid and trustworthy performance for studied operating conditions.

Finally, the GT-Power engine model built for this work is integrated with a MATLAB/Simulink-based estimation and control system. The combination will be used to investigate physical phenomena related to cylinder charge estimation, and to test estimation algorithms using model-in-the-loop strategy.

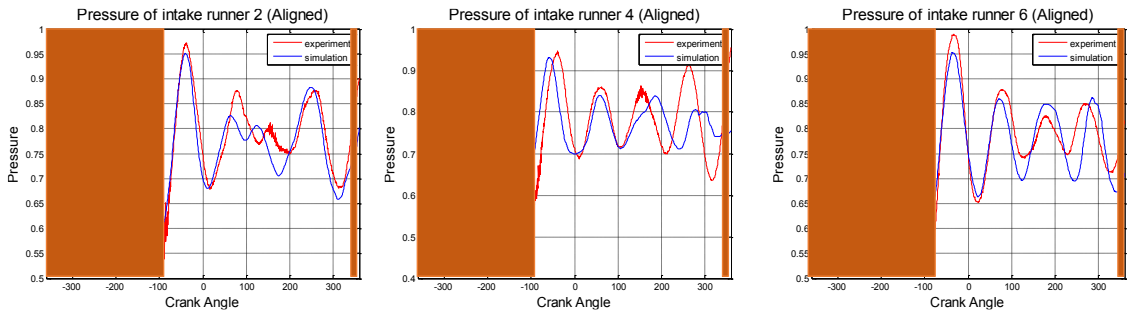

Figure 3.2 GT-POWER model validation (intake runner pressure)

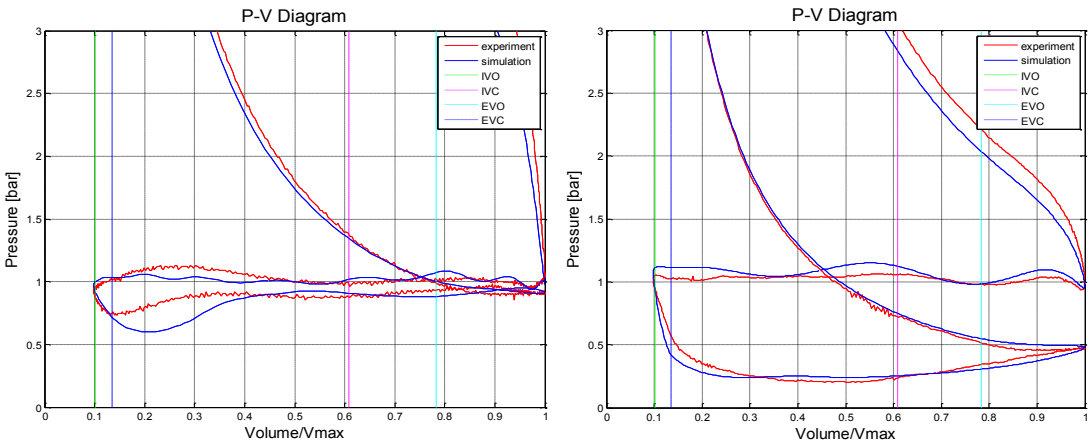

Figure 3.3 GT-POWER model validation (pumping loop)

3.2 Experimental Setup

This experimental test is carried out at Clemson University - International Center for Automotive Research (CU-ICAR). The test engine is installed into a FEV Engine Test Cell located at CU-ICAR. A low-inertia 430KW Alternating Current (AC) dynamometer which is capable to simulate realistic transient engine operation is used to absorb power and regulate engine speed (Figure 3.4 and Figure 3.5).

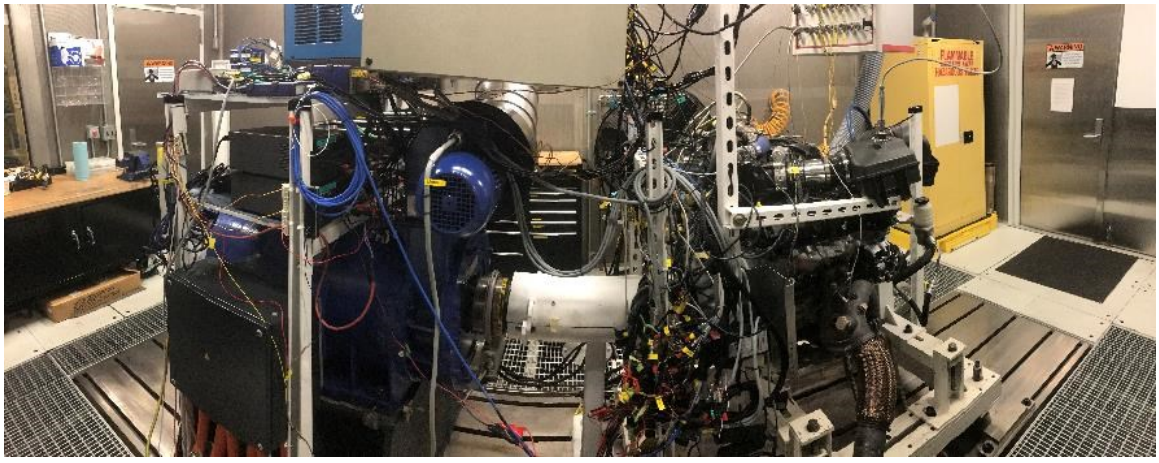

Figure 3.4 FEV AC dynamometer test cell with engine in CU-ICAR

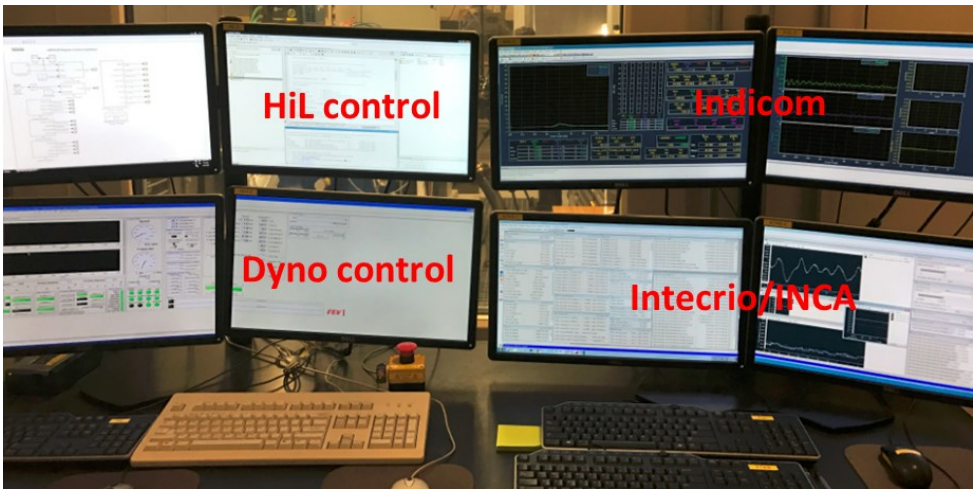

Figure 3.5 FEV test cell control room

The fuel conditioning system of engine test cell, FuelCon, control the fuel temperature and fuel pressure supply to the test engine. The engine coolant conditioning system, CoolCon, assures stable conditions like coolant temperature during the test. Fuel flow rate is measured by SIEMENS Sitrans 2100 mass flow meter. Oil temperature is controlled through a heat exchanger using coolant from engine coolant outlet.

The engine test cell is set up with engine control rapid prototyping system and data acquisition system for this research work which will be explained in the following sections.

3.2.1 Test Engine Description and Setup

A naturally-aspirated 3.6L port fuel injection engine is used for this research. The basic engine specification is listed in Table 3.1.

Table 3.1 Engine specification

Configuration	60° V6
Torque (Nm)	365 @ 4,175 rpm
Horse Power (SAE net)	305 @ 6,400 rpm

Displacement (Liter)	3.6
Cylinder Bore (mm)	96
Piston Stroke (mm)	83
Compression ratio	10.2:1
Valvetrain	dual-independent cam phasing
Oil System	wet sump
Cooling System	water-cooled
Fuel Type	gasoline (87 Pump Octane)
Combustion Type	spark-ignition
Air duct type	naturally-aspirated, no EGR
Fuel injection type	port fuel injected

The existing research engine has been retrofitted with external EGR system. The schematic diagram of the external EGR system is shown in Figure 3.6. An EGR valve is added to the intake manifold. An EGR cooler which is using engine coolant for cooling is added to the middle of EGR pipe. The exhaust manifold is retrofitted to serve as the EGR path inlet before three-way catalyst. The physical photo of the test engine after retrofitting is shown in Figure 3.7.

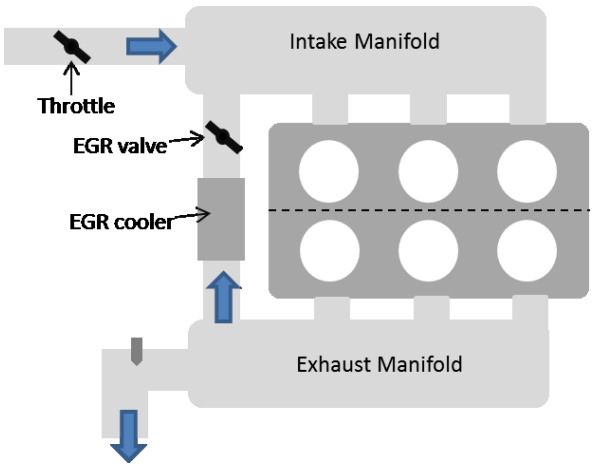

Figure 3.6 External EGR system schematic diagram

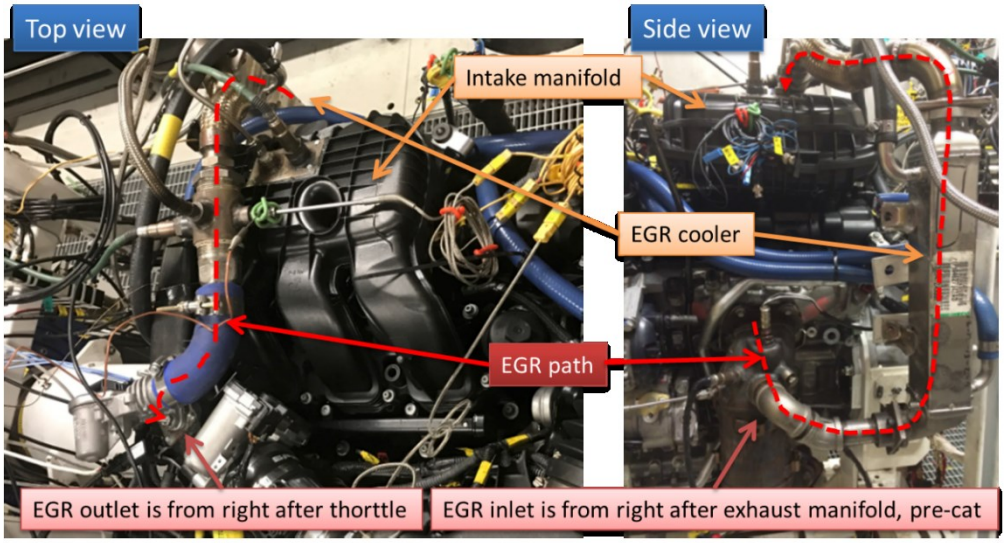

Figure 3.7 The external EGR system after retrofitted

To conduct this research with extra measurements for the validation of the model and estimation algorithm, also to have the ability to investigate the performance of various methods using different combination of sensors, certain instruments and sensors are installed into the test engine and the test cell. The existing engine system consists of a production type mass air flow (MAF) sensor, a stock manifold absolute pressure (MAP) sensor, an wide-band exhaust lambda sensor and intake air charge temperature sensor (ACT) for cylinder charges estimation. Besides these, more sensors and instruments are added to aid estimation algorithm development. A Meriam laminar flow element (LFE) is installed upstream of the engine intake system as a way to calibrate and verify MAF sensor readings. A humidity sensor and a pressure sensor are installed in the air path before throttle for sensitivity analysis and air path modeling. The wide-band lambda sensor based EGR measurement system ECM5230 is used to validate EGR estimation algorithm and provide the intake/exhaust manifold pressure/oxygen concentration. To

track the temperature change for engine intake system with external EGR, six thermocouples are installed in different location in the engine air path side and the EGR path side. The intake port pressures are measured by Piezoresistive Kulite sensors. The cylinder pressures are measure through passage-mounted AVL GH12D piezoelectric cylinder pressure sensors. Besides two stock lambda sensors, two more Bosch LSU 4.9 wide-band lambda sensors have been installed before catalyst at each bank. All installed sensors/instruments are shown in Figure 3.8.

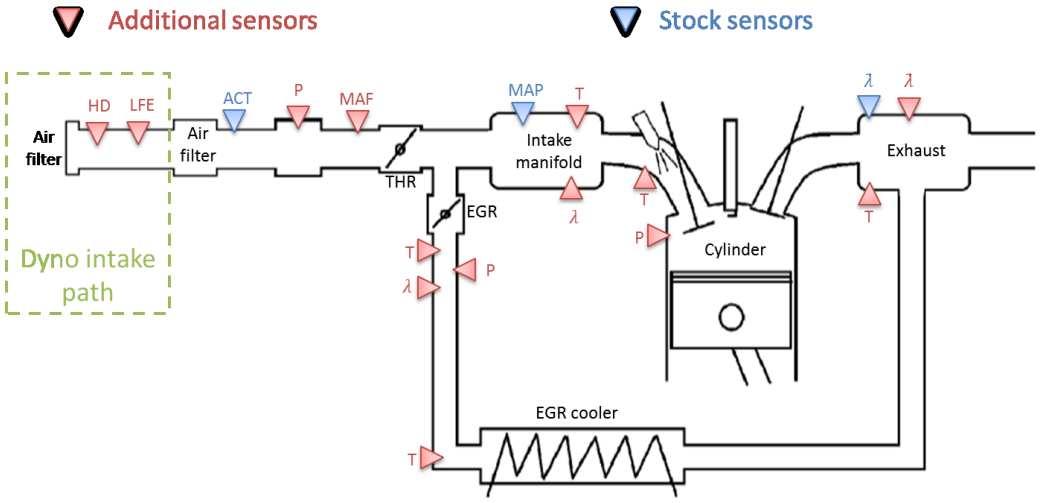

Figure 3.8 Overview of engine sensor location

3.2.2 Data Acquisition and Prototyping System Setup

All signals from these installed sensors/thermocouples/instruments and the stock sensors are collected using AVL Indimaster 671 data acquisition system. This data acquisition system is capable of sampling data with rate up to every 0.025 crank angle intervals to properly capture all relevant engine characteristics with an AVL 365X encoder mounted on a specially designed flywheel. Other signals from test cell such as

fuel rate and engine coolant temperature measured by FuelCon and CoolCon were also fed in to the AVL Indimaster 671. AVL Indicom software is used for online signal monitoring at the test cell control room and AVL concerto software is used for data post processing.

ETAS ES910 prototyping and interface module and ETAS ES930 Multi-I/O Module are used as engine control rapid-prototyping hardware (Figure 3.9).

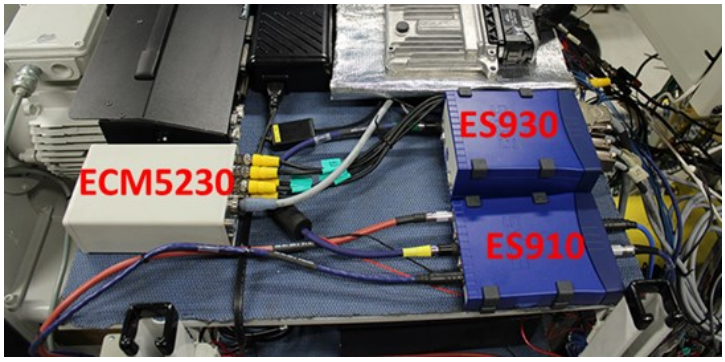

Figure 3.9 Hardware of rapid prototyping system

The rapid-prototyping hardware, interfaced with an ETAS INTECRIO software is used to override the stock engine control system algorithms in real-time when needed. The system allows the adjustment of engine actuators through ETAS INCA and is programmed using MATLAB/Simulink. The structure of the rapid prototyping system is shown in Figure 3.10.

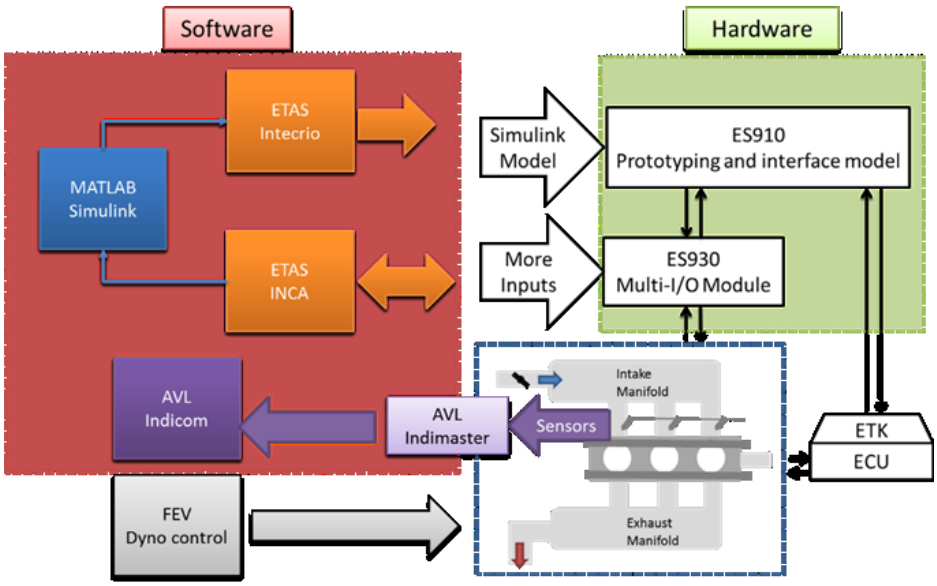

Figure 3.10 Overview of rapid prototyping system and data acquisition system

CHAPTER FOUR

4. ENGINE GAS PATH MODELING

A detailed physics-based model of the whole engine gas path is needed in order to fully understand the cylinder charge process in SI engines, and to provide the basis for estimation-oriented model development. In this chapter, the dynamics of engine gas path for a naturally aspirated port fuel-injected SI engine with external EGR system is investigated. A nonlinear model is developed considering all relevant dynamics of cylinder charge process to maximumly mimic the real engine's behavior. Later the nonlinear model is simplified to an estimation-oriented engine gas path model to capture the key features of the dynamics while keeping the real-time computational load of the proposed estimation algorithm at relatively lower level.

4.1 Model Description

A physics-based model is necessary to capture the cylinder charge dynamics. The literature about engine gas path modeling is exhaustive with various modeling approaches proposed with different objectives and multiple levels of complexities. However, MVEM, which is introduce in Chapter 2, is widely used for engine real time control area due to its physics-based nature, high computational efficiency and decent accuracy. In this research, the MVEM is also chosen as a basis with more in-depth analysis

The proposed engine gas path model includes five sub-models according to their physical causality of the cylinder charge process as shown in Figure 4.1: air path model,

EGR path model, Fuel path model, lambda path model, and intake manifold model. The air path, EGR path and fuel path will be combined as input module. The output signals of this input module are fed to intake manifold model which includes intake manifold pressure, temperature and exhaust gas concentration dynamics. A detailed description of each sub-model will be given in the following sections.

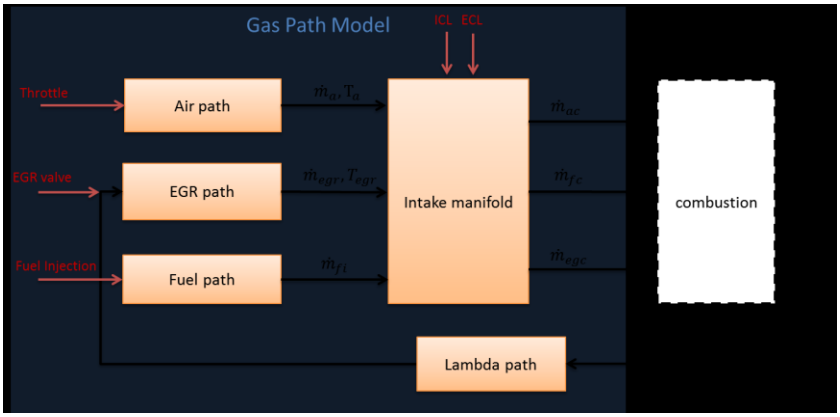

Figure 4.1: gas path model structure

4.2 Input Module Modeling

Input module includes air path model, EGR path model and fuel path model. The output signals of these models are: air mass flow rate goes into the intake manifold $\dot{m}_{thr}$, EGR mass flow rate goes into the intake manifold $\dot{m}_{EGR}$, and the fuel injection mass flow rate from port fuel injector $\dot{m}_{fi}$.These outputs will be fed into intake manifold model.

4.2.1 Air path model

As introduced in section 2.2, an isenthalpic orifice model is widely used to compute throttle valve mass flow. However, the upstream and downstream pressure of throttle valve need to be known in advance. Usually the downstream pressure of throttle valve can be measured by a MAP sensor in intake manifold. The upstream pressure is

always set to be 1 bar as ambient pressure when there is no ambient pressure sensor installed. However, the pressure will drop due to the long air path from air filter to throttle. In the engine test cell, the air path is even longer, thus experimental tests are conducted to evaluate pressure drop from fresh air inlet of test cell to pre-throttle location. It has been observed that the pressure will drop to more than 1 kPa at high speed high load operating condition as shown in the experimental result in Figure 4.2. In conclusion, a pre-throttle pressure drop model is needed for cylinder charge process modeling.

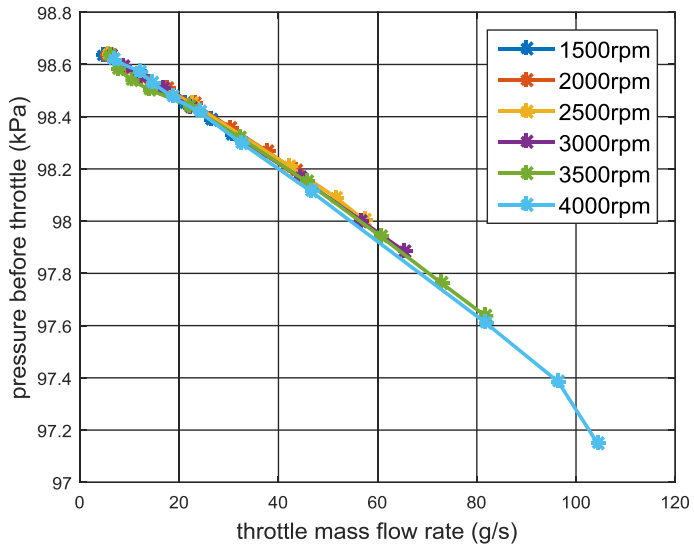

Figure 4.2: Air intake path pressure drop

Most gas flows in engine air path are incompressible flow[64]. Based on the assumption that there is no heat transfer or work transport from the objective pipe, the pressure drop can be modeled based on the energy balance[64]. The proposed pre-throttle pressure drop model is

$$\Delta p = C \cdot \frac{RT_{amb}}{p_{amb}} \cdot \left(a_1 \cdot \dot{m}^{\,2} + a_2 \cdot \dot{m} + a_3\right) \tag{28}$$

where a_1, a_2 and a_3 are calibration parameters, C is a tuning constant that depends on the geometry and air properties of objective pipe, $\dot{m}$ is the air flow rate through the pipe, p_{amb} and T_{amb} are ambient pressure and temperature respectively.

The parameters a_1, a_2 and a_3 are calibrated through experimental test as shown in Figure 4.3, where $R^2 = 0.9977$ and $RMSE = 0.01626$. The experimental validation of the pre-throttle model in Figure 4.4 shows satisfactory performance.

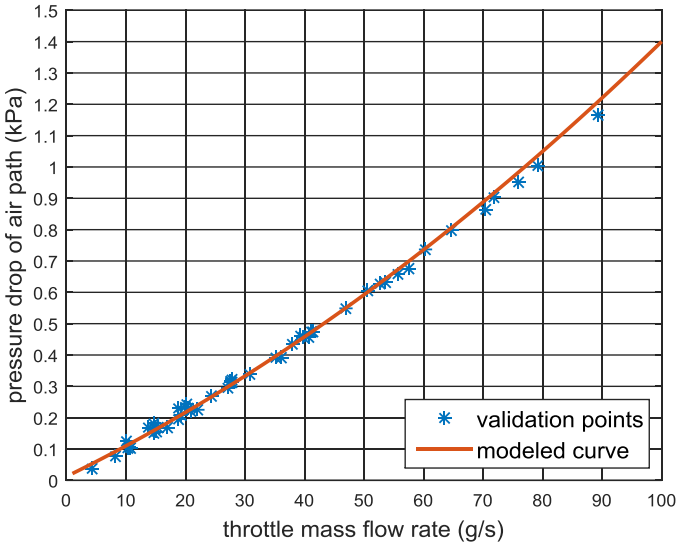

Figure 4.3: Experimental calibration of pre-throttle model

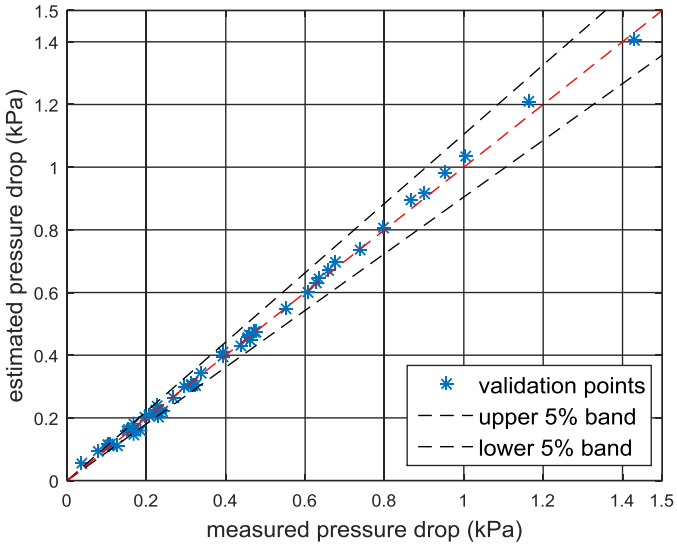

Figure 4.4: Experimental validation of pre-pressure model

When the air goes through the throttle which has a very small cross-section area, the gas velocity is relatively high. And under this condition, the throttle flow can be modeled based on an isenthalpic orifice equation as introduced in section 2.1

$$m(t) = c_d A(t) \frac{p_{pre}(t)}{\sqrt{RT_{amb}(t)}} \Psi\left[\frac{p_{pre}(t)}{p_{im}(t)}\right] \tag{29}$$

$$where, \Psi\left(\frac{p_{pre}}{p_{im}}\right) = \sqrt{\gamma\left(\frac{2}{\gamma+1}\right)^{\frac{\gamma+1}{\gamma-1}}}, \qquad p_o < p_{cr}$$

$$= \left(\frac{p_{im}}{p_{pre}}\right)^{\frac{1}{\gamma}} \sqrt{\frac{2\gamma}{\gamma-1}\left[1-\left(\frac{p_{im}}{p_{pre}}\right)^{\frac{\gamma-1}{\gamma}}\right]}, \qquad p_o \geq p_{cr}$$

$$with\ p_{cr} = \left(\frac{2}{\gamma+1}\right)^{\frac{\gamma}{\gamma-1}} \cdot p_{cr}\ , critical\ pressure$$

where c_d is discharge coefficient, A is the effective flow area of valve, p_{pre} is pre-throttle pressure calculated by the pre-throttle model, p_{im} is intake manifold pressure which is measured by MAP sensor, and T_{amb} is intake air temperature which measured by stock thermocouple installed after air box.

It is known that the orifice based throttle model fails at wide-open-throttle (WOT) situation because at such condition the orifice equation does not fulfill the Lipschitz condition[64]. There are several solutions to address this issue such as, using a linear function around $\Delta p = 0$. Nevertheless, in this research, WOT situation is not considered, thus the orifice based throttle model has enough accuracy for this research. And the discharge coefficient, c_d, and the effective flow area of valve, A, are lumped together for calibration purpose. The calibration result is shown in Figure 4.5 where $R^2 = 0.9948$ and $RMSE = 7.947$. The validation based on different engine operating condition (Figure 4.6) shows reliable performance of throttle model.

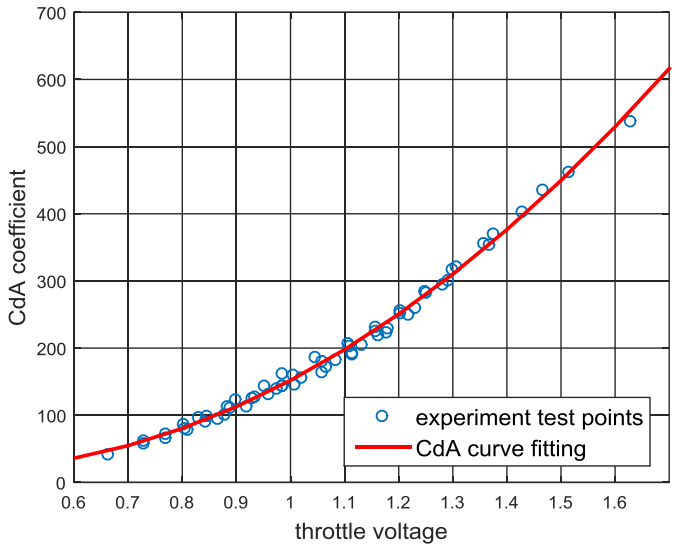

Figure 4.5 Experimental calibration of throttle model

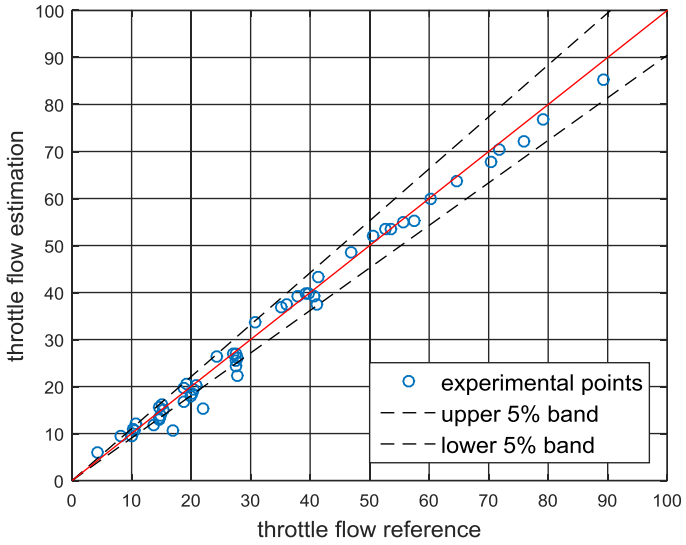

Figure 4.6 Experimental validation of throttle model

4.2.2 EGR path model

The detailed EGR path model includes all related dynamics such as EGR cooler heat transfer dynamics, EGR gas mixing and transport delay dynamics. However, in this research work, only EGR valve flow model is considered for simplicity. The EGR flow can also be modeled using an isenthalpic orifice equation

$$m(t) = c_d A(t) \frac{p_{em}(t)}{\sqrt{RT_{em}(t)}} \Psi\left[\frac{p_{em}(t)}{p_{im}(t)}\right] \tag{30}$$

$$where, \Psi\left(\frac{p_{em}}{p_{im}}\right) = \sqrt{\gamma\left(\frac{2}{\gamma+1}\right)^{\frac{\gamma+1}{\gamma-1}}}, \qquad p_o < p_{cr}$$

$$= \left(\frac{p_{im}}{p_{em}}\right)^{\frac{1}{\gamma}} \sqrt{\frac{2\gamma}{\gamma-1}\left[1-\left(\frac{p_{im}}{p_{em}}\right)^{\frac{\gamma-1}{\gamma}}\right]}, \qquad p_o \geq p_{cr}$$

$$with\ p_{cr} = \left(\frac{2}{\gamma+1}\right)^{\frac{\gamma}{\gamma-1}} \cdot p_{cr}\ , critical\ pressure$$

where c_d is discharge coefficient, A is the effective flow area of valve, p_{ex} is exhaust manifold pressure which is measured or modeled, p_{im} is intake manifold pressure which is measured by MAP sensor, and T_{ex} is EGR gas temperature which is measured by thermocouple installed before EGR valve. The discharge coefficient, c_d, and the effective flow area of valve A are lumped together and calibrated.

The experimental test of this EGR flow model is shown in Figure 4.7 where the blue line is from ECM5230, the red line is model output, and the yellow dotted line is considered as reference which is calculated by MAF and MAP sensors.

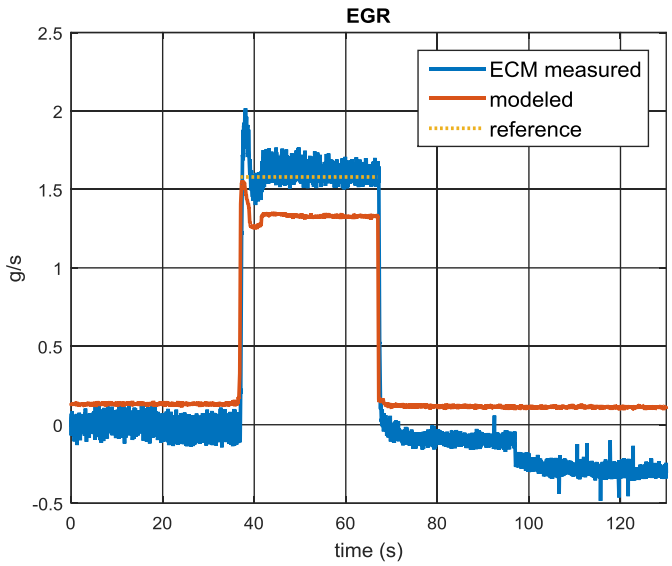

Figure 4.7 Experimental validation of EGR flow model

Accurate EGR concentration in intake manifold is very difficult to estimate. It is found from the experimental test that the orifice model is highly dependent of the

accuracy of calibration parameters and modeled exhaust pressure. This issue will be considered and addressed in Chapter 5.

4.2.3 Fuel path model

For port fuel injection engine, the fuel injection is usually controlled by fuel injector pulse width (PW). The fuel injection amount also depends on a lot of other variables like intake manifold pressure, fuel rail pressure, battery voltage. In this research, for simplicity, only PW is considered as it is the dominating factor.

From experimental test, it is found that there is a linear relationship between fuel injector PW and fuel injection flow rate (Figure 4.8). Thus a fuel injection model as function of engine speed and fuel injector PW is proposed and validated (Figure 4.9)

$$\dot{m}_{fi} = \frac{N}{60} \cdot (c_1 \cdot PW + c_2) \tag{31}$$

where N is enginee speed, PW is fuel injector PW, c_1 and c_2 are calibration parameters.

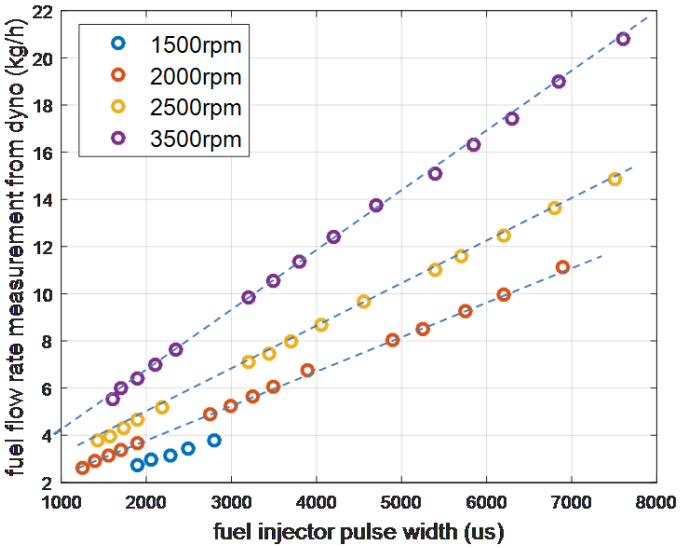

Figure 4.8: Experimental calibration of fuel injection model

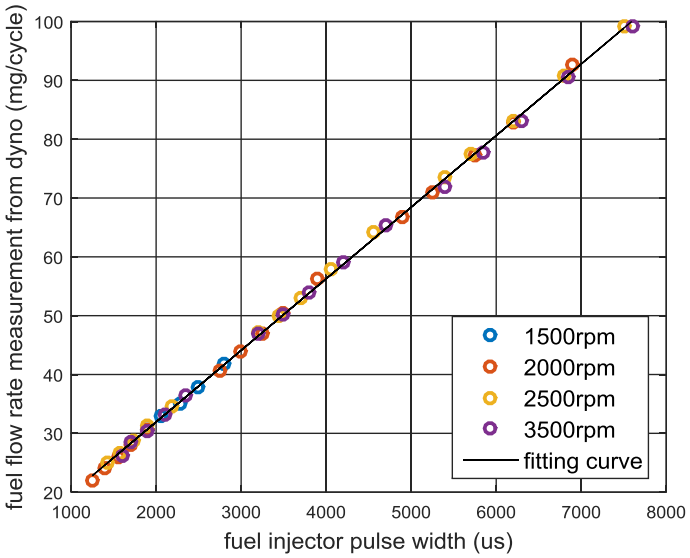

Figure 4.9: Experimental validation of fuel injection model

4.3 Lambda Path Modeling and Padé approximation

The wide-band exhaust lambda sensor can tell the oxygen concentration of exhaust gas with certain time delays. Time delay exists due to engine's characteristics and internal dynamics. For example, the distance from the intake valve to the sensor position, the engine reciprocation, and the sensor characteristics can all cause variable transport delay. Since lambda sensor contains important information for engine cylinder charge process, both its own characteristics and dynamics under certain engine operating conditions should be investigated and modeled properly.

4.3.1 Lambda path model

The lambda path model which represents the time delay from current charged air-to-fuel ratio within cylinder to lambda sensor in the exhaust pipe can be split into three parts: In cylinder delay, transport delay and lambda sensor delay. These delays can be shown visually in Figure 4.10.

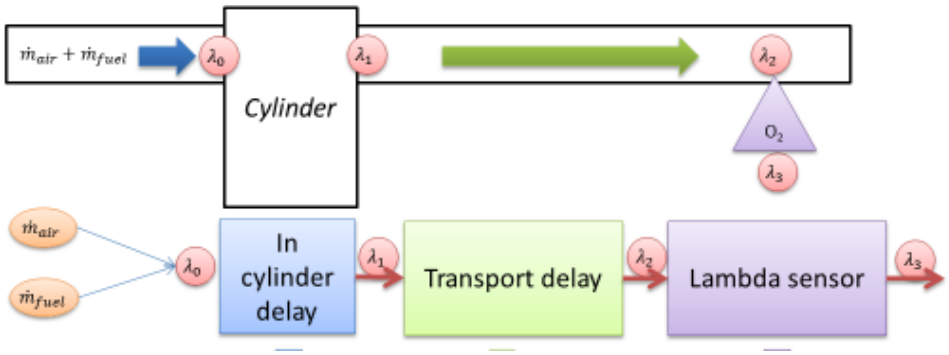

Figure 4.10 lambda path model structure

The fresh air and fuel go into cylinder when the intake valve is open during engine intake stroke. The air-to-fuel ratio at that time is labeled as λ_0 if burnt gas escaped from cylinder is not considered.

The in-cylinder delay is defined as the time duration from engine intake stroke to exhaust stroke. After in-cylinder delay, the air-to-fuel ratio should be

$$\lambda_1(t) = \frac{\dot{m}_{air}(t - \tau_{ICD})}{\dot{m}_{fuel}(t - \tau_{ICD})} \cdot \frac{1}{\lambda_{stoich}} \tag{32}$$

where $\dot{m}_{air}$ is the cylinder air flow charge during engine intake stroke, $\dot{m}_{fuel}$ is cylinder fuel flow charge during engine intake stroke, λ_{stoich} is the stoichiometric air-to-fuel ratio, τ_{ICD} is the in-cylinder delay time which is the function of engine speed

$$\tau_{ICD} \approx \frac{3\pi}{\omega_e} = \frac{90000}{N}[ms] \tag{33}$$

where N is engine speed.

The transport delay is defined as the time duration from exhaust port of cylinder to the lambda sensor location in exhaust pipe. The transport delay can be approximated

by a pure time delay (account for gas transport) plus a first order delay (account for gas mixing). After transport delay, the air-to-fuel ratio should be

$$\lambda_2(s) = e^{-\tau_1 s} \cdot \frac{1}{\tau_2 \cdot s + 1} \cdot \lambda_1(s) \tag{34}$$

where the time constant τ_1 accounts for pure gas transport time delay, and time constant τ_2 accounts for gas mixing time delay.

In this research work, the exhaust lambda sensor is installed right after exhaust manifold. Due to the compact design of engine exhaust system and lambda sensor location, the gas mixing time delay is considered as zero. The time constant τ_1 depends on geometry of engine exhaust system and engine operating conditions. It will be discussed and calibrated later in this section.

The lambda sensor delay is defined as the time needed for lambda sensor sensing the oxygen concentration and reflecting it on its pumping current when the exhaust gas arrived at the lambda sensor location in exhaust pipe. After lambda sensor delay, the air-to-fuel ratio should be

$$\lambda_3(s) = e^{-\tau_4 s} \cdot \frac{1}{\tau_3 \cdot s + 1} \cdot \lambda_2(s) \tag{35}$$

where the combination of a first order delay τ_3 and a pure time delay τ_4 can usually provide a good approximation of exhaust lambda sensor dynamics.

In this research work, a Bosch LSU 4.9 wide-band lambda sensor has been tested. The response time of this sensor without protection tube is identified to 40ms when exhaust temperature is around 700 C. As this specific lambda sensor is used for the

research work, there is only pure time delay needed to be considered in the proposed lambda sensor delay model

$$\tau_3 = 40[ms] \tag{36}$$

In conclusion, the lambda path model includes three various sources of delays. The in-cylinder delay can be calculated by engine speed. And, the sensor delay is assumed as 40 ms. The only unknown term is the transport delay time τ_1 which need to be calculated.

As mention above, the time delay, τ_1, is related to exhaust gas mass flow rate, exhaust temperature, pressure, the geometry of exhaust manifold/pipes, etc. To simplify the delay model, only air mass flow rate is considered as the key factor of the $\tau_1$time delay model.

Figure 4.11 shows lambda path time delay calibration methodology. While the engine actuators are kept still, then fuel injection PWis changed directly, the time duration from fuel command change point (blue line) to lambda sensor change point (red line) is considered as the lambda path total time delay (red bar).

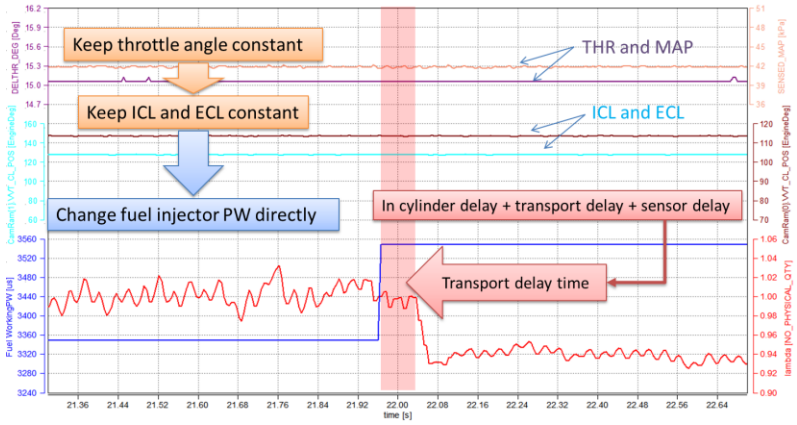

Figure 4.11 Lambda path time delay calibration process

The lambda sensor delay and in cylinder delay is either known or can be calculated as the function of engine speed. The only unknown term is τ_1. It is observed from experimental data that τ_1 is highly dependent of air mass flow rate. The relationship between transport time delay and air mass flow is shown in Figure 4.12.

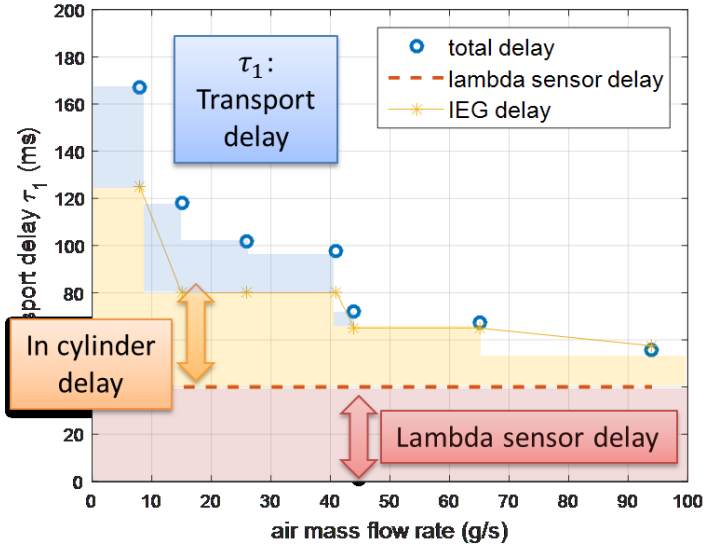

Figure 4.12 Lambda path time delay as function of air mass flow

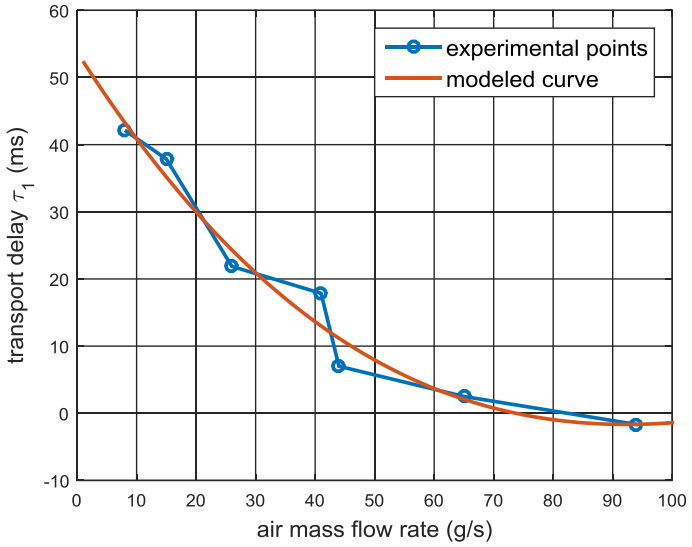

Figure 4.13 Experimental validation of transport delay model

The transport delay is then modeled as function of air mass flow which is validated against experimental data. The accuracy of the model is shown in Figure 4.13.

4.3.2 Padé approximation for time delay

As described in the previous section, varying time delay exists in lambda path model. The lambda sensor sensing value at time step t after simplification is

$$\lambda_3(t) = \lambda_2(t-\tau_3) = \lambda_1(t-\tau_1-\tau_3) = \lambda_0(t-\tau_{ICD}-\tau_1-\tau_3) \tag{37}$$

where τ_{ICD} is the in-cylinder time delay, τ_1 is the gas transport time delay and τ_3 is the lambda sensor response delay.

However, many estimation and control design algorithms cannot handle time delays directly. For example, pole placement as a control algorithm and Luenberger observer as an estimation algorithm do not work properly if time delays are present. To solve this problem, Padé approximation is introduced.

For a system with certain time delay, the transfer function can be expressed as

$$G(s) = e^{-\tau s} \tag{38}$$

where τ is the delay time. Padé approximates the time delay by rational models. The transfer function of the Padé approximation for a time-delay system is

$$G(s) = e^{-\tau s} \approx \frac{\sum_{i=0}^{n} a_i(-\tau s)^i}{\sum_{i=0}^{n} a_i(\tau s)^i} \tag{39}$$

where $a_j = \frac{(2n-i)!n!}{i!(n-i)!(2n)!}$, and n is the order of Padé approximation.

In Figure 4.14 a delayed step response with a 1st, 2nd and 3rd order Padé approximations is simulated to illustrate its performance.

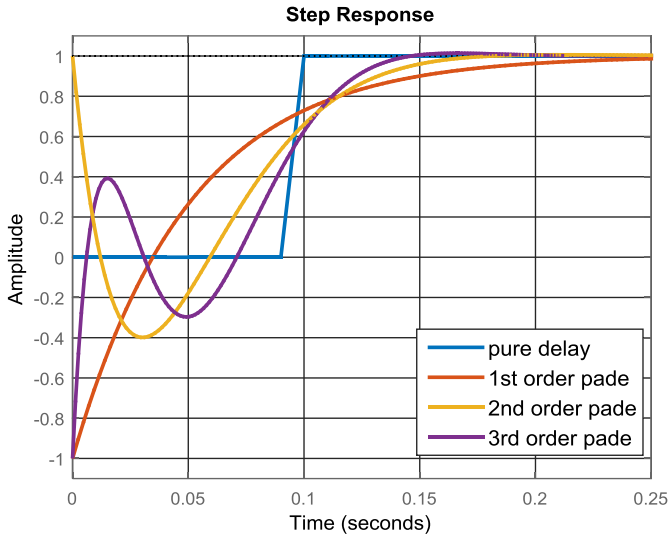

Figure 4.14: Padé approximation for pure time delay system

Padé approximations are useful to model time delay effects such as transport and computation delays within the context of continuous-time systems [65]. Padé approximation is also widely used for engine control with delayed lambda measurements [66–68]. However, Padé approximations have limited performance because a non-minimum phase system zero is introduced and thus experimental test is needed to evaluate the performance for this application. The total time delay at normal engine operating condition is from 50 ms (high speed high load) to 200 ms (low speed low load). To verify the performance of Padé approximation, an experimental test is conducted and the results are shown in Figure 4.15. It shows that 2nd order Padé approximation can model the time delay well with less than 2% lambda estimation error under different operating conditions.

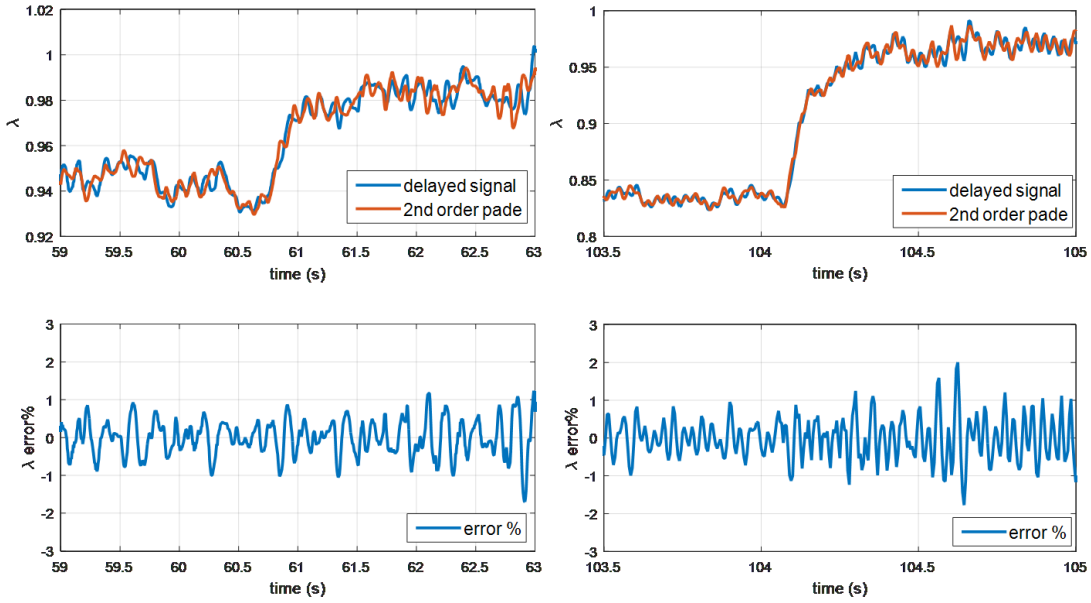

Figure 4.15 Experimental validation for Padé approximation model

With the help of Padé approximation, the state space model of the lambda path without time delay is proposed as

$$\dot{x}_1 = x_2 \tag{40}$$

$$\dot{x}_2 = -\frac{6}{\tau_\lambda}x_1 - \frac{12}{\tau_\lambda}x_2 + \frac{1}{\sigma_o}\cdot\frac{\dot{m}_{air}}{\dot{m}_{fuel}} \tag{41}$$

where the system states x_1 and x_2 do not have any physical meaning and only serve as intermediate variables of Padé approximation, τ_λ is the total time delay of lambda path model, σ_o is the stoichiometric air-to-fuel ratio, $\dot{m}_{air}$ and $\dot{m}_{fuel}$ are the cylinder air charge and cylinder fuel charge at engine intake stroke correspondingly.

The output of lambda path model is the exhaust lambda sensor measurement which can be expressed as

$$y = -\frac{12}{\tau_\lambda} x_1 + \frac{1}{\sigma_o} \cdot \frac{\dot{m}_{air}}{\dot{m}_{fuel}} \tag{42}$$

4.4 Intake Manifold Modeling

4.4.1 Intake manifold pressure/temperature model

In section 2.1, the intake manifold pressure and temperature model is introduced. For most engine control related publications, the intake manifold is usually modeled as a isothermal model without much further investigation. However, there are some questions need to be answered to fully understand the cylinder charge process.

There is not only air but also fuel and exhaust gas which contribute to the intake manifold pressure if purge flow and PCV flow are ignored. The first question is: will partial pressure of fuel influence the intake manifold pressure dynamics? To answer this question, an experimental test is conducted. The result is shown in Figure 4.16. In this experimental test, engine speed, throttle position and valve timing are set as constants. And thus the air flow (red line) is constant. While the fuel injection PW (dark green) is swept to change fuel injection amount, the fast response MAP sensor (blue line) is observed to be unchanged regardless of the alternation of fuel injection PW. In conclusion, the partial pressure of fuel does not influence intake manifold pressure dynamics.

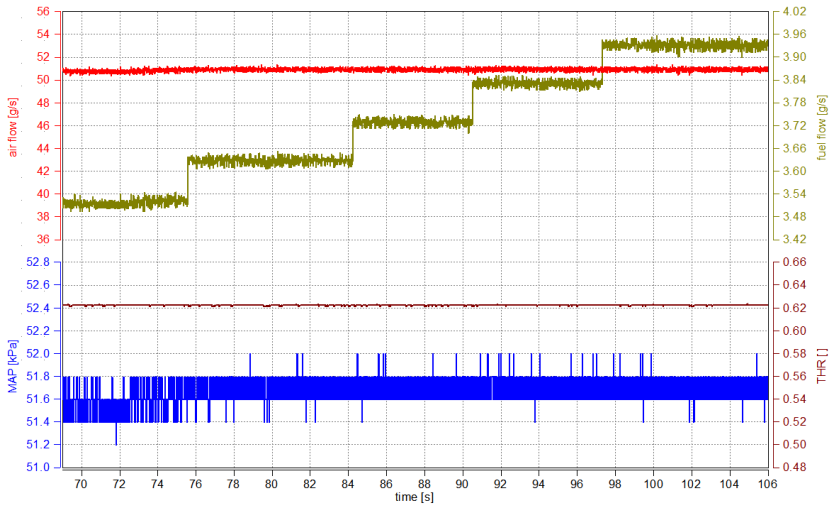

Figure 4.16 Manifold pressure when fuel injection PW is swept

The second question is: what are the differences of isothermal model, adiabatic model and polytropic model for cylinder charge process? The intake manifold model is introduced in section 2.1. Most publications use the isothermal model for the engine control related problem without much more explanation and validations. In this research work, these models are explained in detail and validated with certain simulation and experiment data.

Figure 4.17 depicts an air intake system of the naturally aspirated SI engine equipped with an external EGR system in a mean value approach.

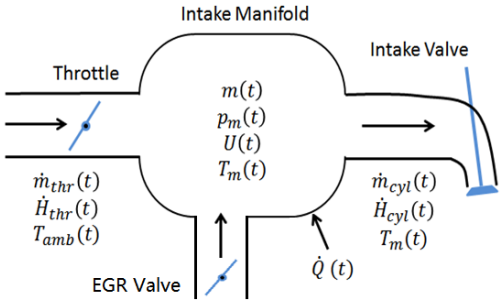

Figure 4.17 Intake system model for engine with external EGR system

Based on the energy balance and mass balance, the polytropic intake manifold model is deduced as

$$\dot{p}_{im} = \frac{\kappa R}{V_{im}}\left(\dot{m}_{thr}T_{thr} + \dot{m}_{egr}T_{egr} - \dot{m}_{cyl}T_{im} + \frac{\dot{Q}}{c_p}\right) \tag{43}$$

$$\begin{aligned}\dot{T}_{im} = \frac{RT_{im}}{p_{im}V_{im}}\big[\kappa\big(\dot{m}_{thr}T_{thr} + \dot{m}_{egr}T_{egr} - \dot{m}_{cyl}T_{im}\big) \\ - T_{im}\big(\dot{m}_{thr} + \dot{m}_{egr} - \dot{m}_{cyl}\big) + \dot{Q}/c_v\big]\end{aligned} \tag{44}$$

where κ is the heat capacity ratio, R is the ideal gas constant, $\dot{Q}$ is the heat transfer through the wall, c_p and c_r are the specific heat capacity at constant pressure and volume respectively. The suffixes im, thr and egr refer to the intake manifold, the throttle and the EGR valve, respectively. $\dot{m}_{cyl}$ is the air and EGR flow go into the cylinder.

If there is no heat transfer, brings $\dot{Q} = 0$ to the polytropic intake manifold model above, the adiabatic intake manifold model is deduced as

$$\dot{p}_{im} = \frac{\kappa R}{V_{im}}\big(\dot{m}_{thr}T_{thr} + \dot{m}_{egr}T_{egr} - \dot{m}_{cyl}T_{im}\big) \tag{45}$$

$$\begin{aligned}\dot{T}_{im} = \frac{RT_{im}}{p_{im}V_{im}}\big[\kappa\big(\dot{m}_{thr}T_{thr} + \dot{m}_{egr}T_{egr} - \dot{m}_{cyl}T_{im}\big) \\ - T_{im}\big(\dot{m}_{thr} + \dot{m}_{egr} - \dot{m}_{cyl}\big)\big]\end{aligned} \tag{46}$$

If there is no temperature change in the system, then the isothermal intake manifold model is deduced as

$$\dot{p}_{im} = \frac{RT_{im}}{V_{im}}(\dot{m}_{thr} + \dot{m}_{egr} - \dot{m}_{cyl}) \tag{47}$$

$$\dot{T}_{im} = 0 \tag{48}$$

The GT-POWER simulation results for intake manifold pressure and temperature of different models are shown in Figure 4.18.

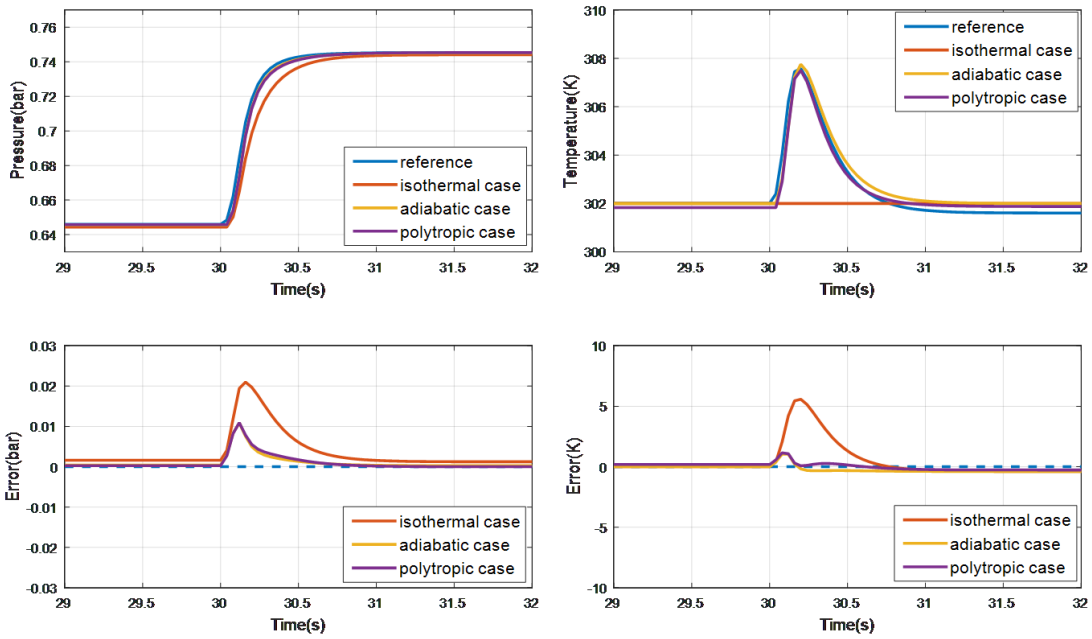

Figure 4.18: Simulation comparison of intake manifold models

From Figure 4.18, it is observed that, the pressure and temperature differences between adiabatic case and polytropic case is very small. At the mean time, the isothermal case has no temperature dynamics and thus the performance will be deteriorated during fast transient condition.

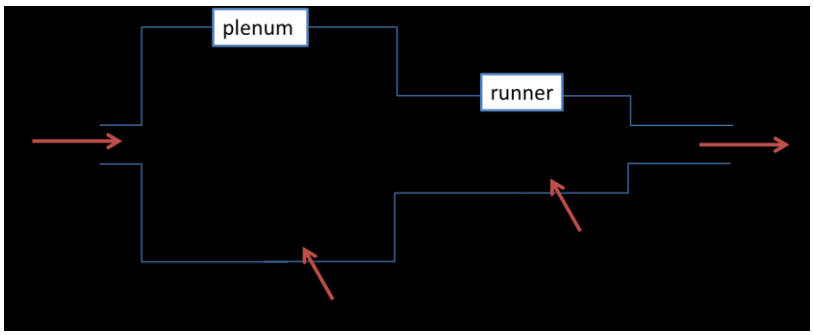

Figure 4.19 Experiment validation on temperature change made by heat transfer

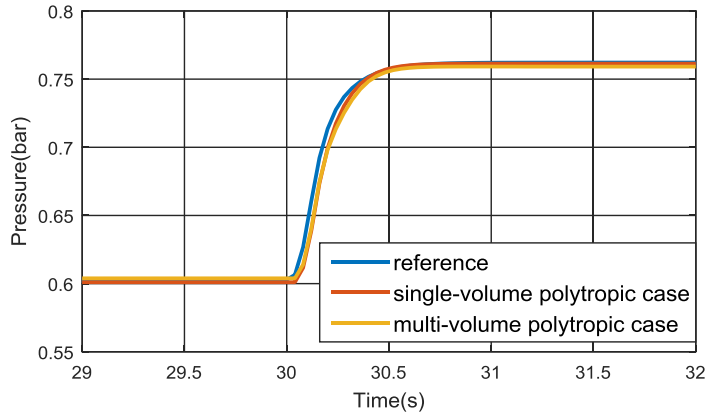

Figure 4.20 Pressure comparison between single volume model and multi-volume model

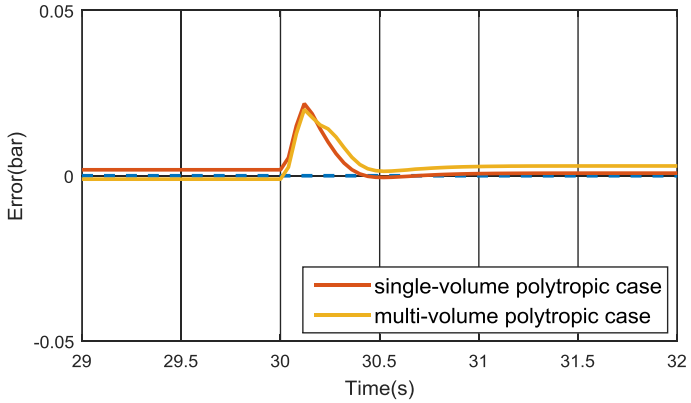

Figure 4.21 Pressure error comparison between single volume model and multi-volume model

It is observed that the heat transfer of plenum and runner are different[69]. Therefore it brings the third question: Do plenum and runner need to be considered separately for cylinder charge process? It is difficult to conduct an experiment since there is no flow rate reference at junction between manifold and runner. Instead, simulation results are compared between single-volume model and multi-volume model. In the GT-POWER model, all parameters related to heat transfer are from OEM manufacturer. The intake manifold pressure calculated by both models are shown in Figure 4.20 and the

pressure errors from these models are shown in Figure 4.21. The simulation results show very minor difference between single-volume model and multi-volume models.

4.4.2 Intake manifold EGR concentration model

For SI engine with external EGR system, the exhaust gas could be recirculated back into the intake manifold through EGR path. Then there is not only fresh air but also exhaust gas in the intake manifold and going into the cylinder. Different from diesel engine, which is usually of lean combustion, the fraction of the air or EGR in intake manifold of SI engine is very important for combustion and emission performance, especially for AFR control system. Similar to the models developed in [70], the dynamics of intake manifold EGR concentration can be approximately described as

$$\dot{F}_{egr} = \frac{RT_{im}}{p_{im}V_{im}}\left(\dot{m}_{egr} - F_{egr}(\dot{m}_{thr} + \dot{m}_{egr})\right) \tag{49}$$

where F_{egr} is intake manifold EGR concentration, $\dot{m}_{egr}$ is the EGR mass flow through EGR valve, $\dot{m}_{thr}$ is the air mass flow through throttle.

EGR concentration during engine transient operating condition is very hard to validate through experiment because of the slow response of intake lambda sensor and slow pressure compensation of ECM 5230. In this research work, the GT-POWER model in Chapter 3 is used for simulation validation of proposed intake manifold EGR concentration model. The results are shown in Figure 4.22 and Figure 4.23 where Figure 4.22 shows the operating condition with only EGR valve movement and Figure 4.23 shows the scenario when throttle plate and EGR valve move at the same time.

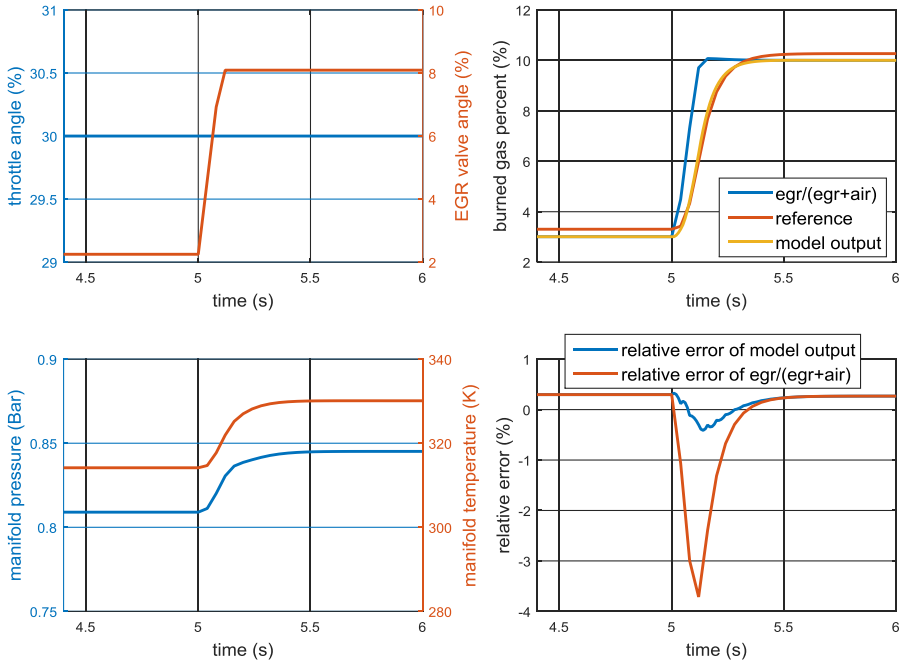

Figure 4.22: Simulation validation of intake manifold EGR concentration model

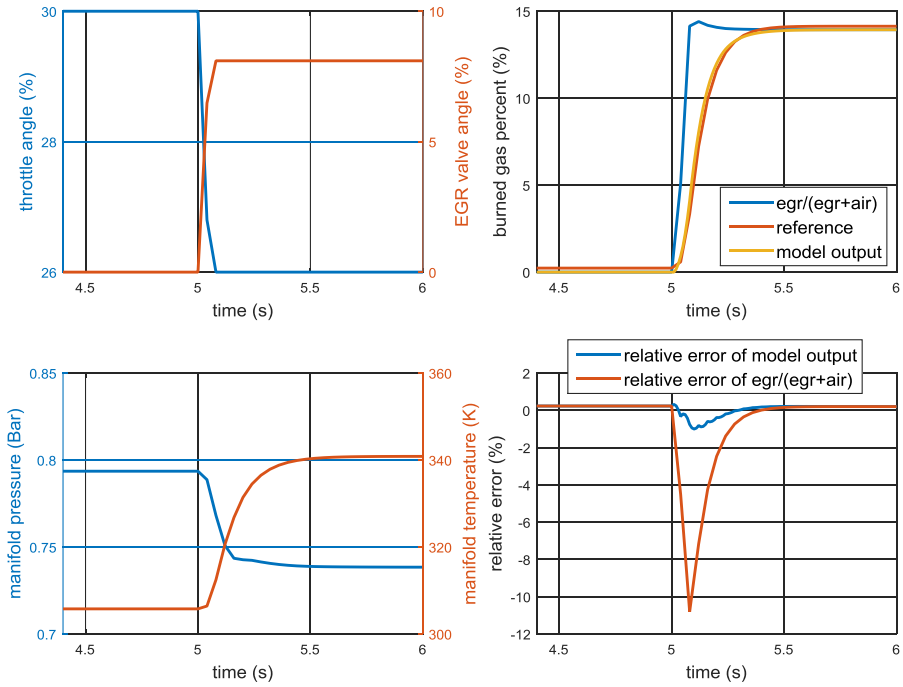

Figure 4.23: Simulation validation of intake manifold EGR concentration model

The top left plot in Figure 4.23 shows the actuators' movement: the throttle plate (blue line) and EGR valve (red line) change at the same time. The bottom left plot shows the manifold pressure (blue line) and temperature (red line) change accordingly. In the top right plot, it can be observed that the modeled intake manifold EGR concentration (yellow line) is following the reference (red line) very well. The bottom right plot shows the relative error of proposed model (blue line) is less than 1% while the direct calculation based on throttle flow and EGR flow has more than 10% error during the tested operating condition.

4.5 Fuel puddle modeling

For direct fuel injection engine, the fuel is delivered inside the cylinder. The cylinder fuel charge amount is identical to the injection amount. For port fuel injection engine, only a fraction of the injected fuel amount is inducted into the cylinder while the rest of the injected fuel is stored at the intake port walls and on the back of intake valve, which is called as "wall-wetting phenomenon". A schematic of the fuel wall-wetting phenomenon is shown in Figure 4.24.

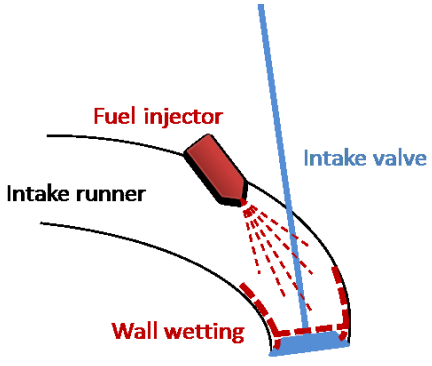

Figure 4.24 Wall wetting phenomenon for PFI engine

To better understand this phenomenon and achieve more accurate control of cylinder fuel charge, different models have been developed in both academic and industry studies[71–76]. Figure 4.25 shows several types of fuel models for PFI engines with analysis of the models' accuracy and computational cost. Due to the computational requirement, although 3D model has better performance, it is too complex to run on-line. Instead, the control-oriented model will be investigated and modified for this research work.

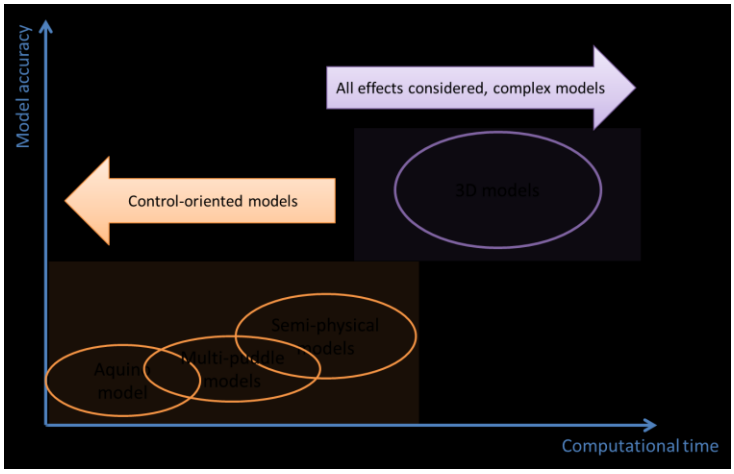

Figure 4.25 Fuel puddle model selection

In the early 1980s Aquino developed a model for fuel puddle dynamics with a very simple structure [77]. The fuel puddle dynamic is modeled as

$$\frac{d}{dt}m_{fp} = -\frac{1}{\tau_f}m_{fp} + X_f\dot{m}_{fi} \tag{50}$$

where τ_f is the evaporation time constant of the fuel in the puddle, X_f is the fraction of the injected fuel that enters the puddle, m_{fp} is the mass of the fuel puddle, and $\dot{m}_{fi}$ is the fuel injection flow rate. The fuel flow goes into the cylinders can be calculated by

$$\dot{m}_{fc} = \frac{1}{\tau} m_{fp} + (1 - X)\dot{m}_{fi} \tag{51}$$

where $\dot{m}_{fc}$ is cylinder fuel charge flow rate.

The Aquino model is widely known as "$\tau - X$" model because of the two parameters τ_f and X_f are needed in this model. These two parameters are usually calibrated as function of engine speed and intake manifold pressure

$$\tau \approx f(N,\, p_{im}) \tag{52}$$

$$X \approx f(N,\, p_{im}) \tag{53}$$

where N is engine speed and p_{im} is intake manifold. But these parameters are also highly dependent of other engine states (e.g. temperature, pressure, etc.) and the fuel properties. Therefore some other calibration tables for compensation are needed. Even if every conditions regarding the engine operating condition are kept constant, the default parameters will still change with the engine aging [78].

Some other more accurate models have been developed after the Aquino's model development. For example, there are the multi-puddle fuel model which makes assumption of more than one wall films on the intake port and on the back of the intake valve with different time constant and also the model considering the back flow of the exhaust gas [79–81]. However, these models are either too complex for estimation/control purposes or calibration-intensive for multiple system parameters.

Because of the complexity and time consuming of calibration process, physics based fuel model appears to be promising. There are a lot of publications discussing this problem and proposing semi-physics models with less calibration and acceptable

performance [82–84]. The semi-physics model proposed in [83] has same model structure as Aquino's model but requires much less experimental calibration. This model is considered to be a good candidate for estimation and control. The basic structure of this semi-physics fuel puddle model is shown in Figure 4.26.

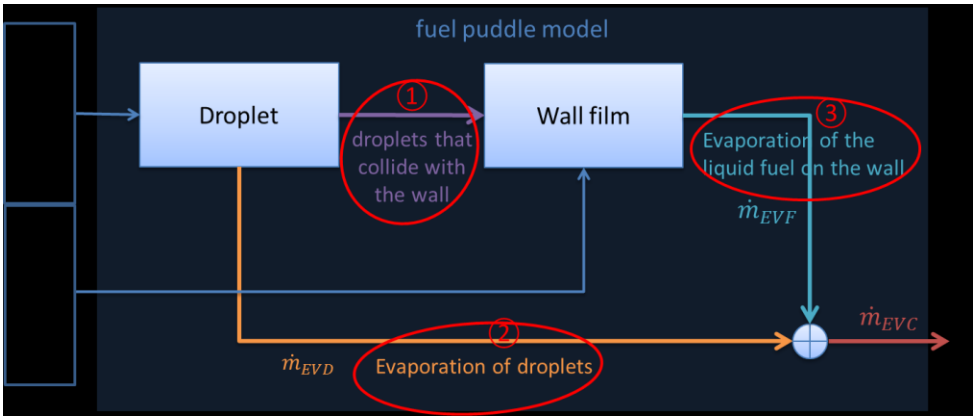

Figure 4.26 Physics based fuel puddle model structure

The model is built based on the assumption that fuel can enter the cylinder only by evaporation. And the cylinder fuel charge amount can be calculated by

$$\dot{m}_{EVC} = \dot{m}_{EVD} + \dot{m}_{EVF} \tag{54}$$

where $\dot{m}_{EVC}$ is cylinder fuel charge flow rate, $\dot{m}_{EVD}$ is the evaporated fuel flow rate from fuel droplets, and $\dot{m}_{EVF}$ is the evaporated fuel flow rate from fuel film.

According to the thermodynamic analogies [16,85], the evaporating fuel mass $\dot{m}_{EV}$ can be modeled as

$$\dot{m}_{EV} = h_m \cdot \rho_f \cdot A_f \cdot ln(1 + B) \tag{55}$$

where, h_m is the mass transfer coefficient, ρ_f is density of the liquid fuel, A_f is the area of the surface on which the evaporation takes place, B is Spalding number. The mass transfer coefficient is

$$h_m = Sh \cdot \frac{D_{AB}}{d_x} \tag{56}$$

where Sh is Sherwood number, D_{AB} is diffusivity coefficient, d_x is the characteristic length. The Sherwood number is calculated by

$$Sh = C_r \cdot Re^{m_r} \cdot Sc^{nr} \tag{57}$$

where C_r is Sherwood number, Re is Reynolds number, Sc is Schmidt number. C_r, m_r and n_r are parameters related to the evaporation process. For fuel puddle model, these parameters have been identified in [16] and listed in Table 4.1 for puddle evaporation process and droplet evaporation process.

Table 4.1 Sherwood number calculation[16]

	C_r	m_r	n_r
Puddle	0.023	0.83	0.44
droplet	0.552	0.50	0.33

It is found that Reynolds number, Re, is a function of air mass flow. And Schmidt number, Sc, is a function of intake manifold pressure and temperature[82]

$$R_e \propto \dot{m}_{air} \tag{58}$$

$$S_c \propto \frac{T_{im}}{p_{im}} \tag{59}$$

where $\dot{m}_{air}$ is air mass flow through the intake runner, p_{im} and T_{im} are intake manifold pressure and temperature correspondingly.

The Spalding number describes the evaporation properties of the fuel and is a function of fuel temperature[16]

$$B = \frac{m_{vs,\%}(T) - m_{vs\infty}}{1 - m_{vs,\%}(T)} \tag{60}$$

where $m_{vs,\%}$ is the mass fraction of fuel vaporized and $m_{vs\infty}$ is the mass fraction of fuel in the surrounding gas flow. If fuel temperature is controlled at 40 degrees centigrade, then the Spalding number can be treated as a constant.

Finally, the semi-physics fuel puddle model can be represented as Aquino's model structure with parameters τ_f and X_f

$$\frac{1}{\tau_f} \propto \dot{m}_{air}^{0.83} \cdot \left(\frac{T_{im}}{P_{im}}\right)^{0.44} = k_1 \cdot \dot{m}_{air}^{0.83} \cdot \left(\frac{T_{im}}{P_{im}}\right)^{0.44} \tag{61}$$

$$X \propto k_2 \cdot \dot{m}_{air}^{0.5} \cdot \left(\frac{T_{im}}{P_{im}}\right)^{0.33} + k_3 = k_2 \cdot \dot{m}_{air}^{0.5} \cdot \left(\frac{T_{im}}{P_{im}}\right)^{0.33} + k_3 \tag{62}$$

where k_1, k_2 and k_3 are the three calibration parameters.

The model is simplified for estimation/control purpose, thus it does not consider influences from fuel temperature, engine coolant temperature, valve timing etc. Only three parameters (k_1,k_2, and k_3) need to be calibrated. The calibration effort is way less than the Aquino model.

The fuel puddle model validation is conducted together with lambda path model. Figure 4.27 shows the experimental validation of fuel and lambda path model at steady

state condition and Figure 4.28 shows the experimental validation of fuel and lambda path model at transient condition. It is believed that the accuracy of this fuel puddle model can be improved with more calibration work.

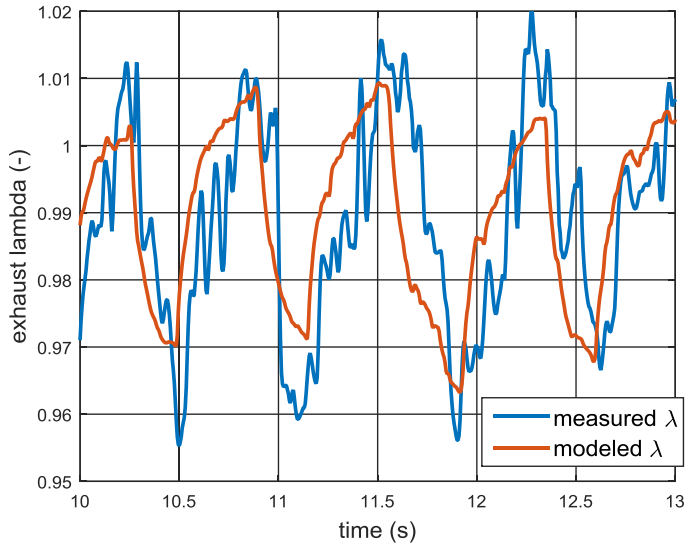

Figure 4.27 Experimental validation of fuel and lambda path model at steady state condition

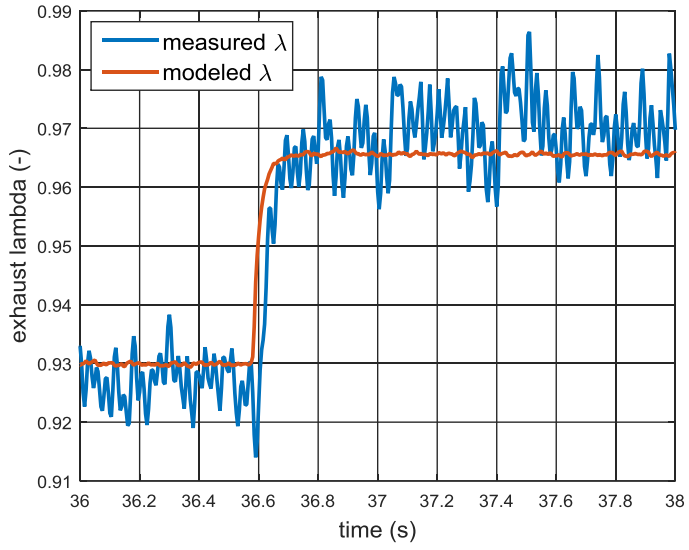

Figure 4.28 Experimental validation of fuel and lambda path model at transient condition

4.6 Estimation-oriented Model

In the previous sections of this chapter, the cylinder charge related dynamics is analyzed in detail. However, the nonlinear model needs to be further transformed and simplified for cylinder charge estimation algorithm design and on-line execution.

The objective of this research work is to estimate cylinder charge amount. However, the state observer techniques can only estimate "system states". There is no cylinder air or EGR charge as a system state in the nonlinear model. To overcome this problem, the speed-density equation is used for converting the intake manifold pressure dynamic to the cylinder air and EGR charge dynamic. The cylinder air and EGR charge dynamic is deduced from isothermal intake manifold model and speed-density equation

$$\dot{m}_{cyl} = \frac{NV_d\eta_{VE}}{120V_{im}}\left(\dot{m}_{thr} + \dot{m}_{EGR} - \dot{m}_{cyl}\right) \tag{63}$$

where $\dot{m}_{cyl}$ is cylinder air and EGR charge mass flow rate, V_d is engine displacement volume, V_{im} is intake manifold volume, and η_{VE} is volumetric efficiency.

After the transformation, the cylinder air charge and cylinder EGR charge can be expressed by the cylinder charge $\dot{m}_{cyl}$ and EGR concentration in intake manifold, $EGR\%$

$$\dot{m}_{cyl.air} = \dot{m}_{cyl} \cdot (1 - EGR\%) \tag{64}$$

$$\dot{m}_{cyl.EGR} = \dot{m}_{cyl} \cdot EGR\% \tag{65}$$

where $\dot{m}_{cyl.air}$ is cylinder air charge, $\dot{m}_{cyl.EGR}$ is cylinder EGR charge, and $EGR\%$ is intake manifold exhaust gas concentration.

For EGR concentration in intake manifold dynamic, equation (49) is used to represent its dynamic.

For fuel charge estimation, the fuel puddle dynamics is used as

$$\frac{d}{dt}m_{fp} = -\frac{1}{\tau_f}\cdot m_{fp} + X_f \cdot \dot{m}_{fi} \tag{66}$$

Then the fuel charge amount can be deduced as

$$\dot{m}_{fc} = \frac{1}{\tau_f}\cdot m_{fp} + (1 - X_f)\cdot \dot{m}_{fi} \tag{67}$$

where $\dot{m}_{fc}$ is cylinder fuel charge flow rate.

For lambda path model, the time delay issue is solved by Padé approximation. The state space equation of 2nd order Padé approximation is used as its dynamics.

In conclusion, the proposed estimation oriented model is

$$\ddot{m}_{cyl} = \frac{NV_d\eta_{VE}}{120V_{im}}(\dot{m}_{thr} + \dot{m}_{egr} - \dot{m}_{cyl}) \tag{68}$$

$$\dot{F}_{egr} = \frac{NV_d\eta_{VE}}{120V_{im}}\frac{1}{\dot{m}_{cyl}}\left[\dot{m}_{egr} - F_{egr}(\dot{m}_{thr} + \dot{m}_{egr})\right] \tag{69}$$

$$\dot{m}_{fp} = -\frac{1}{\tau_f}m_{fp} + X_f\dot{m}_{fi} \tag{70}$$

$$\dot{x}_1 = -\frac{6}{\tau_\lambda}x_1 - \frac{12}{\tau_\lambda^2}x_2 + \frac{1}{\sigma_o}\cdot\frac{\dot{m}_{cyl}(1 - F_{egr})}{(1 - X_f)\dot{m}_{fi} + \frac{1}{\tau_f}m_{fp}} \tag{71}$$

$$\dot{x}_2 = x_1 \tag{72}$$

$$\ddot{m}_{MAF} = -\frac{1}{\tau_{MAF}}\dot{m}_{MAF} + \frac{1}{\tau_{MAF}}\dot{m}_{thr} \tag{73}$$

where τ_f and X_f are parameters of fuel puddle model which is calculated in section 4.5, τ_λ is lambda delay time which is calculated in section 4,3 and τ_{MAF} is MAF sensor 1st order delay time identified by experimental data.

The throttle flow, $\dot{m}_{thr}$, EGR flow, $\dot{m}_{egr}$, and fuel injection flow, $\dot{m}_{fi}$, will be served as model inputs

$$\dot{m}_{thr} = f_{orifice}(p_{amb}, p_{im}, T_{amb}) \tag{74}$$

$$\dot{m}_{egr} = f_{orifice}(p_{im}, p_{em}, T_{im}) \tag{75}$$

$$\dot{m}_{fi} = \frac{N}{60} \cdot (c_1 \cdot PW + c_2) \tag{76}$$

where $f_{orifice}$ is orifice equation, N is engine speed and PW is fuel injector pulse width, c_1 and c_2 are the calibrated parameters.

The measurements used for this research work are MAP sensor, MAF sensor, and exhaust lambda sensor

$$\overline{MAP} = \frac{1}{k_1} \frac{RT_{im}}{V_{im}} \dot{m}_{cyl} \tag{77}$$

$$\bar{\lambda}_{ex} = -\frac{12}{\tau_\lambda} x_1 + \frac{1}{\sigma_o} \cdot \frac{\dot{m}_{cyl}(1 - F_{egr})}{(1 - X_f)\dot{m}_{fi} + \frac{1}{\tau_f} m_{fp}} \tag{78}$$

$$\overline{MAF} = \dot{m}_{MAF} \tag{79}$$

where $\overline{MAP}$ is MAP sensor measurement, $\bar{\lambda}_{ex}$ is exhaust lambda sensor measurement, and $\overline{MAF}$ is MAF sensor measurement.

In conclusion, the nonlinear model for SI engine gas path has been developed and then converted to an estimation oriented model. Certain dynamics is ignored such as the intake manifold temperature dynamics and the exhaust gas dynamics of rich or lean combustion. MAF sensor dynamics is added. The time delay issue is solved by Padé approximation. This estimation-oriented model will serve as the basis of cylinder charge

estimation algorithms and is modified for different applications and objectives in the following chapters.

CHAPTER FIVE

5. CYLINDER AIR CHARGE ESTIMATION WITH MAF AND MAP SENSORS

For engine without external EGR system, or when EGR valve is closed, the cylinder charge is only fresh air thus the problem would be simplified to cylinder air charge estimation. Some methods have been investigated in Chapter 2. Their performances have been compared and the pros and cons for different approach have been listed in section 2.6. It is observed that observer based estimation technique is promising from the literature review. In this Chapter, several observer based methods for cylinder air charge estimation utilizing both MAF and MAP sensors are developed. The purpose is to apply observer based methods to reduce calibration work while providing acceptable transient and steady-state accuracy with low computational load.

5.1 State Estimation Introduction

5.1.1 Observer introduction

The use of a dynamic system to provide estimates of the unmeasurable states goes back to the earliest work with state-space methods in the early 1960s[86]. Luenberger's work of the mid-1960s systematized and generalized much of the earlier results. In his research work, the term "*observer*" was introduced into linear system theory [87–89].

Consider a linear time invariant continuous system in state space representation:

$$\dot{x} = Ax + Bu \tag{80}$$

$$y = Cx + Du \tag{81}$$

where, x is system states, u is system inputs, y is system output. An artificial dynamic system can be construct with an estimated initial state value

$$\dot{\hat{x}} = A\hat{x} + Bu \tag{82}$$

$$\hat{y} = C\hat{x} + Du \tag{83}$$

where, $\hat{x}$ is the estimated states, $\hat{y}$ is the estimated system output. An error signal can be generated from the difference between $\bar{y}$ and $\hat{y}$, where $\bar{y}$ is the measured output. The Luenberger observer then can be designed as

$$\dot{\hat{x}} = A\hat{x} + Bu + L(\bar{y} - \hat{y}) \tag{84}$$

$$\hat{y} = C\hat{x} + Du \tag{85}$$

where L is the observer gain. If the state error is defined as

$$e = x - \hat{x} \tag{86}$$

Then the observer error satisfies the equation:

$$\dot{e} = \dot{x} - \dot{\hat{x}} = Ax + Bu - A\hat{x} - Bu - L(\bar{y} - \hat{y}) = (A - LC)e \tag{87}$$

The objective of the observer is to reduce the state estimation error $e(t)$ as much as possible. If the eigenvalues of the matrix $(A - LC)$ can be made Hurwitz, then the observer error $e(t)$ will approach zero asymptotically. Similar with the controllability check when designing a feedback controller, if the observability test matrix

$$O = \begin{bmatrix} C \\ AC \\ \vdots \\ A^{n-1}C \end{bmatrix} \tag{88}$$

is of rank n, where n is the number of the states in the system, the eigenvalues of the matrix $(A - LC)$ can be placed at arbitrary location. In conclusion, for any observable linear system, by adjusting the observer gain L, an observer can be designed having the property that the estimation error can be made to go to zero as fast as one may desire. An illustration of how an observer works is shown in Figure 5.1.

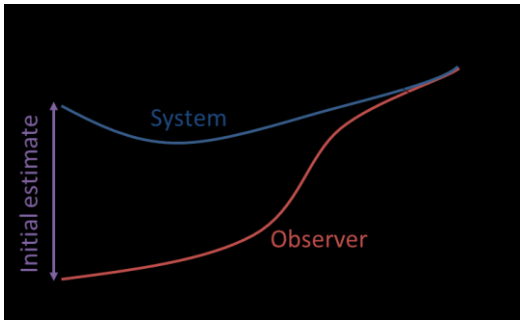

Figure 5.1 Illustration of observer based estimation

Luenberger observer works only for linear system without any noise and disturbances. However, due to the complexity of the real system, a lot of observer techniques have been developed to solve different problems. For example, Kalman filter is developed in early 1960s to optimally estimate system states for linear system with zero mean white noise. It is widely recognized since it was used for the Apollo human spaceflight program. Although Kalman filter is the most widely used estimator and has been successfully used in a number of applications, it only works when the objective system meets the assumption: the model must be sufficiently accurate, the noises from process and measurements are stochastic, zero mean, and Gaussian with known covariances. To solve nonlinear model problem, the extended Kalman filter and Unscented Kalman filter have been developed. To deal with the unknown disturbance,

sliding mode observer have been developed. Sliding mode techniques were known for their potential as a robust control methods. The advantage of sliding mode observer is robustness for system modeling uncertainties and unmodeled disturbances[90]. H-infinity observer is trying to minimize the maximum or worst case disturbance[91]. Or Particle filter technique can be used for system which has non-Gaussian distributions[92]. For nonlinear system with non-Gaussian distribution noise and inequality constraints, moving horizon estimation has been developed[93]. In this research work, different observer techniques are investigated and compared. The result is shown in Table 5.1.

Table 5.1 Observer techniques comparison

Algorithm	Model required	Estimation Type	Computational cost	Robustness	limitation
Luenberger observer	linear	deterministic	low	low	Accurate model &measurement
Sliding mode observer	nonlinear	deterministic	low	high	Known bond of disturbance
Kalman filter	linear	Bayesian estimation	low	Good only for white noise	Linear with known w, v
Extended KF	nonlinear	Bayesian estimation	moderate (low)	Good only for white noise	Fails on highly nonlinear sys
Unscented KF	nonlinear	Bayesian estimation	moderate (high)	Good only for white noise	Does not consider constrains
H infinity observer	linear	optimization	high	high	Only avoid worst scenario
MHE	nonlinear	optimization	high	high	Online running
Particle filter	nonlinear	Monto Carlo	high	high	Online running

From the investigation and comparison of different observer techniques, it is found that extended Kalman filter is the best compromise solution considering performance, model limitation, robustness and computational requirement. It will be introduced in the next section.

5.1.2 Extended Kalman filter

As introduced in previous section, Kalman filter, as an observer technique, is widely used in different applications. The basic principle of Kalman filter is explained as follows.

Given a discrete-time linear dynamic system with state space representation

$$x_k = Ax_{k-1} + Bu_{k-1} + w_{k-1} \tag{89}$$

$$y_k = Cx_k + Du_k + v_k \tag{90}$$

where w_k represents process noise accounting for the unmodeled dynamics and unknown disturbance, v_k represents measurement noise. They are assumed to be independent, with zero mean Gaussian probability distribution

$$p(w) \sim N(0, Q) \tag{91}$$

$$p(v) \sim N(0, R) \tag{92}$$

where Q matrices is the process noise covariance and R matrices is the measurement noise covariance.

Kalman filter is the optimal state observer for unconstrained linear system by producing the optimal estimation with noisy measurements and inaccurate dynamic model. More details for Kalman filter derivation can be found in [94]. Here the Kalman filter algorithm can be simply explained as two steps: prediction and correction.

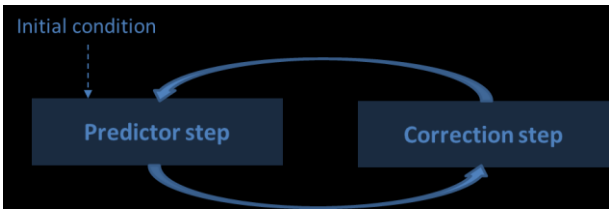

Figure 5.2 Kalman filter running cycle

At time step zero, an initial condition is defined as

$$\hat{x}_{0|-1} = x_0 \ ; \ \hat{P}_{0|-1} = P_0 \tag{93}$$

where $\hat{x}$ is estimate state, $\hat{P}$ is estimate error covariance. Then in prediction step, the state and error covariance is updated from time step k to step $k+1$

$$\hat{x}_{k+1|k} = A\hat{x}_k + bu_k \tag{94}$$

$$P_{k+1|k} = AP_{k|k}A^T + Q \tag{95}$$

where $\hat{x}_{k+1|k}$ is a priori estimate of x_{k+1}, $P_{k+1|k}$ is a priori estimate error covariance.

In correction step, the measurement residual is calculated by

$$\tilde{y}_k = \bar{y}_k + C\hat{x}_{k+1|k} \tag{96}$$

where $\bar{y}_k$ is the measurement. Then the Kalman gain is

$$K_k = P_{k|k-1}C^T\left(R_k + CP_{k|k-1}C_k^T\right)^{-1} \tag{97}$$

The state estimate and covariance estimate deduced in the prediction step is corrected by Kalman gain where an a posteriori state estimation in obtained in Equation (94) and an a posteriori error covariance estimation is obtained in Equation (95).

$$x_{k|k} = x_{k|k-1} + K_k\tilde{y}_k \tag{98}$$

$$P_{k|k} \ = (I - K_kC)P_{k|k-1} \tag{99}$$

Then it goes back to prediction step recursively. Due to its recursive property, it can run on-line efficiently using only current measurements and previously estimated state and uncertainty matrix.

Kalman filter works as an optimal estimation algorithm only for linear system models. However, almost all physical models in engine application are nonlinear models. Some adapted techniques have been made to apply Kalman filter to nonlinear system, such as extended Kalman filter and unscented Kalman filter. The extended Kalman filter is probably the most widely used estimation algorithm for nonlinear system[46,95,96].

Given a discrete-time nonlinear dynamics system with state space representation

$$x_k = f(x_{k-1}, u_{k-1}) + w_{k-1} \tag{100}$$

$$y_k = h(x_k, u_k) + v_k \tag{101}$$

where, w_k is process noise, v_k is measurement noise. These noises are independent, with zero mean Gaussian probability distribution. The extended Kalman filter has the same steps of Kalman filter. The mean propagation and measurement residual is obtained through the full nonlinear model

$$\hat{x}_{k+1|k} = f(x_k, u_k) \tag{102}$$

$$\tilde{y}_k = \bar{y}_k + h\left(\hat{x}_{k|k-1}, u_k\right) \tag{103}$$

But the covariance updates and Kalman gain are obtained through the linearized model

$$P_{k+1|k} = F_k P_{k|k} F_k^T + Q_k \tag{104}$$

$$K_k = P_{k|k-1} H^T \left(R_k + H P_{k|k-1} H\right)^{-1} \tag{105}$$

where the state transition and observation matrices F and H are calculated by Jacobian matrix

$$F_k = \left.\frac{\partial f}{\partial x}\right|_{\hat{x}_{k|k}, u_k} \tag{106}$$

$$H_k = \left.\frac{\partial h}{\partial x}\right|_{\hat{x}_{k|k-1}} \tag{107}$$

5.2 Cylinder Air Charge Estimation Design with Both MAF and MAP Sensors

Since volumetric efficiency for the speed-density approach is pre-calibrated, it is difficult to compensate for engine aging and it may contain error. This error can be accounted for as the variation of VE, and it is denoted as $\Delta\eta$. The speed-density equation can be rewritten as

$$\dot{m}_{cyl} = (\eta_{ss} + \Delta\eta)\frac{p_m N V_d}{120 R T_m} \tag{108}$$

where η_{ss} is pre-calibrated volumetric efficiency; $\Delta\eta$ is the variation of VE. Using observer based methods, the variation $\Delta\eta$ can be identified as a system state in real time by augmenting the system model. From Equation (5) and (7), the intake manifold dynamics can be derived as

$$\frac{d}{dt}p_m = \frac{RT_m}{V_m}\left[\dot{m}_{MAF} - (\eta_{ss} + \Delta\eta)\frac{p_m N V_d}{120 R T_m}\right] \tag{109}$$

or

$$\frac{d}{dt}p_m = f(p_m, \Delta\eta) \tag{110}$$

Considering slow variations of $\Delta\eta$, the system dynamics can be written in state space representation

$$\begin{cases} \dfrac{d}{dt}p_m = f(p_m, \Delta\eta) \\ \dfrac{d}{dt}\Delta\eta = 0 \\ y = p_m \end{cases} \tag{111}$$

The system described by equation (xx) has two states, p_m and $\Delta\eta$. While p_m is measured from the MAP sensor, $\Delta\eta$ cannot be measured directly and needs to be estimated. In order to implement the observer with digital processors, the continuous-time system is discretized as

$$\begin{cases} x_1(k+1) = f(x_1, x_2, \Delta t) + w_1 \\ x_2(k+1) = x_2(k) + w_2 \\ y(k) = x_1(k) + v \end{cases} \tag{112}$$

where x_1 is the engine intake manifold pressure; x_2 is the variation of volumetric efficiency; $y(k)$ is the MAP sensor measurement; Δt is sampling time of the discretization; $w = [w_1, w_2]^T$ is the process noise, $w \sim N[0, Q]$; v is the measurement noise, $v \sim N[0, R]$.

The EKF algorithm is initiated with Equations (12) and (13), using given initial values of the system states $\hat{x}(0|0)$ and error covariance matrix $P(0|0)$

$$\hat{x}(k+1|k) = f(\hat{x}(k|k)) \tag{113}$$

$$P(k+1|k) = F(k)P(k|k)F^T(k) + Q(k) \tag{114}$$

where $\hat{x}(k+1|k)$ are estimated engine states with knowledge of the previous step; $P(k+1|k)$ is estimated error covariance with knowledge of the previous step; $F(k)$ is

the state transition matrix based on the Jacobian matrix and $Q(k)$ is the error covariance of process noise.

The state transition matrix $F(k)$ is calculated at each step using the following Jacobian matrix

$$F(k) = \frac{\partial f(k)}{\partial x}|_{x=\hat{x}(k|k)} \tag{115}$$

$$F(k) = \begin{bmatrix} -\frac{V_d N \eta_{ss}}{120 V_m \tau} - \frac{x_2(k) V_d N}{120 V_m \tau} + 1 & -\frac{x_1(k) V_d N}{120 V_m \tau} \\ 0 & 1 \end{bmatrix} \tag{116}$$

After predicting system states and error covariance through Equations (12) and (13), the Kalman gain, error covariance estimate, and state estimate are updated

$$\tilde{y}(k) = y(k) - \hat{x}_1(k|k-1) \tag{117}$$

$$K(k) = P(k|k-1)C^T\left(R(k) + CP(k|k-1)H^T(k)\right)^{-1} \tag{118}$$

$$P(k|k) = (I - K(k)C)P(k|k-1) \tag{119}$$

$$x(k|k) = x(k|k-1) + K(k)\tilde{y}(k) \tag{120}$$

where, $\tilde{y}(k)$ is the measurement residual, $K(k)$ is the optimal Kalman gain, $P(k|k)$ is the updated error covariance estimate, $x(k|k)$ is the updated estimation of states and $R(k)$ is the error covariance of measurement noise.

Finally the cylinder air charge is calculated by

$$\widehat{m}_{cyl}(k) = \hat{x}_1(k)[\eta_{ss} + \hat{x}_2(k)]\frac{NV_d}{120RT_m} \tag{121}$$

where $\hat{x}_1$ and $\hat{x}_2$ are estimated system states from the EKF algorithm.

The EKF method previously discussed requires a calibrated VE table. To eliminate the calibration of VE, an integration-based method is designed. First, the manifold pressure is estimated based on the isothermal manifold model

$$\hat{p}_m(t) = \frac{RT_m}{V_m}\int \left(\dot{m}_{MAF}(\tau) - \hat{\dot{m}}_{cyl}(\tau)\right)d\tau \tag{122}$$

where, $\hat{\dot{m}}_{cyl}$ is the estimated cylinder air charge estmation from the previous time step.

Then, the pressure estimation error is

$$e(t) = \hat{p}_m(t) - \bar{p}_m(t) \tag{123}$$

where $\hat{p}_m$ is the estimated manifold pressure from equation (21) and $\bar{p}_m$ is the measured manifold pressure from the MAP sensor.

Finally, cylinder air charge is estimated by

$$\hat{\dot{m}}_{cyl}(t) = K_P \cdot e(t) + K_I \int e(\tau)d\tau \tag{124}$$

where K_P is the proportional gain and K_I is the integral gain of the PI controller. The algorithm for the integration-based method is shown in Figure 5.3.

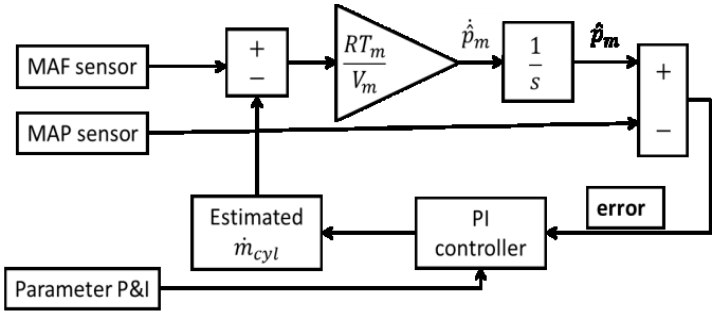

Figure 5.3 Calculation flow for the integration-based air flow estimation method

This integration-based method can estimate cylinder air charge without a calibrated VE, but sensor noise affects the estimation result. To avoid the need for VE

calibration and performance degradation caused by sensor noise, a Kalman filter based method is also derived. After proper system model design, the air path dynamics can be written as

$$\begin{cases} \dot{p}_m(k+1) = \dfrac{RT_m}{V_m}\left(\dot{m}_{MAF} - \dot{m}_{cyl}\right) + w_1 \\ p_m(k+1) = \Delta t \cdot \dot{p}_m(k) + p_m(k) + w_2 \\ \dot{m}_{MAF}(k+1) = \dot{m}_{MAF}(k) + w_3 \\ \dot{m}_{cyl}(k+1) = \dot{m}_{cyl}(k) + w_4 \end{cases} \tag{125}$$

Since $\frac{RT_m}{V_m}$ changes slowly compared with the engine air path dynamics, the system can be assumed to be linear time-invariant. Thus the model can be represented in a more compact linear state-space form

$$x(k+1) = Ax(k) + w \tag{126}$$

$$y(k) = Cx(k) + v \tag{127}$$

where $w = [w_1, w_2, w_3, w_4]^T$ is the process noise, $w \sim N[0, Q]$; v is the measurement noise, $v \sim N[0, R]$. The system states, x, and matrices A and C are

$$x = [\dot{p}_m \quad p_m \quad \dot{m}_{MAF} \quad \dot{m}_{cyl}]^T \tag{128}$$

$$A = \begin{bmatrix} 0 & 0 & \dfrac{RT_m}{V_m} & -\dfrac{RT_m}{V_m} \\ \Delta t & 1 & 0 & 0 \\ 0 & 0 & 1 & 0 \\ 0 & 0 & 0 & 1 \end{bmatrix} \tag{129}$$

$$C = \begin{bmatrix} 0 & 1 & 0 & 0 \\ 0 & 0 & 1 & 0 \end{bmatrix} \tag{130}$$

The observability matrix, o, of this system is

$$o = [C \quad CA \quad CA^2 \quad CA^3]^T \tag{131}$$

The rank of the observability matrix is four, which is equal to the number of system states. Therefore, this system is observable. The Kalman filter can be applied to estimate the system states. Formulation and execution of the KF is similar to the EKF methods previously discussed. The most important difference is replacement of the Jacobian matrix, F, with the state transition matrix A. Finally, cylinder air charge is estimated by

$$\hat{m}_{cyl}(k) = [0 \quad 0 \quad 1 \quad 0]\hat{x}(k) \tag{132}$$

5.3 Experimental Validation for Cylinder Air Charge Estimation

Stability and convergence of the proposed cylinder air charge estimation are validated through dynamometer test over a wide range of engine operating conditions (Table 5.2).

Table 5.2 Engine operating conditions

Engine Speed	1500RPM – 4000 RPM
Engine Load (p_m)	0.3bar -0.8 bar
Valve Timing	Controlled by stock ECU

To verify real-time performance of the proposed estimation algorithms, a throttle tip-in condition is used for demonstration. Figure 5.4 shows the engine operating conditions for this test. During the throttle tip-in period, engine speed is held at ~1500 RPM by the engine dynamometer. Intake manifold pressure increases gradually during

this process due to manifold filling and emptying dynamics. The intake camshaft position, ICL, and exhaust camshaft position, ECL, are controlled according to the stock calibration.

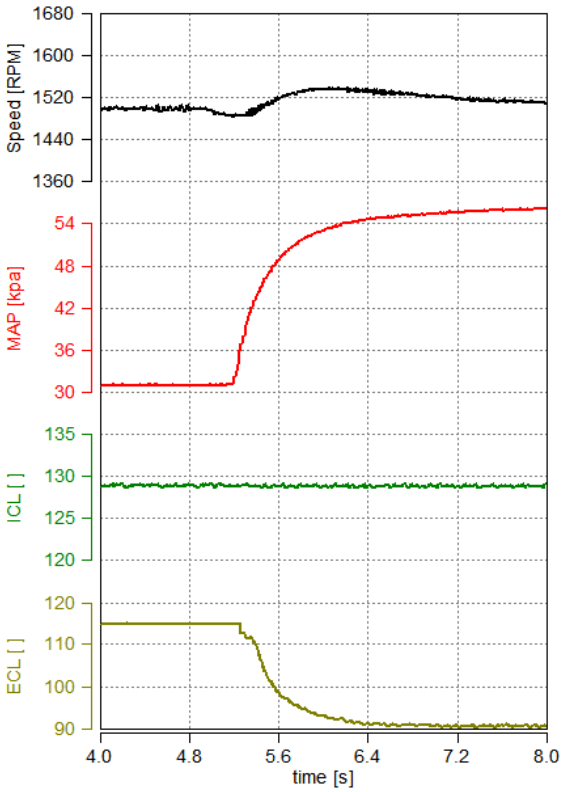

Figure 5.4 Engine operating conditions for algorithm performance 'tip-in' test

Figure 5.5 shows the experimental results of the proposed EKF method (Equation 20), compared with the MAF sensor reading and the speed-density approach. At steady-state conditions, the MAF sensor reading should be the same as the cylinder air mass charge. The speed density approach has steady state error due to the VE calibration error. It can also be observed from Figure 5.5 that the cylinder air charge flow has significant delay from the MAF sensor output during the tip in process because of manifold filling

and emptying dynamics. The proposed EKF method, utilizing both MAP and MAF sensors, can estimate cylinder air charge with more accuracy than both the MAF sensor or speed density approach individually. The EKF captures manifold filling and emptying dynamics during transient situations while preserving the steady state accuracy of the MAF sensor with less noise power. In the meantime, the variation of VE is also estimated by the EKF, the estimation results are shown in Figure 5.6.

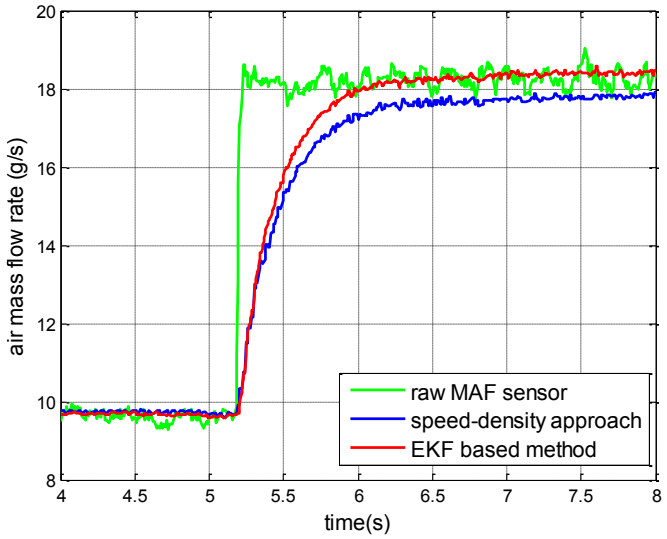

Figure 5.5 Experimental results of the EKF based estimation method

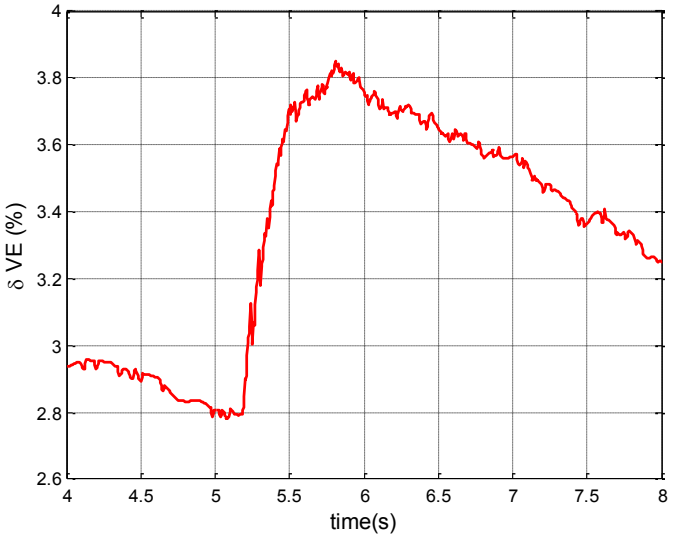

Figure 5.6 Variation in VE estimation from the EKF based method

Figure 5.7 shows experimental results for the KF based method (Equation 31) compared with the raw MAF sensor signal and speed-density approach. Similar to the EKF based method, the KF generates close to MAF sensor steady state results with less noise. During transient operating conditions, the KF results are closer to the speed-density approach.

The two proposed methods are further evaluated with a continuous tip-in and tip-out operating condition test. In this test, these two approaches are also compared with other engine air charge estimation algorithms.

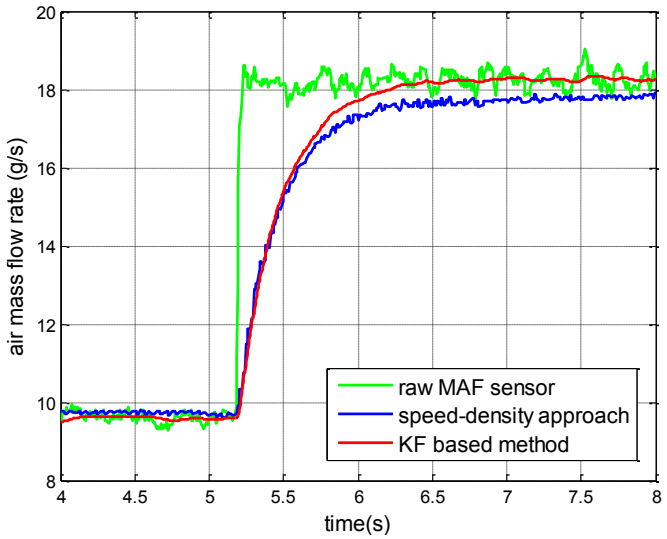

Figure 5.7 Experimental results of the KF based estimation method

The high gain input observer proposed by *Stotsky et al.* [17] is used for benchmarking the proposed EKF based method. This method was unmodified from its original form, details can be found in [12,17]. Both algorithms use volumetric efficiency as a model input and estimate the variation of VE in real time. The integration method is chosen to compare with the KF based method since both algorithms eliminate VE calibration.

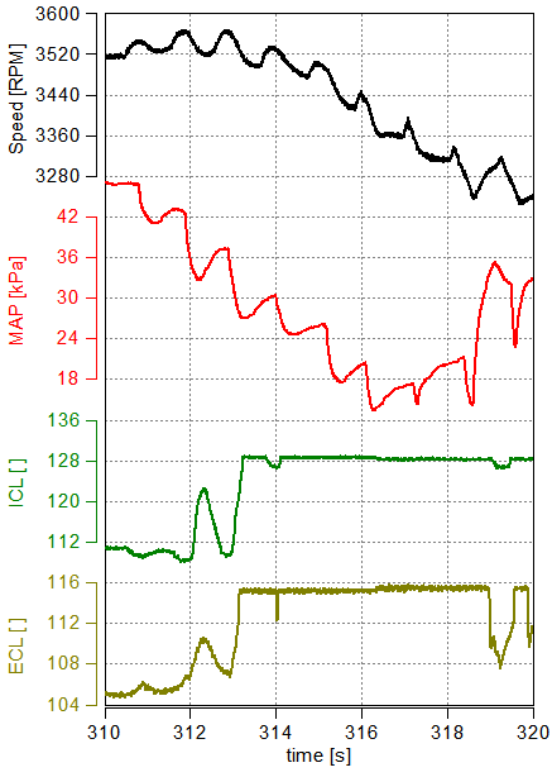

Figure 5.8 Transient engine operating conditions used for method comparison

The proposed EKF and KF methods, together with the high gain input observer and integration methods, are compared over the transient cycle in Figure 5.8. Estimation results for all algorithms are shown in Figure 5.9 and Figure 5.10 where INTE, HGIO, EKF w/ VE and KF w/o VE are the integration method (Equation 23), high gain input observer, proposed EKF method (Equation 20), and KF method (Equation 31) respectively. The reference signal in these figures is from the stock engine calibration. Figure 5.11 shows the errors of these four estimation approaches against the reference signal. In general, the proposed approaches track the reference closely through the test, with noticeable improvement over the high gain observer and integration methods. The

increased estimation error after 316 seconds is caused by inaccurate MAF sensor calibration at low engine MAP.

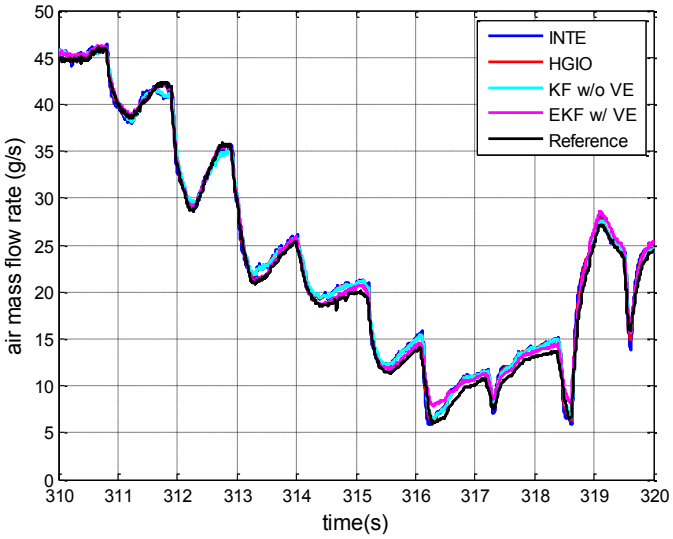

Figure 5.9 Comparison of the proposed estimation algorithms and other methods (in time domain)

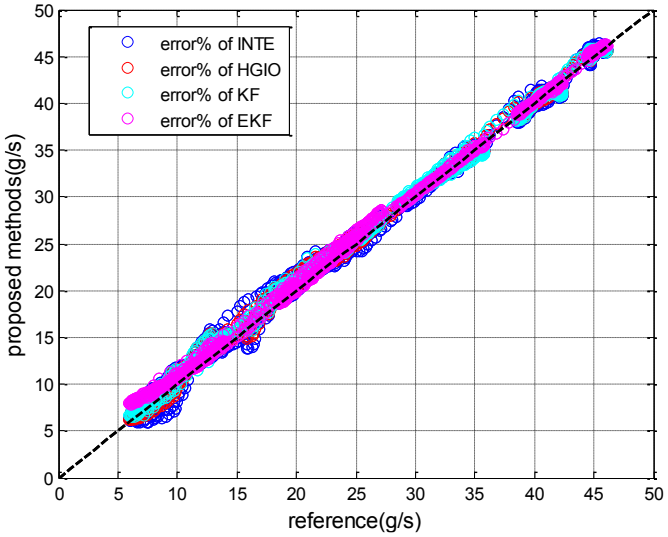

Figure 5.10 Error comparison of the proposed estimation algorithms

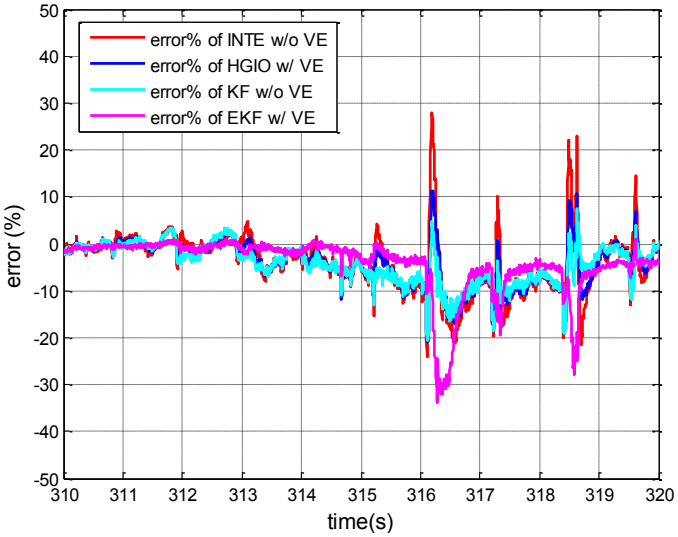

Figure 5.11 Error% of all proposed estimation methods

Table 5.3 RSMEs of different estimation algorithms

Method	**RSME**
Integration + PI controller	0.9988
High gain input observer	0.8843
Kalman Filter	0.8621
Extended Kalman Filter	0.7322

The root mean squared errors (RSME) for each algorithm are listed in Table 5.3. RSME values of the integration and high gain input observer methods are larger compared with the EKF and KF based methods. The reason of this performance difference is that they cannot filter out MAF sensor noise at steady-state conditions. The high gain input observer has better performance than the integration based method due to the use of calibrated VE. The EKF based method demonstrates the lowest RSME for

cylinder air charge estimation because it uses calibrated VE as a model input. Furthermore, it can filter out sensor noise.

The KF based method is not as good as the EKF based method, but it still outperforms the integration and high gain input observer methods. More importantly, the fact that it does not use VE as a model input significantly reduces calibration effort, possibly making it favorable during early engine development.

5.4 Conclusions

The aim of this chapter is to take advantage of both MAF and MAP sensors for cylinder air charge estimation. Several observer based cylinder air charge estimation methods are proposed utilizing both sensors. The first method is based on extended Kalman filter and needs calibrated volumetric efficiency as a model input. This algorithm can help to correct calibrated volumetric efficiency on-line with system dynamics and sensor feedback while estimating cylinder air charge. An integration method is also proposed with the intent of eliminating volumetric efficiency, but performance is limited because of sensor noise. To overcome sensor noise issues, a Kalman filter based method is proposed which also eliminates volumetric efficiency after proper model design and parameter tuning. These algorithms are compared using transient tests with a rapid-prototype engine controller in an engine dynamometer cell. The results show EKF and KF based methods have better performance during steady and transient operating conditions as compared with a high gain input observer and the integration based method.

CHAPTER SIX

6. CYLINDER CHARGE ESTIMATION WITH DISTURBANCE OBSERVER

In Chapter 5, cylinder air charge flow rate is estimated based on both MAF and MAP sensors. However, the cylinder fuel charge flow rate and EGR charge flow rate are not yet evaluated in the estimation problem. In this chapter, the cylinder air charge, fuel charge and EGR charge are all considered with the exhaust lambda sensor involved. The objective is to develop an observer based cylinder charge estimation algorithm that can identify and reject disturbances caused by input modeling error. In section 6.1, as the inputs of the gas path model come from three upstream models (the throttle flow model, the EGR valve flow model and fuel injection flow model) and these input models drift due to a lot of reasons such as engine aging, inaccurate calibration and low pressure differential across the valve, the performance of the traditional observer methods will be compromised accordingly. Therefore, an EKF based disturbance observer algorithm for cylinder charge estimation is developed to overcome this issue. The experimental validation results of the developed estimation algorithm are shown in section 6.2.

6.1 Disturbance Observer based Cylinder Charge Estimation Design

To estimate not only the cylinder air charge but also cylinder EGR charge and cylinder fuel charge, the fuel and EGR dynamics need to be considered. Therefore, the dynamic model deduced in chapter 4 is used for cylinder charge estimation. Besides the MAF sensor and MAP sensor, the exhaust lambda sensor is also used for this cylinder

charge estimation work. The structure of the proposed observer based cylinder charge estimation is shown in Figure 6.1.

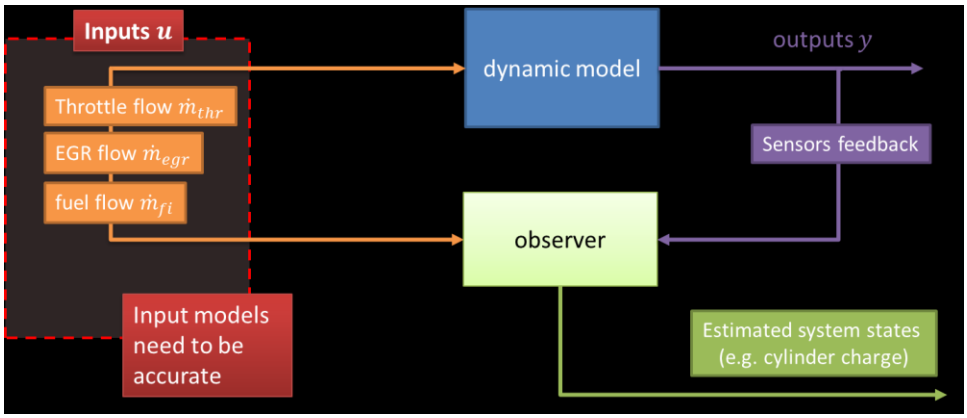

Figure 6.1 observer based cylinder charge estimation structure

With $\boldsymbol{x}$ as the system states, the dynamic model derived in chapter 4 can be represented as

$$\dot{x}_1 = k_1(u_1 + u_2 - x_1) \tag{133}$$

$$\dot{x}_2 = \frac{k_1}{x_1}[u_2 - x_2(u_1 + u_2)] \tag{134}$$

$$\dot{x}_3 = -\frac{1}{\tau_f}x_3 + X_f u_3 \tag{135}$$

$$\dot{x}_4 = -\frac{6}{\tau_\lambda}x_4 - \frac{12}{\tau_\lambda^2}x_5 + \frac{1}{\sigma_o}\cdot\frac{x_1(1-x_2)}{(1-X_f)u_3 + \frac{1}{\tau_f}x_3} \tag{136}$$

$$\dot{x}_5 = x_4 \tag{137}$$

$$\dot{x}_6 = -\frac{1}{\tau_{MAF}}x_6 + \frac{1}{\tau_{MAF}}u_1 \tag{138}$$

where x_1 is the cylinder air and EGR charge $\dot{m}_{cyl}$, x_2 is the EGR concentration in intake manifold F_{egr}, x_3 is the fuel puddle mass m_{fp}, x_4 and x_5 are states for Padé approximation, x_6 is MAF sensor measurement $\dot{m}_{MAF}$. The inputs u_1, u_2, and u_3 are the throttle flow $\dot{m}_{thr}$, the EGR flow $\dot{m}_{egr}$, and the fuel injection flow $\dot{m}_{fi}$ respectively. These inputs are modeled in section 4.2. The parameters τ_f and X_f are fuel model parameters and calculated by the proposed semi-physics fuel puddle model. Parameter τ_λ is lambda delay time and calculated by the proposed transport delay model. Parameter σ_o is the stoichiometric AFR. And τ_{MAF} is the 1st order delay time for MAF sensor. The parameter k_1 can be expressed as

$$k_1 = \frac{NV_d\eta_{VE}}{120V_{im}} \tag{139}$$

The measurements used of the entire dynamic systems are the sensing values from the MAP sensor, the MAF sensor and the exhaust lambda sensor. In the dynamic system, these three variables are treated as outputs, calculated from system states $\boldsymbol{x}$ and inputs $\boldsymbol{u}$, and then compared with the real sensor signals to feed the error to the observer. The system outputs are expressed as

$$y_1 = \frac{1}{k_1}\frac{RT_{im}}{V_{im}}x_1 \tag{140}$$

$$y_2 = -\frac{12}{\tau_\lambda}x_4 + \frac{1}{\sigma_o}\cdot\frac{x_1(1-x_2)}{(1-X_f)u_3 + \frac{1}{\tau_f}x_3} \tag{141}$$

$$y_3 = x_6 \tag{142}$$

where, y_1 is the modeled MAP sensor output, y_2 is the modeled exhaust lambda sensor output, and y_3 is the modeled MAF sensor output.

However, from a lot of experimental tests, it is found that the input models are inaccurate. It is introduced earlier that the inputs of system dynamic models are the throttle flow, the EGR valve flow and the fuel injection flow. The throttle flow and EGR valve flow can be calculated by isentropic orifice model. However, the orifice model needs more accurately calibrated parameter C_d to achieve acceptable performance. The calibrated parameter will also change along with engine aging. Furthermore, the ambient pressure as upstream pressure of throttle and the exhaust manifold pressure as upstream pressure of EGR valve are always modeled with calibration tables. These calibrations, if with deficiency, will also lead to estimation performance deterioration of orifice model based flow. Also, the isentropic orifice model only works when the pressure differential across throttle or EGR valve is large enough. Thus, when engine is running at wide open throttle(WOT) condition, the throttle flow model and EGR valve flow model all fail. The throttle flow model is taken as an example in Figure 6.2 where “thr ais flow” (blue line) is throttle orifice model using OEM calibrated parameter, “MAF” (red line) is the well-calibrated MAF sensor measurement, “modeled thr flow” (yellow line) is throttle orifice model using re-calibrated parameter, and “total air port mass flow” is OEM calibrated cylinder air charge flow.

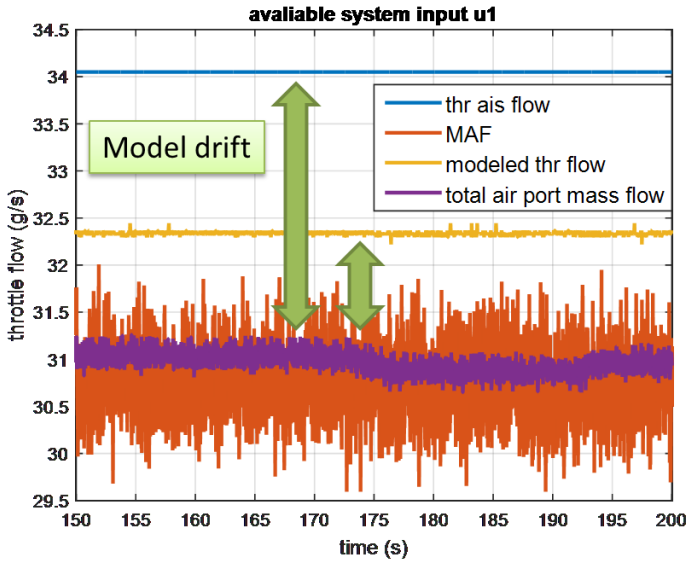

Figure 6.2 Input model drift

From Figure 6.2 it is found that the orifice model based throttle flow estimation is not as accurate as expected. Even after re-calibration of the parameter C_d, the performance of orifice model will deteriorate over time. Same issue happens for EGR flow estimation since it is also based on orifice model. For fuel injection flow, as described in Chapter 4, it is calibrated as function of engine speed and fuel injector pulse width without considering other factor which may influence fuel injection amount such as coolant temperature and battery voltage. So, the fuel injection flow estimation might also be inaccurate. In conclusion, all these models as inputs to observer based estimation algorithm in this section might not be accurate enough and may drift over time and lead to the failure of the observer based cylinder charge estimation algorithm. Due to the issue with the input models, the observer based estimation algorithm cannot work. Thus, a EKF based disturbance observer is proposed here to address this concern.

Disturbance observer is an estimation tool to compensate disturbances. It can estimate unknown disturbances in addition to system states. This concept has been introduced, analyzed and used in different applications[100–102]. In section 6.1 it is found that the input models of the proposed KEF based cylinder charge estimation algorithm are not accurate. Thus, for the system

$$\dot{x} = Ax + Bu \tag{143}$$

$$y = Cx + Du \tag{144}$$

it can be assumed that the disturbances are on inputs as

$$\dot{x} = Ax + B(u + \delta u) \tag{145}$$

$$y = Cx + D(u + \delta u) \tag{146}$$

where δu represents the disturbance to the input u. The disturbance δu can be treated as system state, then the new augmented system is

$$\begin{bmatrix} \dot{x} \\ \dot{\delta u} \end{bmatrix} = \begin{bmatrix} A & B \\ 0 & 0 \end{bmatrix} \cdot \begin{bmatrix} x \\ \delta u \end{bmatrix} + \begin{bmatrix} B \\ 0 \end{bmatrix} \cdot u + \begin{bmatrix} w_x \\ w_{\delta u} \end{bmatrix} \tag{147}$$

$$y = \begin{bmatrix} C & D \end{bmatrix} \cdot \begin{bmatrix} x \\ \delta u \end{bmatrix} + Du + \begin{bmatrix} v_x \\ v_{\delta u} \end{bmatrix} \tag{148}$$

If the augmented system is observable, the system states which include the disturbance can be estimated by an appropriately designed observer. The observability can be checked by the observability matrix

$$O = \begin{matrix} C_{aug} \\ A_{aug}C_{aug} \\ \vdots \\ \left[A_{aug}^{n-1}C_{aug}\right] \end{matrix} \tag{149}$$

where A_{aug} and C_{aug} are from the augmented system

$$A_{aug} = \begin{bmatrix} A & B \\ 0 & 0 \end{bmatrix} \tag{150}$$

$$C_{aug} = [C \quad D] \tag{151}$$

For the studied system, the distances are added to the three input models and treated as the additional system states

$$\delta u_1 = x_7 \tag{152}$$

$$\delta u_2 = x_8 \tag{153}$$

$$\delta u_3 = x_9 \tag{154}$$

where δu_1 represents the disturbance from the throttle flow model, δu_2 represents the disturbance from the EGR flow model, and δu_3 represents the disturbance of the fuel injection flow model. After discretization, the complete system dynamic model with disturbances is

$$x_1(k+1) = x_1(k) + \delta t \cdot k_1[u_1(k) + u_2(k) - x_1(k)] \tag{155}$$

$$x_2(k+1) = x_2(k) + \delta t \cdot \frac{k_1}{x_1(k)}\{u_2(k) - x_2(k)[u_1(k) + u_2(k)]\} \tag{156}$$

$$x_3(k+1) = \left[1 - \frac{\delta t}{\tau_f}\right] x_3(k) + \delta t \cdot X_f u_3(k) \tag{157}$$

$$x_4(k+1) = \left[1 - \delta t \cdot \frac{6}{\tau_\lambda}\right] x_4(k) - \delta t \cdot \frac{12}{\tau_\lambda^2} x_5(k) + \delta t \cdot \frac{1}{\sigma_o} \cdot \frac{x_1(k)[1 - x_2(k)]}{[1 - X_f] u_3(k) + \frac{1}{\tau_f} x_3(k)} \tag{158}$$

$$x_5(k+1) = x_5(k) + \delta t \cdot x_4(k) \tag{159}$$

$$x_6(k+1) = \left(1 - \frac{\delta t}{\tau_{MAF}}\right) x_6(k) + \frac{\delta t}{\tau_{MAF}} u_1(k) \tag{160}$$

$$x_7(k+1) = x_7(k) \tag{161}$$

$$x_8(k+1) = x_8(k) \tag{162}$$

$$x_9(k+1) = x_9(k) \tag{163}$$

where x_7, x_8, x_9 are the added disturbance states. The system outputs are

$$y_1 = \frac{1}{k_1} \frac{RT_{im}}{V_{im}} \left(x_1(k) + x_7(k)\right) \tag{164}$$

$$y_2(k) = -\frac{12}{\tau_\lambda} x_4(k) + \frac{1}{\sigma_o} \cdot \frac{\left(x_1(k) + x_7(k)\right)[1 - x_2(k) - x_8(k)]}{[1 - X_f] u_3(k) + \frac{1}{\tau_f}\left(x_3(k) + x_9(k)\right)} \tag{165}$$

$$y_3(k) = x_6(k) \tag{166}$$

One of the most important prerequisites for observer based estimator design is the observability of the objective system. There are different ways to deal with observability check for nonlinear systems [97–99]. For the case of this research work, the observability is checked through the observability matrix of the linearized system dynamic equations

across the full range of engine operating condition. The observability matrix is calculated as

$$O = \begin{bmatrix} C \\ AC \\ \vdots \\ A^{n-1}C \end{bmatrix} \tag{167}$$

where A and C are system Jacobian matrix after linearization at each engine operating points, which are properly discretized in a certain interval. Using such method, it has been verified that the objective system is observable within the whole engine operating range. Though lack of rigor of grounded theory and thus without 100% guarantee towards the system observability, the proposed observability verification method can be applied to this application with reasonable density of discretization. The observability of this methods has also been experimentally verified under examined operational conditions.

Another important prerequisite for observer based estimation is to make sure that the assumptions made to build the system dynamic model and estimation algorithm are all within reasonable range. For general EKF algorithm, the estimation will only work when the process noise and sensor noise are both zero-mean Gaussian-distributed white noise. For the studied system, the sensor signal histograms for the three measurements are shown in Figure 6.3, Figure 6.4 and Figure 6.5. The test is conducted with no disturbance to the sensor, the output of which should be constant/offset added with sensor noise.

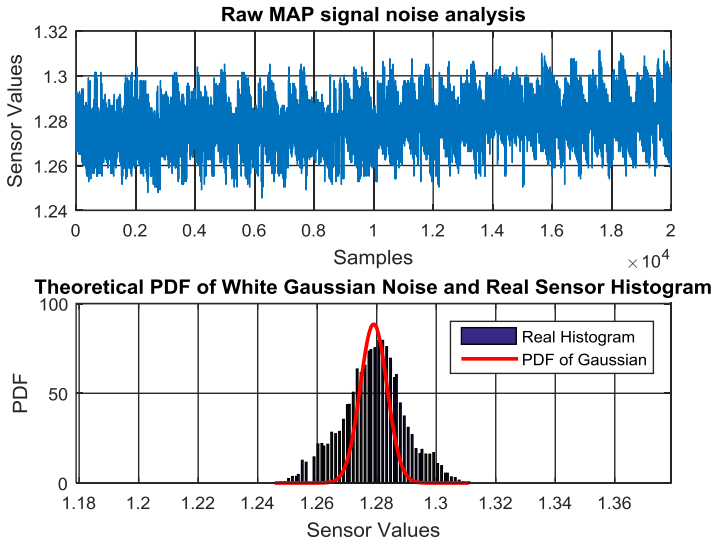

Figure 6.3 MAP sensor signal histogram

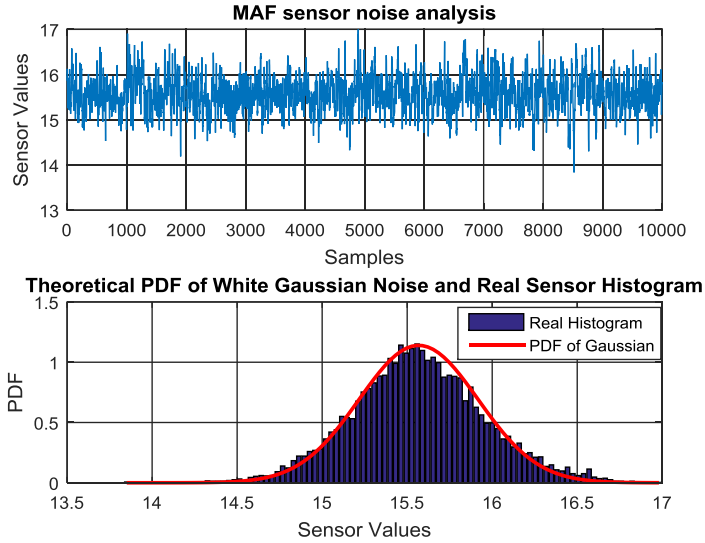

Figure 6.4 MAF sensor signal histogram

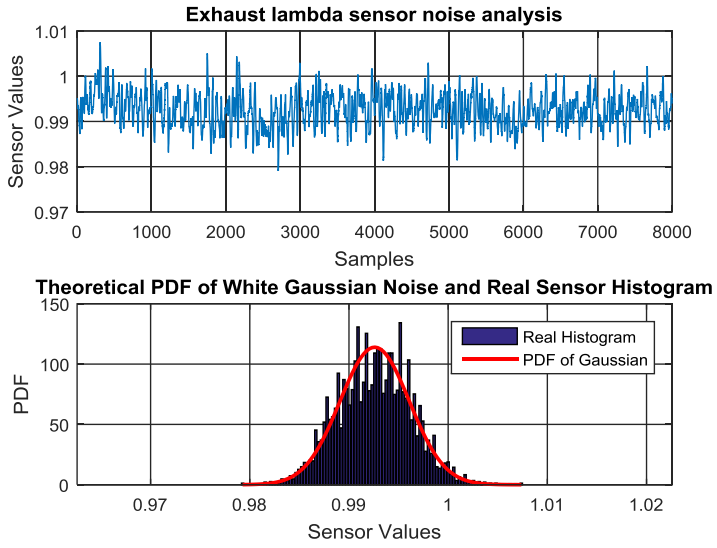

Figure 6.5 Exhaust lambda sensor signal histogram

It cannot be concluded from Figure 6.3, Figure 6.4 and Figure 6.5 that these sensors exhibit pure white noises without thoroughly analysis such as power spectral density analysis and sensor behavior at different engine operating condition. Also, it still inconclusive if the process noise is zero-mean white noise. However, to facilitate the estimation work, it is acceptable to assume that the sensors exhibit characteristics of white noise as the profile of the test data histograms can roughly follow the probability density function (PDF) of Gaussian noise.

6.2 Experimental Validation for Cylinder Charge Estimation

To verify the feasibility of the proposed disturbance observer, an experimental test is designed (Figure 6.6). In this experiment, the pseudo inputs with designed disturbance are fed into disturbance observer artificially. The errors will be induced to

different pseudo inputs at different time to verify if the disturbance observer can reject the artificially added error from input models.

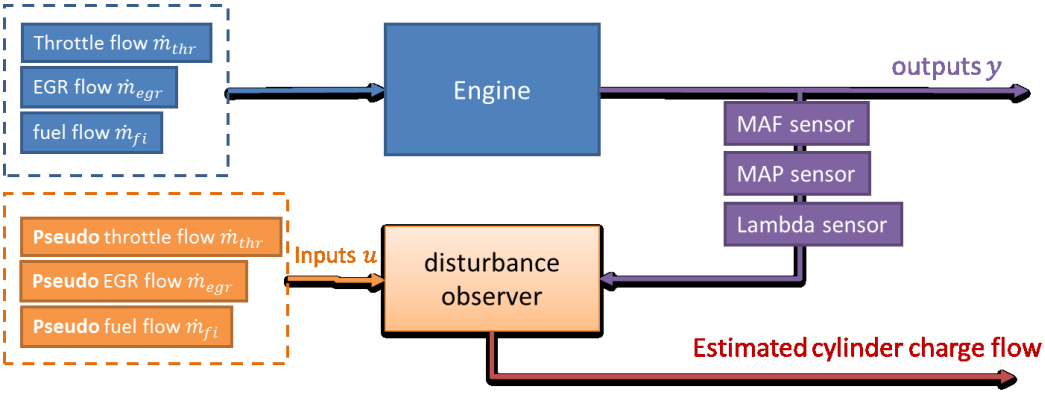

Figure 6.6 Experimental design with pseudo inputs

Three tests are performed in this experiment as explained in Table 6.1. In test scenario 1, the error is induced on throttle flow model without telling the disturbance observer. The objective is to verify if the developed algorithm can reject air flow error. In test scenario 2, the error is induced on throttle flow model first. Then error is added on fuel injection flow model without telling the disturbance observer either. The objective is to verify if the developed algorithm can reject not only air flow error but also fuel flow error. In test scenario 3, all three input models are designed to be added with errors at different time to verify if the developed algorithm works when all input models are biased. The engine operating condition for scenario 1, 2 and 3 is shown in Figure 6.7 where all engine actuators are kept constant. The fuel injection flow is controlled by the OEM's stock AFR controller during the time range from 65 second to 95 second.

Table 6.1 Experiment test scenario 1 to 4

Test Number	Operating condition
Scenario 1	Induce air flow error without telling EKF
Scenario 2	Induce air error, then add fuel error without telling EKF
Scenario 3	Induce air error, then add fuel error, and finally add EGR error without telling EKF
Scenario 4	Induce air error, fuel error, and EGR error at the same time without telling EKF

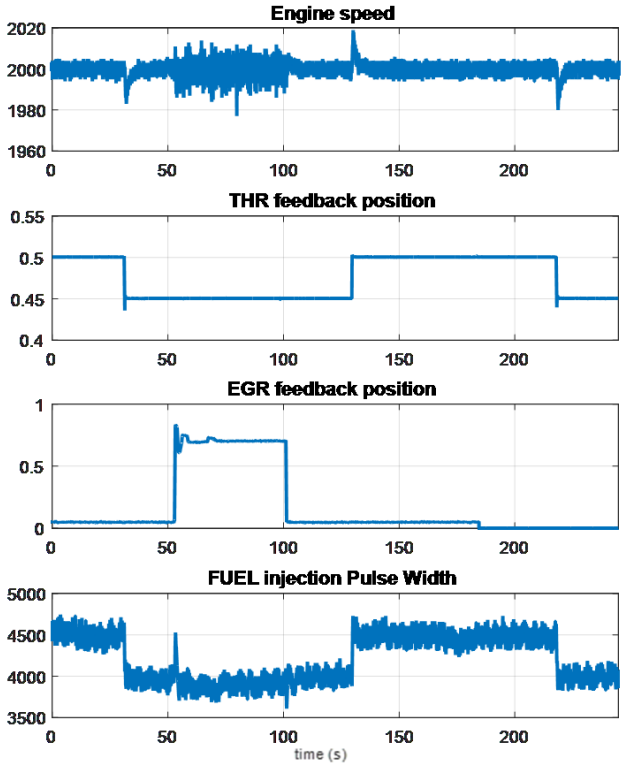

Figure 6.7 Engine operating condition for experiment test 1 to 4

For the test scenario 1, 5g/s error is induced on throttle flow model starting from 80 second with no error induced on EGR flow model and fuel injection flow model (Figure 6.8). The experimental results of air flow, EGR flow, and exhaust lambda estimation are shown in Figure 6.9, Figure 6.10 and Figure 6.11 respectively.

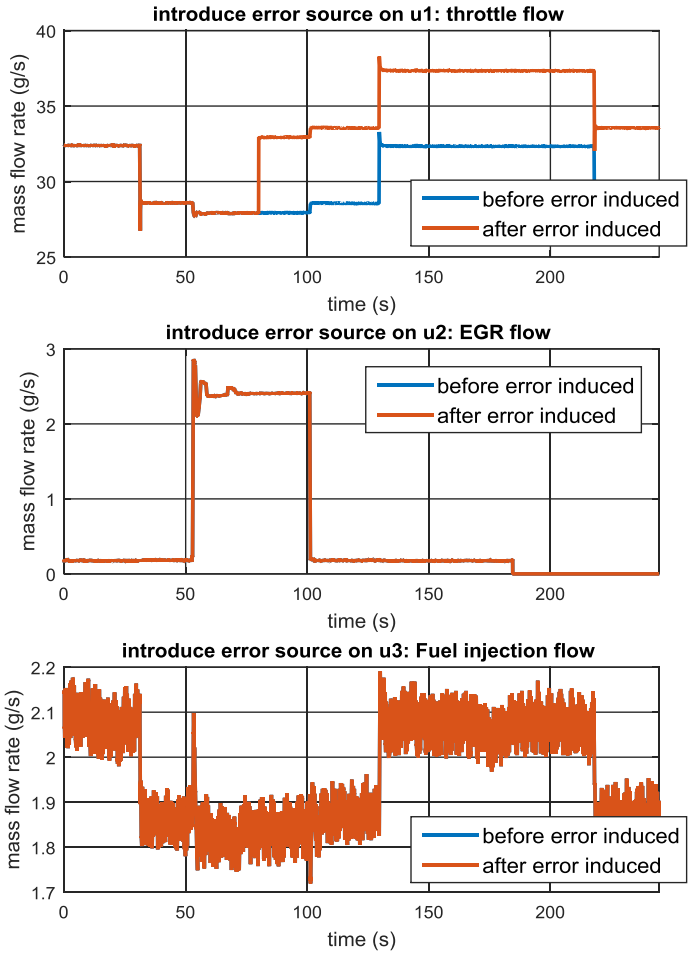

Figure 6.8 Pseudo inputs for scenario 1

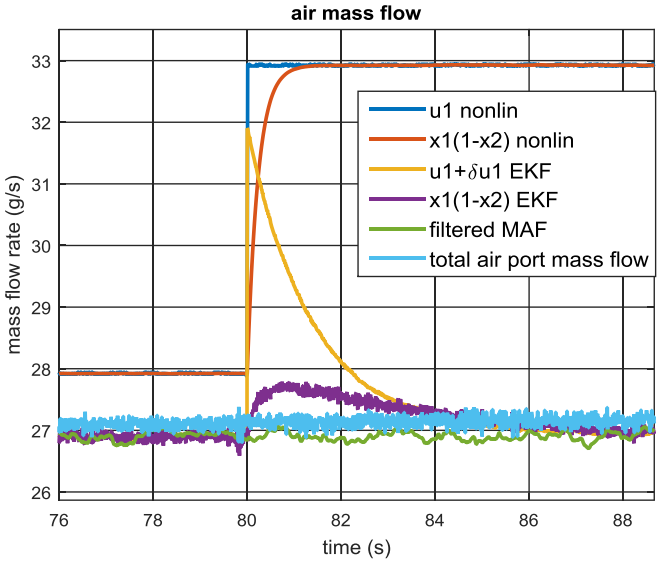

Figure 6.9 Air mass flow estimation for scenario 1 (zoom in)

In Figure 6.9, the air flow estimation results of test scenario 1 is presented. In this figure, the blue line is the modeled throttle flow, the red line is the modeled cylinder air charge flow. The yellow line is the estimated throttle flow from the developed disturbance observer based estimation algorithm. The purple line is the estimated cylinder air charge flow from the developed disturbance observer based estimation algorithm. The green line is the filtered MAF sensor measurement. The cyan line is OEM calibrated cylinder air charge flow. It is observed that when error is induced on throttle flow model starting from 80 second, the flow calculation is following the wrong throttle flow model. Thus, the cylinder air charge estimation is also inaccurate due to the faulty throttle flow input. After a few sampling cycles, the developed disturbance observer based estimation algorithm starts to sense that the throttle flow model is inaccurate, and gradually correct the inaccurate throttle flow estimation. Finally the throttle flow estimation is able to converge to the same value as that of the MAF sensor which is assumed to be the

reference (green line). Because at engine steady state operating condition the MAF sensor value is equal to the cylinder air charge, the cylinder air charge estimation (purple line) is also driven by disturbance observer to the value of the MAF sensor signal. The small difference between the filtered MAF sensor and the OEM calibrated cylinder air charge flow at steady state operating condition might be caused by the inaccurate calibration.

In Figure 6.10, the EGR flow estimation results of test scenario 1 are shown. In this figure, it is observed that when engine is running with no actuator and environmental change the estimated EGR flow and cylinder EGR charge flow drop incorrectly when error is induced on throttle flow model. Then these estimations can be rectified by the developed disturbance observer based estimation algorithm. Same results are shown in Figure 6.11,where the estimated exhaust lambda (yellow line) is following the lambda sensor measurement (green line) even when the modeled exhaust lambda value (red line) gets disrupted due to the induced error on throttle flow model.

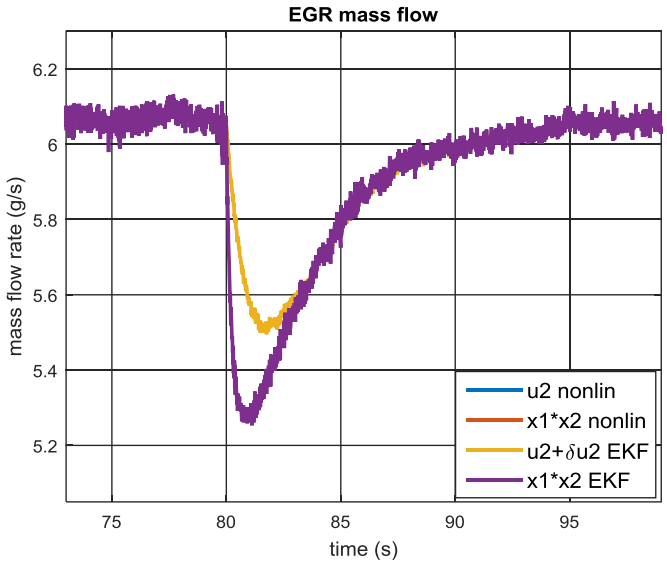

Figure 6.10 EGR mass flow estimation for scenario 1 (zoom in)

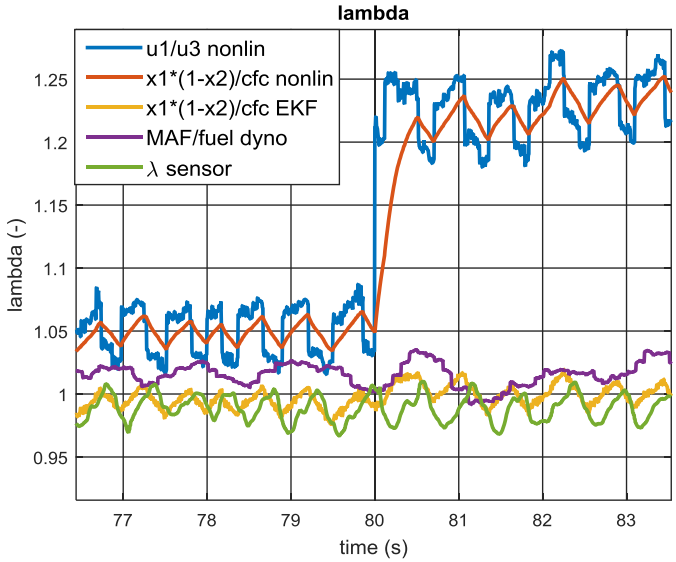

Figure 6.11 Exhaust lambda estimation for scenario 1 (zoom in)

For the test scenario 2, 5g/s error is induced on throttle flow model starting from 80 second and then 0.5g/s error is induced on fuel flow model starting from 85 second with no error induced on EGR flow model (Figure 6.12). The experimental results of air flow, EGR flow, fuel flow and exhaust lambda estimation are shown in Figure 6.13, Figure 6.14, Figure 6.15, and Figure 6.16 respectively.

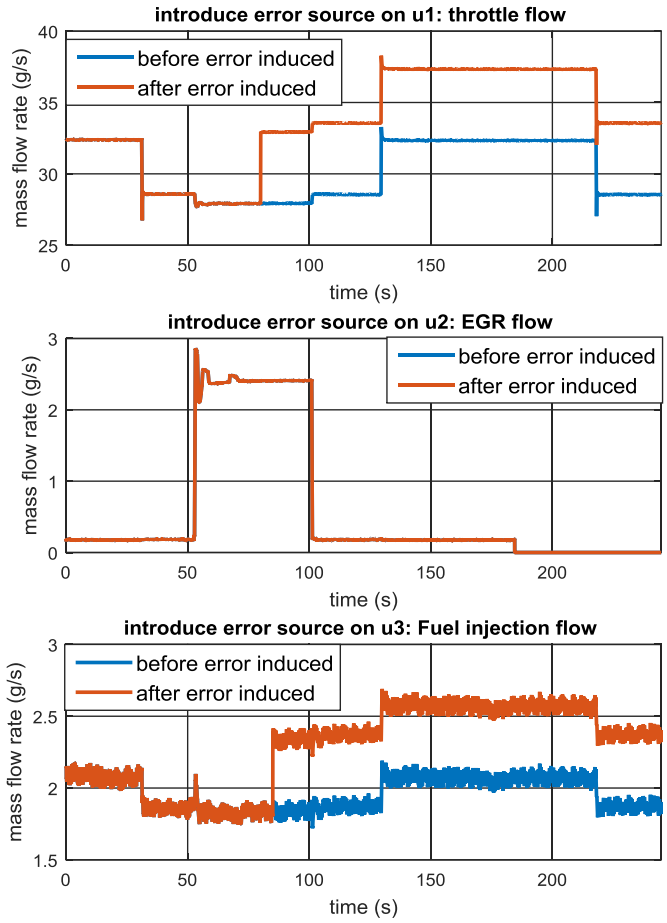

Figure 6.12 Pseudo inputs for scenario 2

The air flow estimation and EGR flow estimation results of test scenario 2 are shown in Figure 6.13 and Figure 6.14 respectively. A few sampling cycles after 80 second when error is induced on throttle flow model, it is observed that the air estimation and EGR estimation both recover from the wrong value and converge to the correct number with the help of the developed disturbance observer based estimation algorithm.

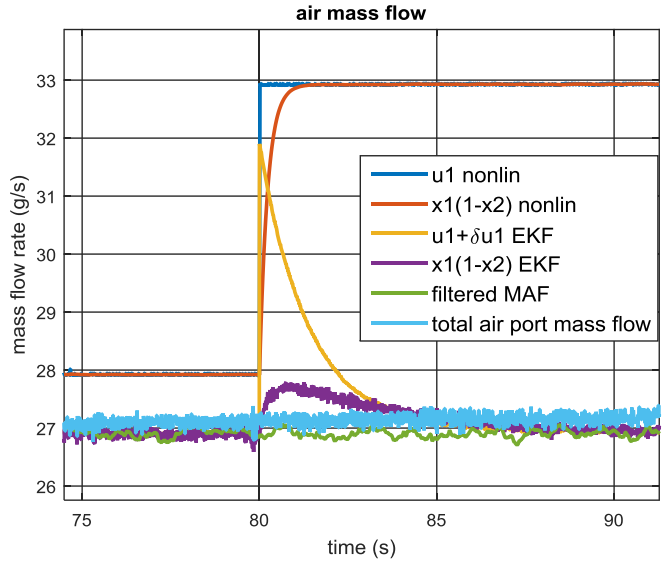

Figure 6.13 Air mass flow estimation for scenario 2 (zoom in)

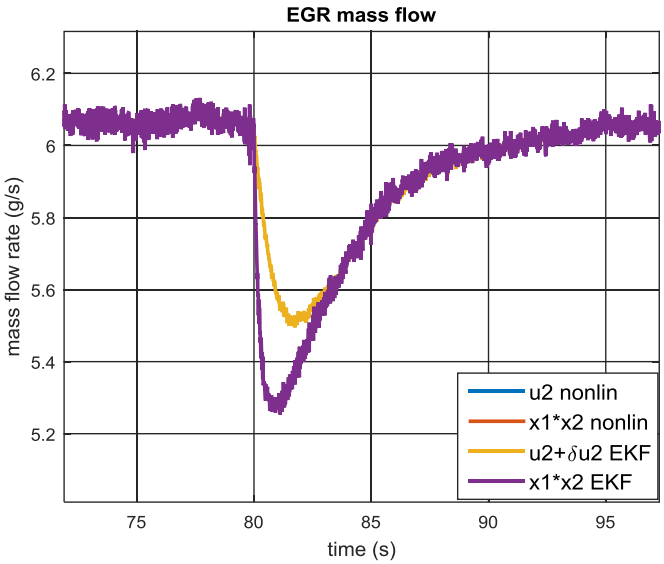

Figure 6.14 EGR mass flow estimation for scenario 2 (zoom in)

In Figure 6.15, the fuel flow estimation results of test scenario 2 is shown. In this figure, the blue line is the modeled fuel injection flow and the red line is the modeled cylinder fuel charge flow. The yellow line is the estimated fuel injection flow from the developed disturbance observer based estimation algorithm. The purple line is the

estimated cylinder fuel charge flow from the developed disturbance observer based estimation algorithm. The green line is the OEM calibrated fuel injection flow. And, the cyan line is the measured fuel flow in the engine test cell. It is observed that when error induced on throttle flow model starting from 80 second, there is no not much influence on fuel flow estimation. However, at the instance of the 85th second when error is induced on fuel flow model, the estimated fuel injection flow goes wrong and which leads to a miscalculated cylinder fuel charge flow estimation. The developed disturbance observer based estimation algorithm then drives the inaccurate fuel flow estimation back to the value around the fuel flow measurement which is assumed to be the reference (cyan line).

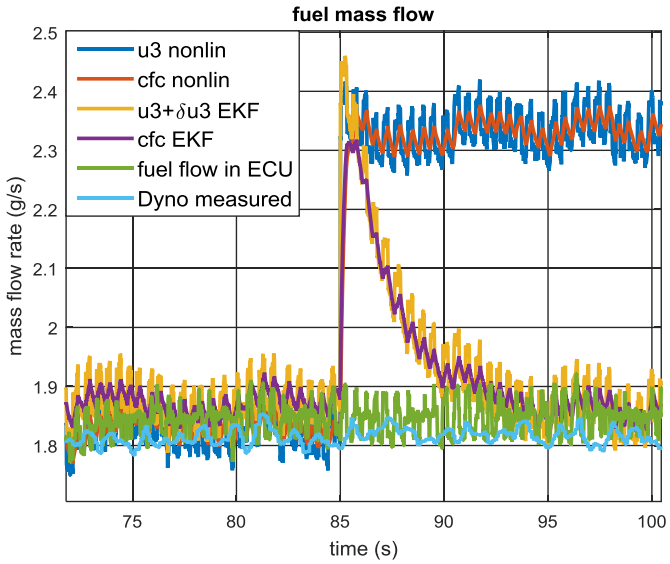

Figure 6.15 Fuel mass flow estimation for scenario 2 (zoom in)

In Figure 6.16, the exhaust lambda estimation results of test scenario 2 are shown. In this figure, it is observed that when errors are induced on the throttle flow model or fuel flow model, the estimated exhaust lambda (yellow line) can recover to the value

around that of the measured exhaust lambda (green line) with the help of the developed disturbance observer based estimation algorithm as expected.

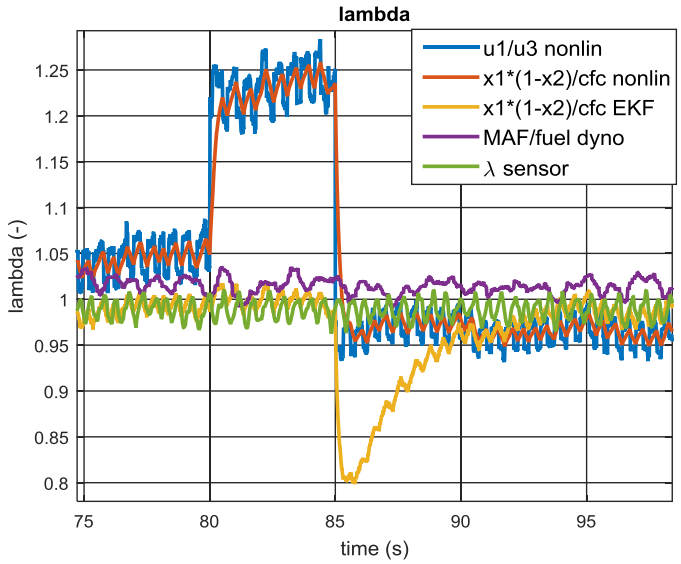

Figure 6.16 Exhaust lambda estimation for scenario 2 (zoom in)

For the test scenario 3, the errors are induced to three input models successively at different time. The detail is shown in Figure 6.17 where 5g/s error is induced on the pseudo throttle flow input model at 70 second, 1g/s error is induced on the pseudo EGR flow input model at 80 second, and 0.5g/s error is induced on the pseudo fuel flow input model. The experimental results of air flow, EGR flow, fuel flow and exhaust lambda estimation are shown in Figure 6.18, Figure 6.19, Figure 6.20, and Figure 6.21 respectively.

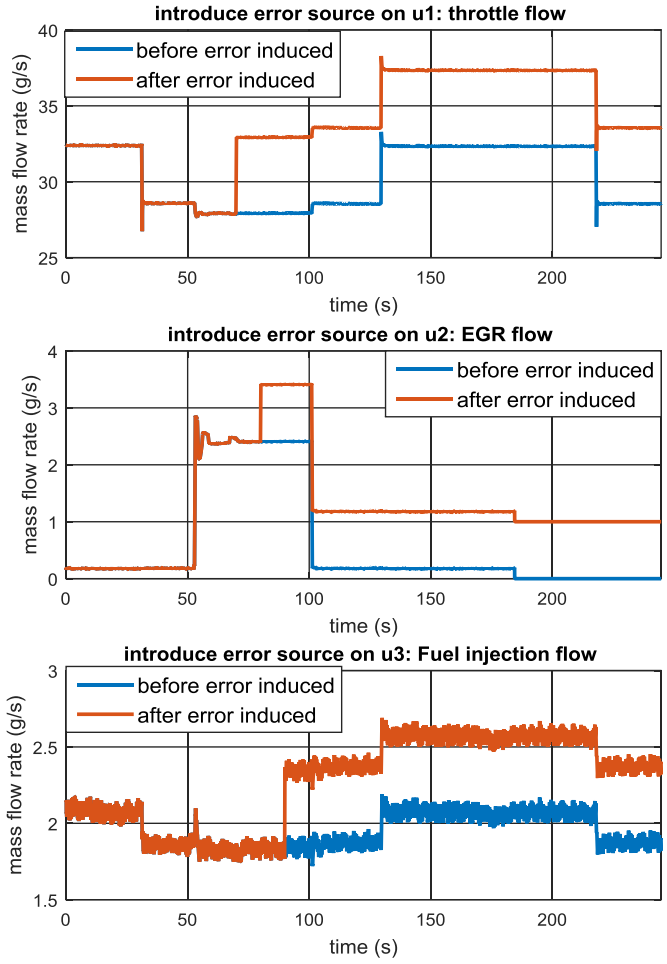

Figure 6.17 Pseudo inputs for scenario 3

The air flow estimation results of test scenario 3 is shown in Figure 6.18. It is observed that when errors induced on all the three input models one after another at different time, the estimated throttle flow (yellow line) and estimated cylinder air charge flow (purple line) can be recovered from the wrongly modeled throttle flow (blue line) and wrongly modeled cylinder air charge flow (red line) respectively with the help of the developed disturbance observer based estimation algorithm as expected.

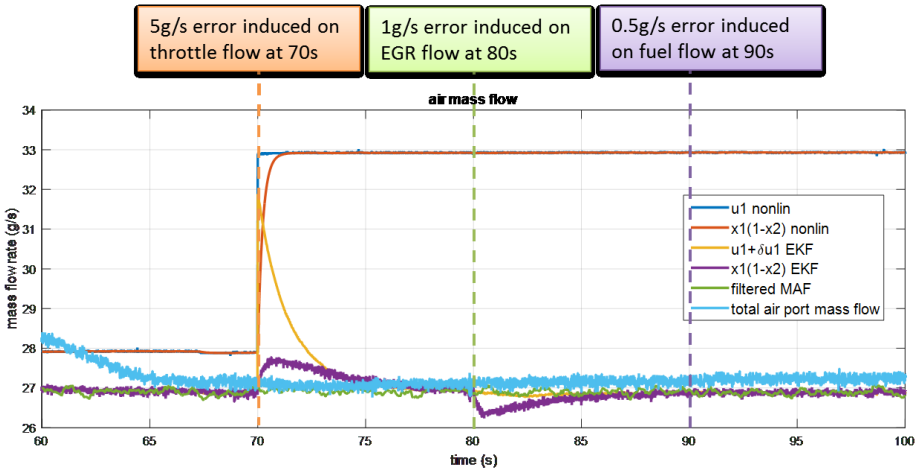

Figure 6.18 Air mass flow estimation for scenario 3

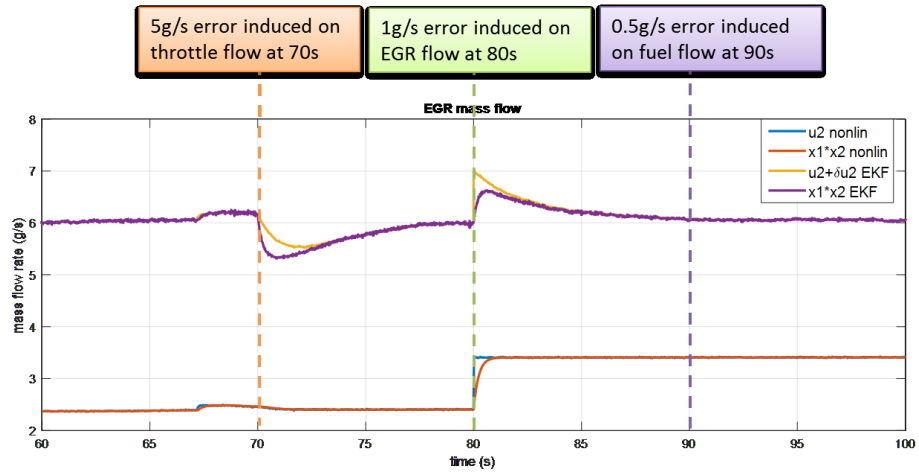

Figure 6.19 EGR mass flow estimation for scenario 3

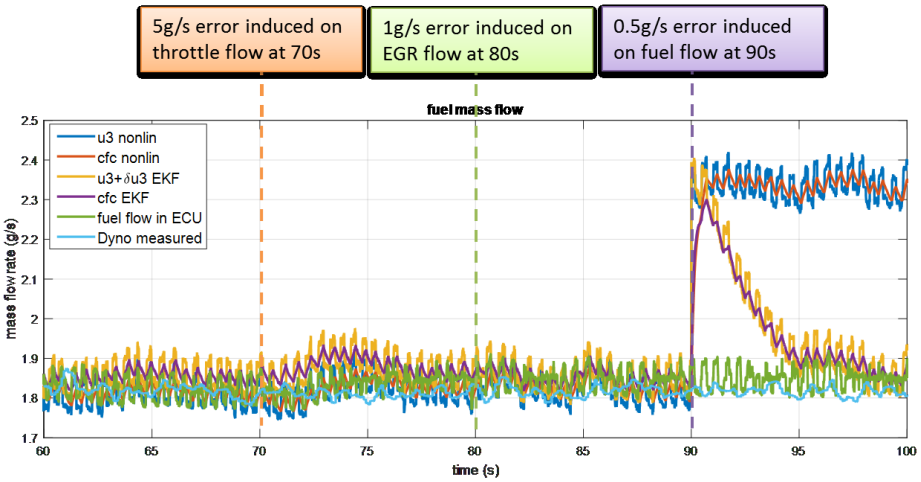

Figure 6.20 Fuel mass flow estimation for scenario 3

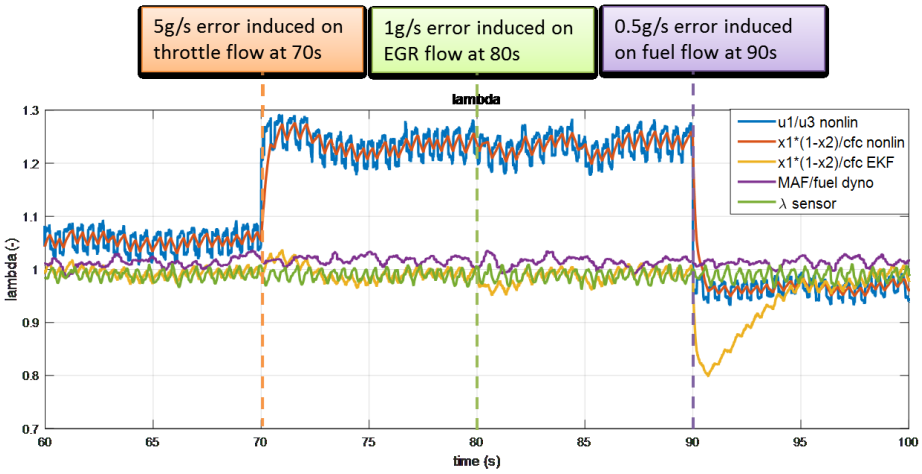

Figure 6.21 Exhaust lambda estimation for scenario 3

Same conclusion can be made on EGR flow estimation (Figure 6.19), fuel flow estimation (Figure 6.20), and exhaust lambda estimation (Figure 6.21). The estimated cylinder charge flow can all be recovered even with the disturbances of the wrong input models.

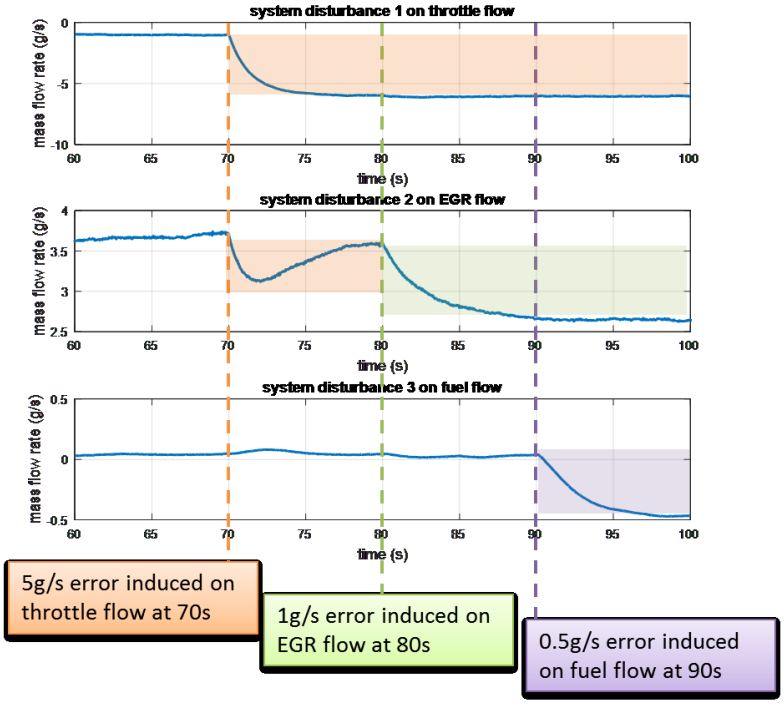

Figure 6.22 Disturbance estimation for scenario 3

Figure 6.22 shows the trajectory of three estimated disturbances. In the first plot on this figure, the disturbance δu_1 is a non-zero value even at initial steady state condition without artificial input model error. It is because of the small disagreement between MAF sensor and throttle flow model. Since MAF sensor is more trusted, the throttle model is compensated by disturbance δu_1. It is observed that the 5g/s error induced on throttle flow model at 70s is corrected by disturbance observer after several seconds. The disturbance δu_1 is able to compensate the inaccurate throttle flow model in a timely and accurate way. In the second plot on this figure, it is observed that the 1g/s error induced on EGR flow model at 80s is corrected by disturbance observer as well. The disturbance δu_2 can compensate the inaccurate EGR flow model. However, due to the inaccurate model parameter, the disturbance δu_2 is far away from zero at the initial steady state operating condition. The EGR flow estimation can be improved if more accurate volumetric efficiency model or calibration table is available. In the third plot on this figure, it is observed that the 0.5g/s error induced on fuel injection flow model at 90s is corrected by disturbance observer. The disturbance δu_3 compensate the inaccurate fuel injection flow model.

For the test scenario 4, the errors are induced to three input models at same time. The detail is shown in Figure 6.23 where 5g/s error is induced on the pseudo throttle flow input model, 1g/s error is induced on the pseudo EGR flow input model, and 0.5g/s error is induced on the pseudo fuel flow input model all at 80 seconds. The experimental results of disturbance estimation are shown in Figure 6.24.

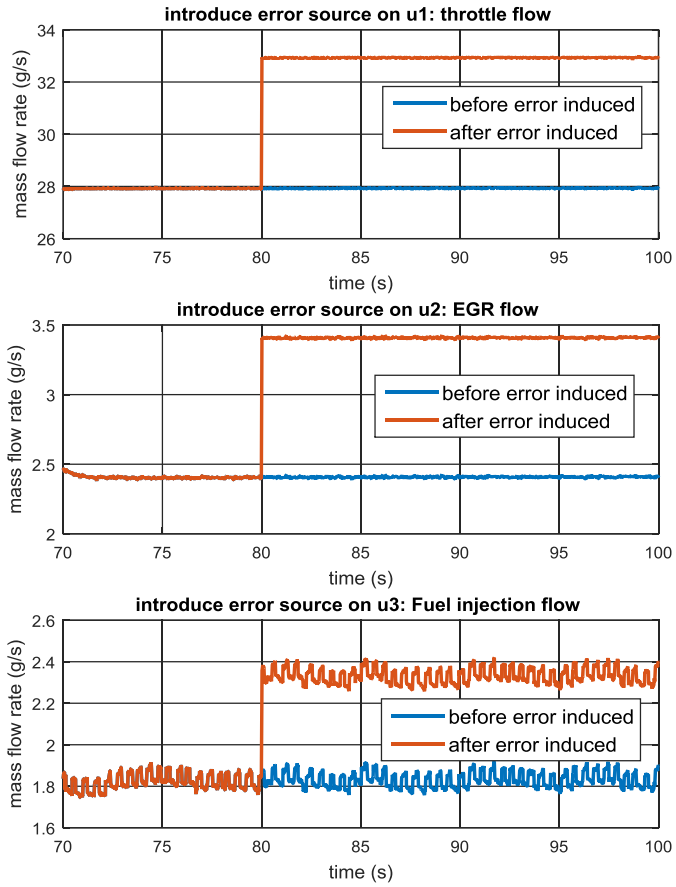

Figure 6.23 Pseudo inputs for scenario 4

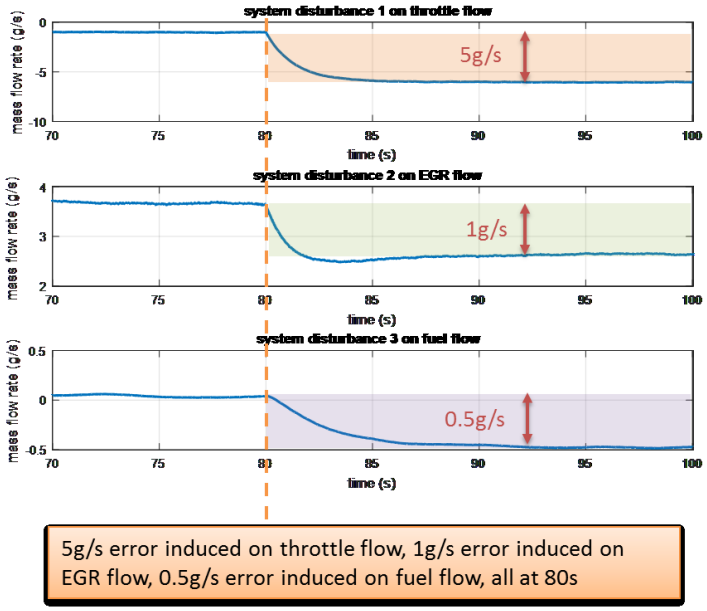

Figure 6.24 Disturbance estimation for scenario 4

From experiment test scenario 1 to 4, it can be concluded that the developed disturbance observer based cylinder charge estimation algorithm can reject the errors artificially added to input models as expected. When error is induced on throttle flow model, the throttle flow u_1 can be corrected by disturbance δu_1. When error is induced on EGR flow model, the EGR flow u_2 can be corrected by disturbance δu_2. When error is induced on fuel injection flow model, the fuel injection flow u_3 can be corrected by disturbance δu_3.

For the test scenario 1 to 4, the input modeling errors are induced by purpose to see if the disturbance observer works. The developed disturbance observer based estimation works as expected based on the designed experimental tests. However, extra experimental tests are needed to evaluate the performance of the developed algorithm under the real engine operating condition besides the previous tests with merely the error

induced artificially. The experimental design structure with non-ideal inputs is shown in Figure 6.25.

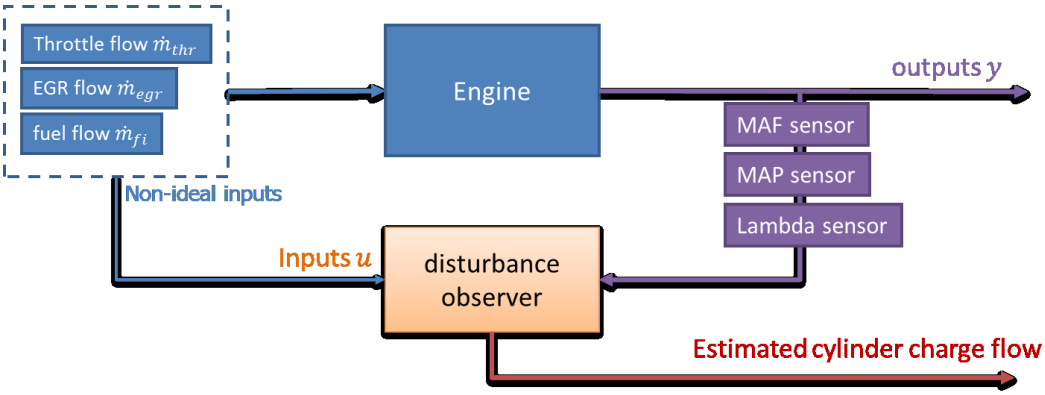

Figure 6.25 Experimental design with non-ideal inputs

For the experiment with non-ideal inputs, there are three tests with different engine operating conditions listed in Table 6.2. In test scenario 5, the EGR valve and fuel PW are kept unchanged while throttle position is moving. In test scenario 6, the throttle plate and EGR valve are kept unchanged while fuel PW is changed. In test scenario 7, the throttle plate is kept unchanged and the fuel PW is controlled by the stock closed-loop AFR controller while the EGR valve is changed.

Table 6.2 Experiment test scenario 5 to 7

Test Number	Operating condition
Scenario 5	Keep fuel PW and EGR valve constant, change throttle
Scenario 6	Keep throttle and EGR valve constant, change fuel PW
Scenario 7	Keep throttle constant, change EGR valve

Figure 6.26 shows the engine operating condition for test scenario 5 with all engine actuators kept unchanged except for the throttle plate. The throttle plate starts to change at 110 second.

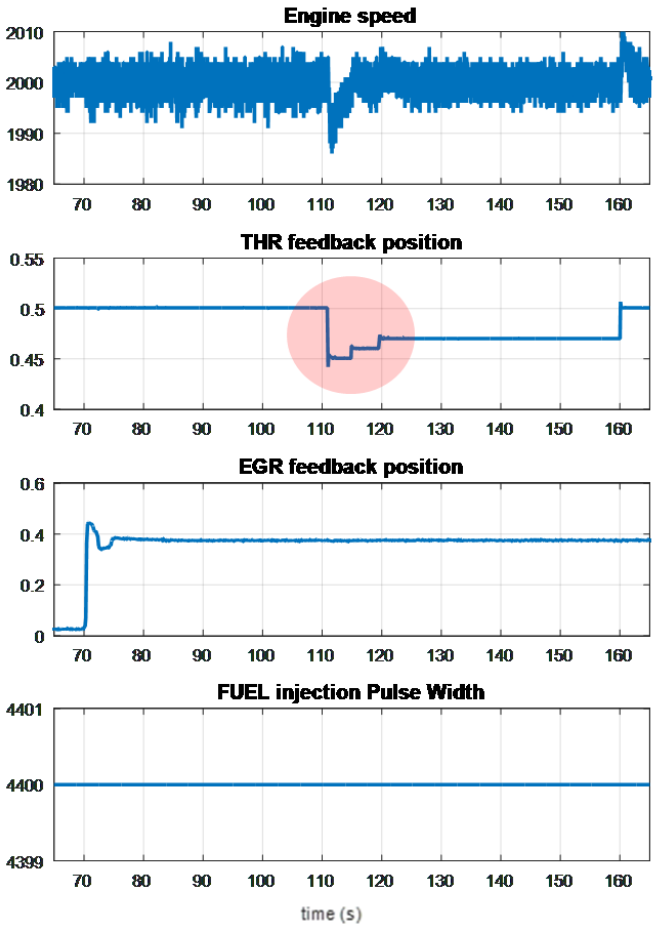

Figure 6.26 Engine operating condition for experiment test 5

The air mass flow estimation result is shown in Figure 6.27 where the estimated throttle flow is corrected by the developed disturbance observer based estimation algorithm even with the presence of the poorly calibrated throttle flow model. And the estimated cylinder air charge flow (purple line) is following the MAF sensor measurement (green line) as expected.

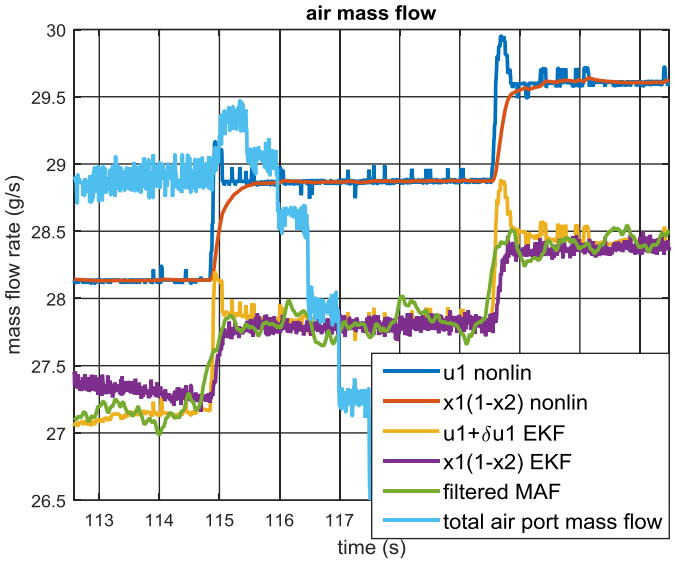

Figure 6.27 Air mass flow estimation for scenario 5 (zoom in)

The EGR mass flow estimation result is shown in Figure 6.28 where the estimated EGR flow (yellow line) and the estimated cylinder EGR charge flow (purple line) are corrected by the developed algorithm. As explained previously, the EGR flow estimation works as expected with the ability to reject the input model disturbance with some inaccuracy caused by the inaccurate model parameter.

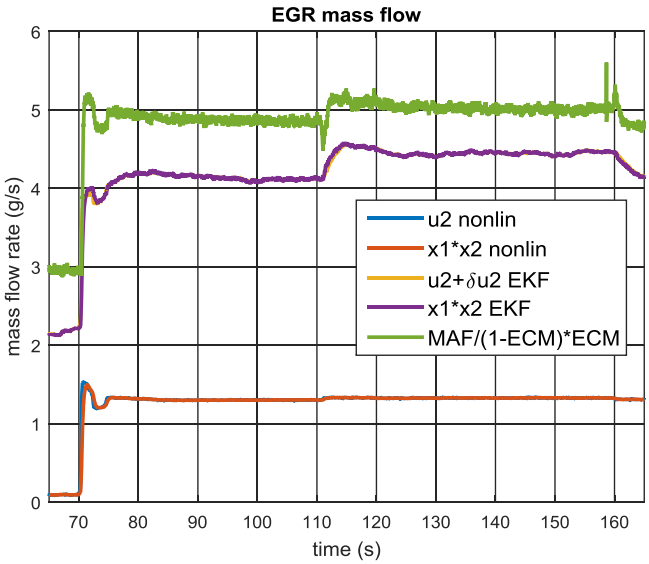

Figure 6.28 EGR mass flow estimation for scenario 5 (zoom in)

The fuel mass flow estimation result is shown in Figure 6.29 where the estimated cylinder fuel charge flow (purple line) is following the trend of the measured fuel flow (cyan line) with some drift. There is approximately 2.5% error for the estimated fuel flow, the reason of which might be the inaccurate fuel flow measurement.

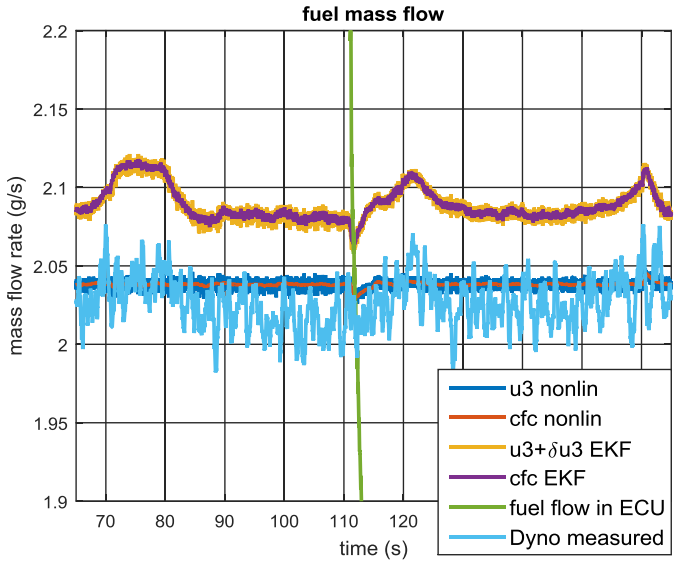

Figure 6.29 Fuel mass flow estimation for scenario 5 (zoom in)

The exhaust lambda estimation result is shown in Figure 6.30 where the estimated exhaust lambda (yellow line) is following the measurement (green line) as expected.

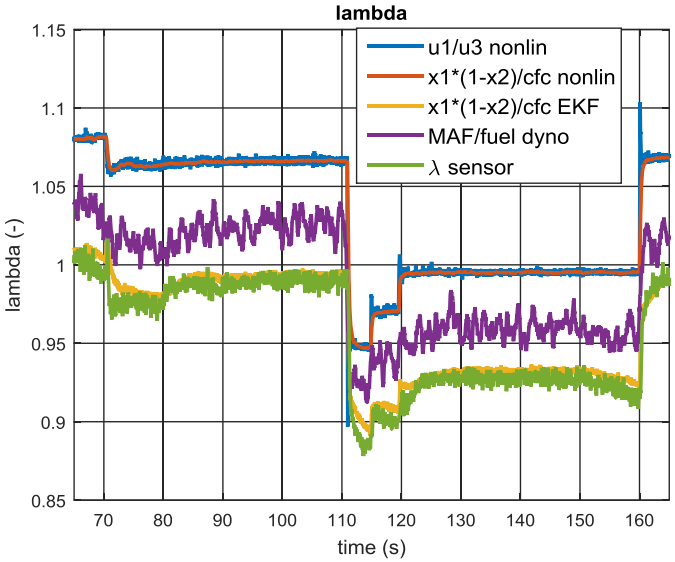

Figure 6.30 Exhaust lambda estimation for scenario 5 (zoom in)

Figure 6.31 shows the engine operating condition for test scenario 6 where all engine actuators except fuel PW kept unchanged.

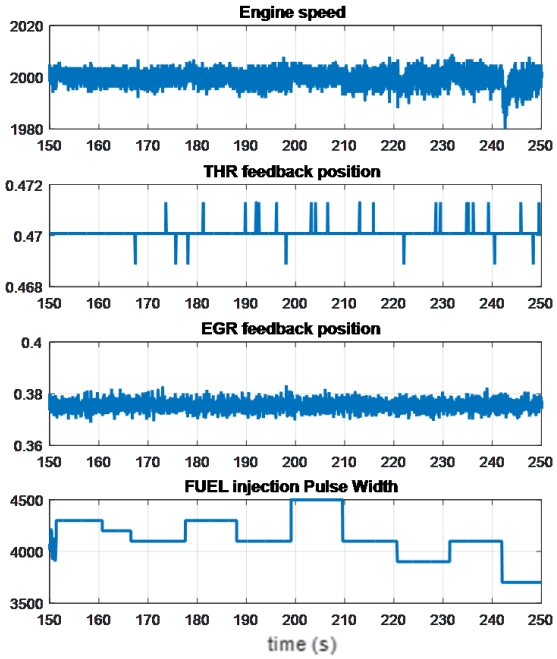

Figure 6.31 Engine operating condition for experiment test 6

The air mass flow estimation result is shown in Figure 6.32 where the estimated throttle flow is corrected by the developed disturbance observer based estimation algorithm even with the poorly calibrated throttle flow model. And the estimated cylinder air charge flow (purple line) is following the measurement (green line) as expected.

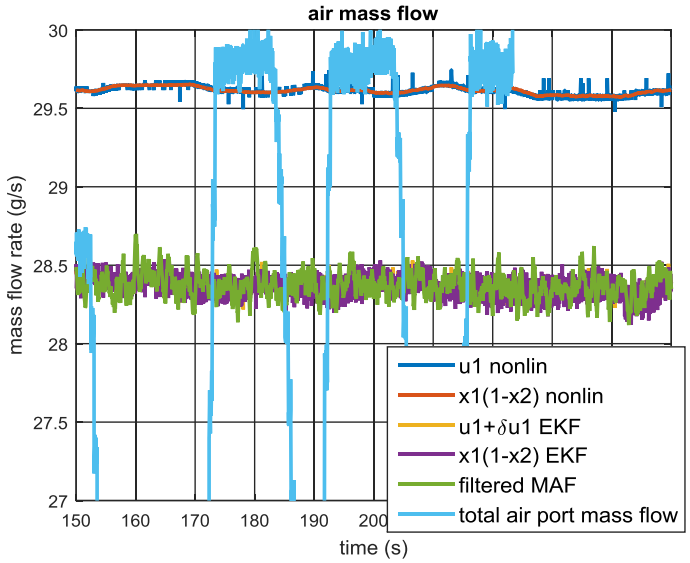

Figure 6.32 Air mass flow estimation for scenario 6 (zoom in)

The EGR mass flow estimation result is shown in Figure 6.33 where the estimated EGR flow (yellow line) and the estimated cylinder EGR charge flow (purple line) are corrected by the developed algorithm.

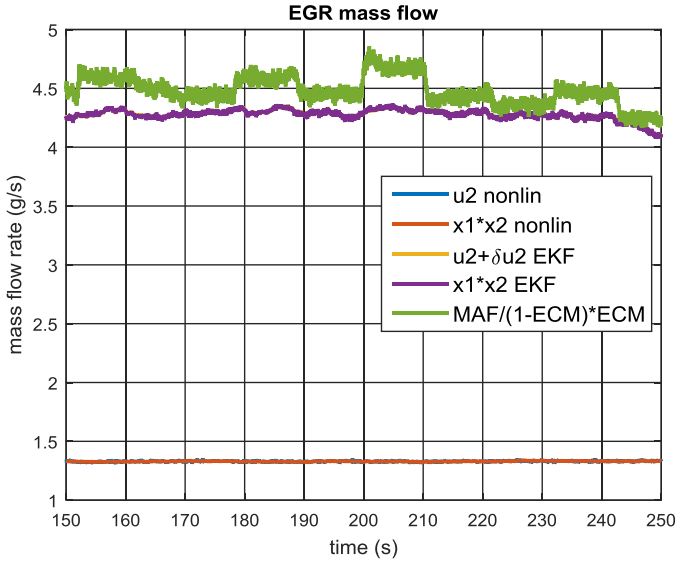

Figure 6.33 EGR mass flow estimation for scenario 6 (zoom in)

The fuel mass flow estimation and the exhaust lambda estimation results are shown in Figure 6.34 and Figure 6.35 respectively with the same conclusion: The developed disturbance observer based estimation algorithm works as expected.

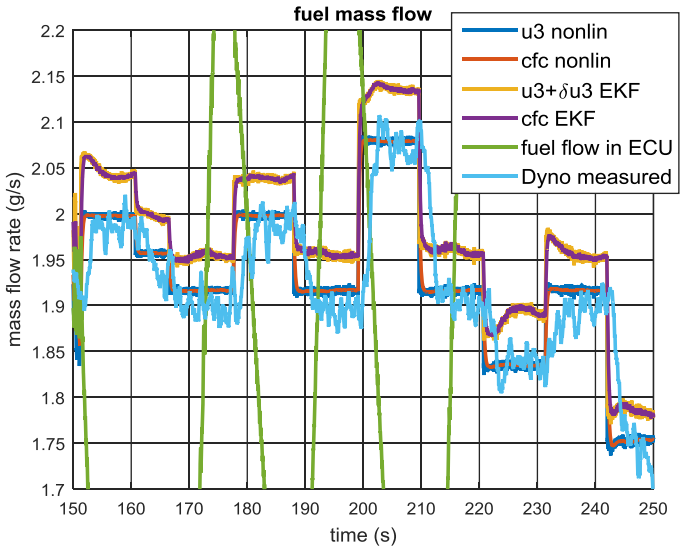

Figure 6.34 Fuel mass flow estimation for scenario 6 (zoom in)

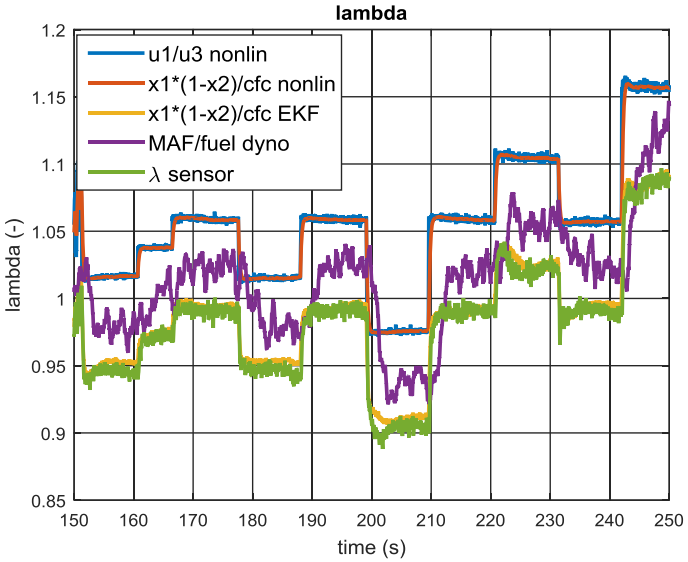

Figure 6.35 Exhaust lambda estimation for scenario 6 (zoom in)

Figure 6.36 shows the engine operating condition for test scenario 7 where all engine actuators are kept unchanged except for EGR valve. In this test, the fuel PW is controlled by the OEM's AFR controller to simulate the real-world condition.

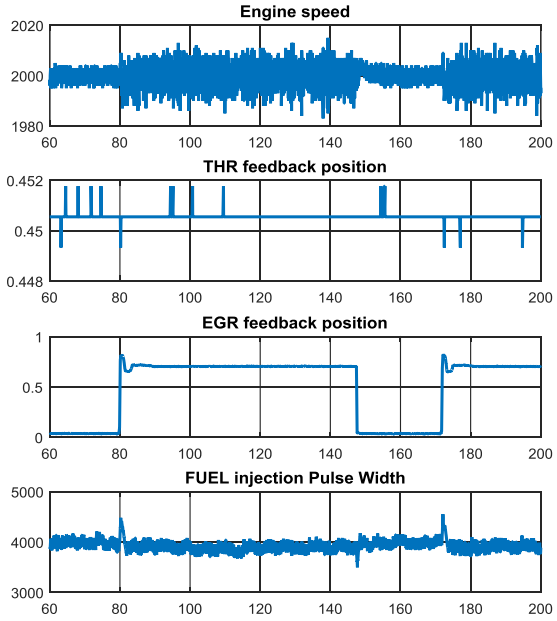

Figure 6.36 Engine operating condition for experiment test 7

The air mass flow estimation result is shown in Figure 6.37 where the estimated throttle flow is corrected from the input of the poorly calibrated throttle flow model by the developed disturbance observer based estimation algorithm. And the estimated cylinder air charge flow (purple line) is following the MAF sensor measurement (green line) as expected. The OEM calibrated air mass flow at intake port (cyan line) exhibits a high spike whenever the EGR valve moves, the reason of which is that the stock engine controller is not designed for the engine system with external EGR. However, it still able to converge with the feedback information from the exhaust lambda sensor.

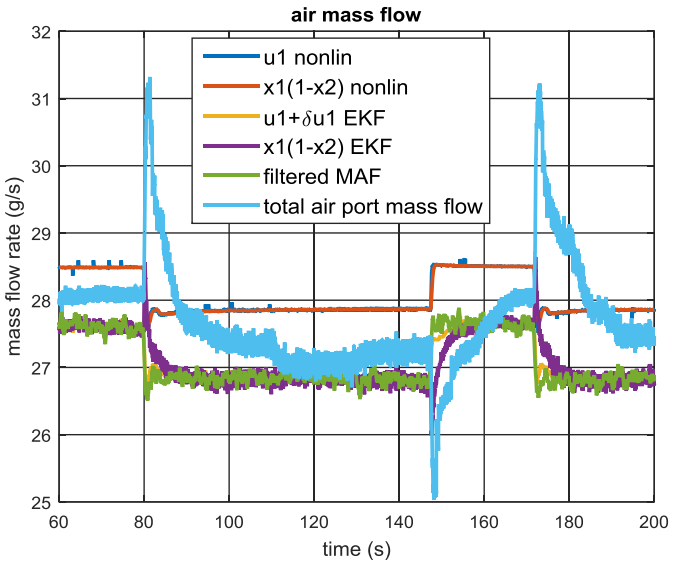

Figure 6.37 Air mass flow estimation for scenario 7 (zoom in)

The EGR mass flow estimation result is shown in Figure 6.38 where the estimated cylinder EGR charge flow (purple line) is corrected by the developed algorithm.

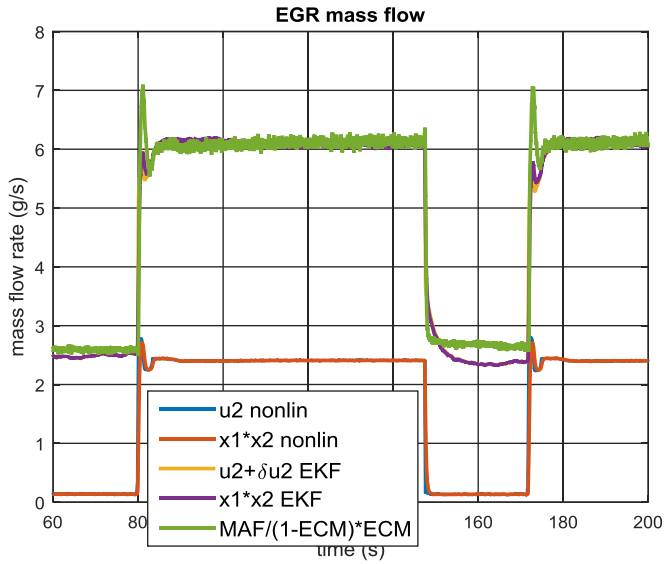

Figure 6.38 EGR mass flow estimation for scenario 7 (zoom in)

The fuel mass flow estimation and the exhaust lambda estimation results are shown in Figure 6.39 and Figure 6.40 respectively. The same conclusion can be drawn that the developed disturbance observer based cylinder charge estimation can reject the input model errors from the experimental tests as designed.

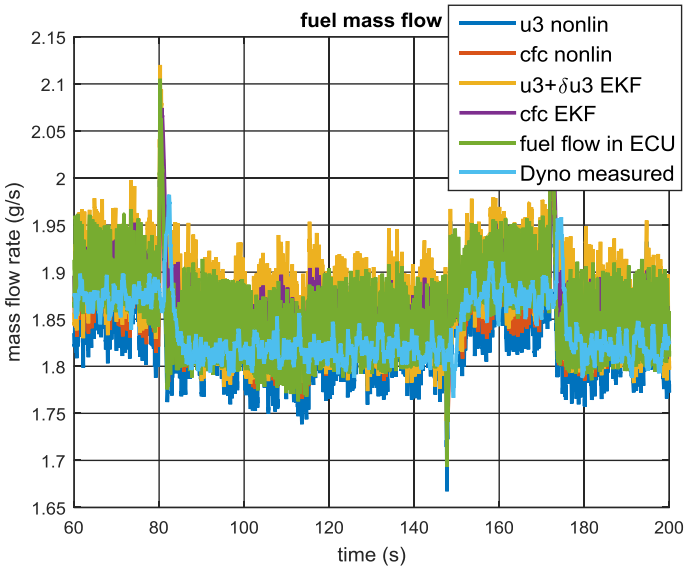

Figure 6.39 Fuel mass flow estimation for scenario 7 (zoom in)

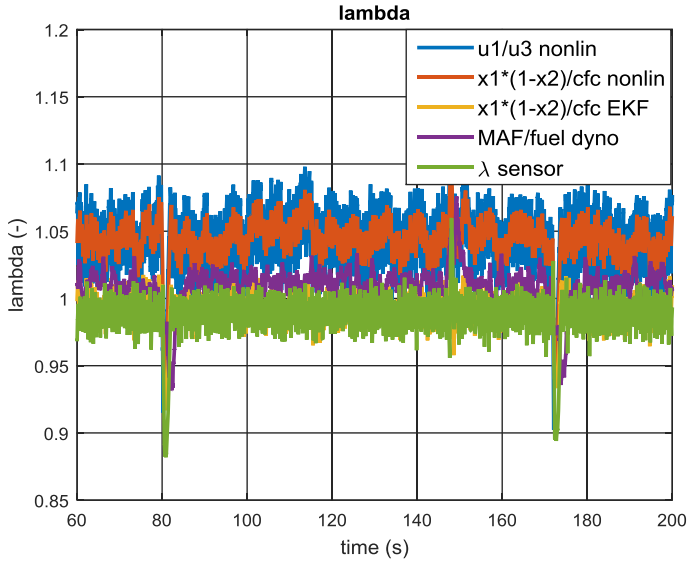

Figure 6.40 Exhaust lambda estimation for scenario 7 (zoom in)

From section 5.1, it is inferred that the elements of matrix Q and R can be tuned for better performance of EKF based estimation algorithm. Here for the disturbance observer based cylinder charge estimation algorithm, the tuning of the Q matrix and R matrix will influence the estimation convergence rate and noise level. Three parameter sets are selected and the air mass flow estimation results based on these parameter sets are compared to investigate the tuning parameters' influence on estimation convergence rate and noise level.

In Figure 6.41 an error is induced on throttle flow model starting from 70 seconds. The nonlinear modeled throttle flow (red line) thus deviates from the MAF sensor measured value (blue line). The throttle flow estimation results based on different parameter sets (yellow, purple and green line) show that the convergence rate varies with the application of different parameters to the disturbance observer. After the disturbance observer estimation results are settled with the induced error, in Figure 6.42 it is observed

that the steady state estimation noise level changes accordingly while applying different parameter sets.

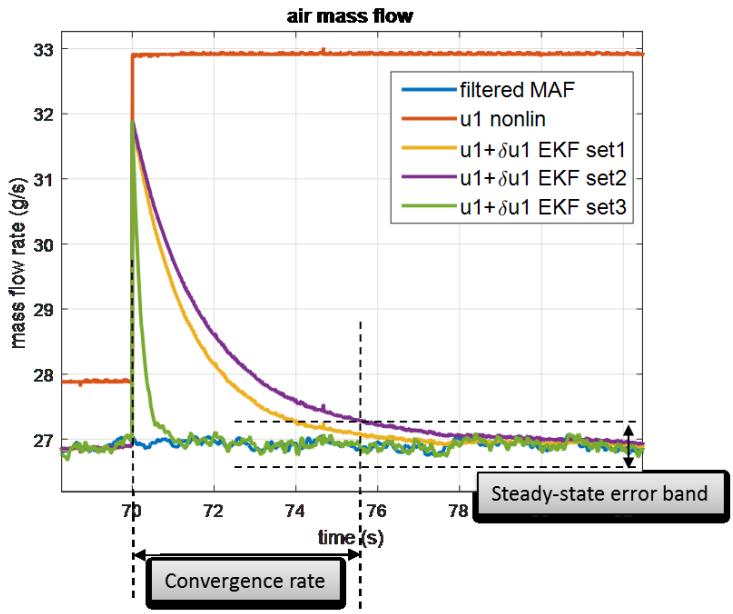

Figure 6.41 Parameter tuning effect on convergence rate

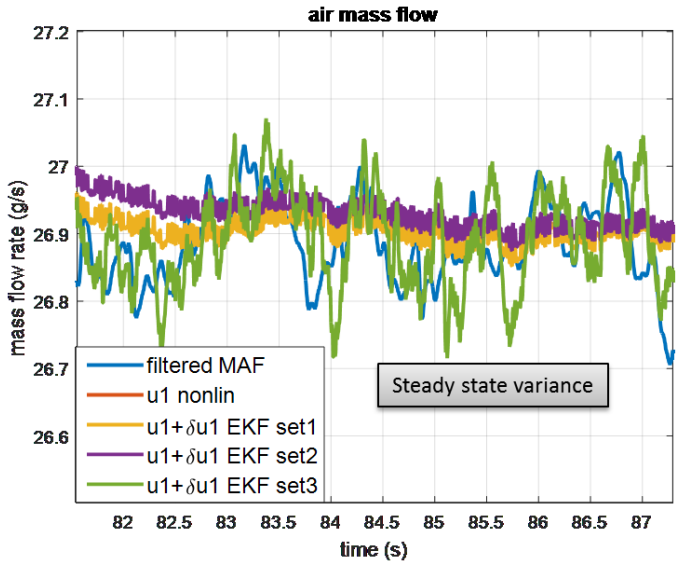

Figure 6.42 Parameter tuning effect on steady state variance

6.3 Conclusions

In this chapter, a disturbance observer based cylinder charge estimation algorithm is developed and validated experimentally with the ability to estimate cylinder air, fuel and EGR charge, and most importantly, to identify the throttle flow, EGR valve flow and fuel injection flow model error with readings of the MAF sensor, the MAP sensor and the exhaust lambda sensor. The errors from throttle flow estimation, EGR valve flow estimation and fuel injection flow estimation are treated as system disturbances respectively in the system dynamic equations. The EKF based disturbance observer is designed to estimate the system states and disturbances simultaneously, which allows the estimator to reject input model errors and identify the sources of the errors/disturbances. The developed method enables more accurate AFR control, torque estimation and physical based combustion modeling. Moreover, the research achievements of this chapter could be used for development of model based engine control strategy. It could help automobile manufacturers to build more fuel-efficient engines to meet the standards of government mandates for fuel economy and remit serious air-quality problems gradually.

CHAPTER SEVEN

7. CONCLUSIONS AND FUTURE WORKS

7.1 Dissertation Summary

The objective of this research work was to develop an observer based cylinder charge estimation technique utilizing a combination of sensors including MAF, MAP, and exhaust lambda sensors to improve the engine cylinder charge estimation accuracy and pin point the sources of the input model errors. The structure of the proposed algorithm can adapt to most SI engine configurations.

After the introduction in Chapter 1, Chapter 2 gives a detailed literature review on different cylinder charge estimation approaches along with the research gaps found between current methodologies and potential advanced estimation methods to be developed. Evaluation is also conducted for certain existing methods using data gathered from massive specifically designed experimental tests.

Chapter 3 introduces the simulation and experiment setup for model and estimation algorithm validation. A physics-based gas path model is developed in Chapter 4. The gas path model has been separated into five modules. Each section has been investigated and modeled separately. The nonlinear engine gas path model includes the air path module, EGR path module, fuel path module, manifold module, and the lambda path module. This nonlinear model is further simplified to an estimation-oriented model for online application.

In Chapter 5, the observer based estimation techniques are used to estimate cylinder air charge based on both MAF and MAP sensors. Several algorithms have been

developed and experimentally verified. The performances of these algorithms are compared under continuous tip-in and tip-out operational conditions. The developed observer based algorithms can reduce calibration work load while providing acceptable transient and steady-state estimation accuracy with low computational load.

In Chapter 6, besides the estimation of only the air charge as studied in Chapter 5, the estimation of fuel charge and EGR charge is further explored. Observer based estimation algorithms can give an optimal estimation for cylinder air/fuel/EGR charge if the model is sufficiently accurate. However, due to the inaccuracy of the throttle flow model, EGR valve flow model and fuel injection flow model under certain operational conditions, the performance of observer based algorithms could be compromised. To solve this issue, disturbance observer technique has been selected because of its potential to reject the disturbances. The developed disturbance observer based cylinder charge estimation algorithm can identify the error sources from air, fuel or EGR under the circumstances when uncertain disturbances on input models are presented.

7.2 Significant Contributions and Findings

Contributions and improvements are identified in four distinct areas: (1) Review of cylinder air charge estimation; (2) Modeling of estimation oriented physics based gas path; (3) Design of cylinder air charge estimator with both MAF and MAP sensors; (4) Design of disturbance observer based cylinder charge estimator. Significant findings in each category are described separately in the following sections.

7.2.1 Review of cylinder air charge estimation

The existing research work on cylinder air charge estimation for spark ignition engines has been reviewed thoroughly. Particular focus is given to methods utilizing MAF sensors, speed-density algorithms, input estimation, and closed-loop observers. Both the advantages and disadvantages of each method are discussed and massive simulation and experimental tests are conducted using various methods with their results compared and analyzed for performance evaluation. The large number of experimental tests conducted for this particular research is also a leverage to further verify the feasibility of the developed method in real engine state estimation.

7.2.2 Physics based gas path model

In this research work, a physics based gas path model is developed. This model is further simplified to an estimation oriented model for real-time operation. Different from the models in literatures, a detailed analysis of engine mean value gas path model has been conducted. The pressure drop of the engine intake system is considered in the developed air path model. The intake manifold isothermal model, adiabatic model, and polytropic model have been investigated. And the single-volume model and multi-volume model have been compared. A new semi-physics based fuel puddle model has been developed which inherits the simple Aquino model structure with less calibration parameters. Padé approximation is used for the lambda delay thus the exhaust lambda path can be combined with the other models without the interference of its time delay. The developed gas path model includes all the dynamics related to cylinder charge thus paves the way for the future model based engine estimation and control techniques which could significantly improve the estimation/control performance.

7.2.3 Cylinder air charge estimation with both MAF and MAP sensors

Some production vehicles are equipped with both MAF and MAP sensors to offer air charge estimation and other benefits. In order to take advantage of both MAF and MAP sensors for cylinder air charge estimation, several observer based cylinder air charge estimation methods are proposed utilizing both sensors. With appropriate tuning, the developed KF based algorithm has been experimentally verified to have to the ability to reduce calibration work while providing acceptable transient and steady-state accuracy with low computational load.

7.2.4 Disturbance observer based cylinder charge estimation

The disturbance observer technique is a very promising tool for engine state estimation and model based control. With appropriate design, the observer technique can estimate system unmeasured disturbances with current sensor sets. In this research work, this technique is used for identifying and rejecting the errors of the upstream throttle flow model, EGR flow model and fuel injection flow model while estimating cylinder charge flow. The successful development and experimental validation of this disturbance observer based cylinder charge estimation algorithm significantly helps improve the accuracy of cylinder air, fuel and EGR estimation and identify the error sources from the inaccurate upstream models. More importantly, the developed algorithm can further help the controller to mitigate modeling error thus improve the performance of physical model based engine control especially AFR control.

7.3 Future Directions

Future research on several areas could improve the estimation accuracy and robustness of the proposed observer based cylinder charge estimation algorithm. A list of suggested areas of the further exploration is as follows:

- Development of physics based model

In this research work, a relatively simplified model is proposed and used as the basis for the observer design. To improve the estimation performance, a more comprehensive physics based model which can capture more detailed dynamics is needed. One example is, in Chapter 4, the EGR flow is considered to come from the complete combustion. However, the exhaust gas might have extra air under lean combustion operating condition or extra "fuel" under rich combustion operating condition. This phenomenon could be considered in a more detailed model.

- The introduction of more sensors

The system observability is highly dependent of the number of measurements available. A sensor set of MAF sensor, MAP sensor and exhaust lambda sensor is utilized in this research work. With more information provided by different sensors, the developed estimation algorithm could identify and reject more disturbances. If the production engine is not able to add more sensors due to the cost control, the virtual sensor could be a good choice. For example, if the cylinder charge flow virtual sensor developed in [58] is added to the system, the MAF sensor drift can be identified and parameter calibration workload will be reduced using the developed disturbance observer based estimation algorithm structure.

- Long-term adaptation

The model errors identified from the developed disturbance observer based estimation algorithm in this research work can further be used for developing a long-term adaptation methods for model inaccuracy due to engine aging, environment change or low pressure differentials across the valve.

REFERENCES

[1] Yacobucci, B. D., Canis, B., and Lattanzio, R. K., 2012, "Automobile and truck fuel economy (CAFE) and greenhouse gas standards." CRS Report for Congress 7-5700. Washitong, DC.

[2] Sanchez, F. P., Bandivadekar, A., and German, J., 2012, "Estimated cost of emission reduction technologies for light-duty vehicles," Int. Counc. Clean Transp.

[3] Jensen, P. B., Olsen, M. B., Poulsen, J., Hendricks, E., Fons, M., and Jepsen, C., 1997, "A New Family of Nonlinear Observers for SI Engine Air/Fuel Ratio Control," SAE Technical Paper 970615.

[4] Chang, C., 1993, "AFR control in an IC engine using an event based observer," PhD Dissertation, Stanford University.

[5] Chang, C.-F., Fekete, N. P., Amstutz, A., and Powell, J. D., 1995, "Air-fuel ratio control in spark-ignition engines using estimation theory," Control Syst. Technol. IEEE Trans., **3**(1), pp. 22–31.

[6] Lauber, J., Guerra, T. M., and Dambrine, M., 2011, "Air-fuel ratio control in a gasoline engine," Int. J. Syst. Sci., **42**(2), pp. 277–286.

[7] Ault, B. A., 1994, "System identification and AFR control of a SI engine," PhD Dissertation, Standford University.

[8] Wang, S., Prucka, R., Zhu, Q., Prucka, M., and Dourra, H., 2016, "A Real-Time Model for Spark Ignition Engine Combustion Phasing Prediction," SAE Int. J. Engines, **9**(2), pp. 2016-01–0819.

[9] Zhu, Q., Wang, S., Prucka, R., Prucka, M., and Dourra, H., 2015, "Model-Based

Control-Oriented Combustion Phasing Feedback for Fast CA50 Estimation," SAE Int. J. Engines, **8**(3), pp. 997–1004.

[10] Abd-Alla, G. H., 2002, "Using exhaust gas recirculation in internal combustion engines: A review," Energy Convers. Manag., **43**(8), pp. 1027–1042.

[11] Wei, H., Zhu, T., Shu, G., Tan, L., and Wang, Y., 2012, "Gasoline engine exhaust gas recirculation - A review," Appl. Energy, **99**(X), pp. 534–544.

[12] Wang, Z., Zhu, Q., and Prucka, R., 2016 "A Review of Spark-Ignition Engine Air Charge Estimation Methods," SAE Technical Paper 2016-01-0620.

[13] Hendricks, E., and Sorenson, S. C., 1990, "Mean Value Modelling of Spark Ignition Engines," SAE Technical Paper 900616.

[14] Hendricks, E., 1997, "Engine Modelling for Control Applications : A Critical Survey," Meccanica, **32**(5), pp. 387–396.

[15] Hendricks, E., Chevalier, A., Jensen, M., Sorenson, S. C., Trumpy, D., and Asik, J., 1996, "Modelling of the Intake Manifold Filling Dynamics," SAE International, p. 960037.

[16] Guzzella, L., and Onder, C. H., 2004, Introduction to Modeling and Control of Internal Combustion Engine Systems, Springer Berlin Heidelberg, Berlin, Heidelberg.

[17] Stotsky, A., and Kolmanovsky, I., 2002, "Application of input estimation techniques to charge estimation and control in automotive engines," Control Eng. Pract., **10**(12), pp. 1371–1383.

[18] Leroy, T., Chauvin, J., Le Solliec, G., and Corde, G., 2007, "Air path estimation

for a turbocharged SI engine with variable valve timing," Proc. Am. Control Conf., pp. 5088–5093.

[19] Chevalier, A., Müller, M., and Hendricks, E., 2000, "On the Validity of Mean Value Engine Models During Transient Operation," SAE Technical, pp. 2000-01–1261.

[20] Heywood, J. B., 1988, Interal Combustion Engine Fundamentals, Mcgraw-hill, New York.

[21] Taglialatela, F., Cesario, N., and Lavorgna, M., "Soft Computing Mass Air Flow Estimator for a Single-Cylinder SI Engine," SAE Technical Paper 2006-01-0010.

[22] Jankovic, M., 2001, "Cylinder air-charge estimation for advanced intake valve operation in variable cam timing engines," JSAE Rev., **22**(4), pp. 445–452.

[23] Grizzle, J. W., Cook, J. a., and Milam, W. P., 1994, "Improved cylinder air charge estimation for transient air fuel ratio control," Proceedings of 1994 American Control Conference - ACC '94, IEEE, pp. 1568–1573.

[24] Magner, S., Jankovic, M., and Cooper, S., 2004, "Methods to Reduce Air-charge Characterization Data for High Degree of Freedom Engines," SAE Technical Paper, pp. 2004-01–0903.

[25] Smith, L. a, Fickenscher, T., and Osborne, R. P., 1999, "Engine Breathing - Steady Speed Volumetric Efficiency and Its Validity Under Transient Engine Operation," SAE Technical Paper Series, pp. 1999-01–0212.

[26] Malaczynski, G. W., Mueller, M., Pfeiffer, J., Cabush, D., Hoyer, K., and Corp, D., 2010, "Replacing Volumetric Efficiency Calibration Look- up Tables with

Artificial Neural Network-based Algorithm for Variable Valve Actuation."

[27] Wu, B., Filipi, Z., Assanis, D. N., Kramer, D. M., Ohl, G. L., Prucka, M. J., and DiValentin, E., 2004, "Using Artificial Neural Networks for Representing the Air Flow Rate through a 2.4 Liter VVT Engine," SAE Technical Paper 2004-01-3054.

[28] El Hadef, J., Colin, G., Talon, V., and Chamaillard, Y., 2013, "Neural Model for Real-Time Engine Volumetric Efficiency Estimation," SAE Technical Paper, pp. 2013-24–0132.

[29] Turin, R. C., Zhang, R., and Chang, M.-F., 2008, "Volumetric Efficiency Model for Variable Cam-Phasing and Variable Valve Lift Applications," SAE Technical Paper 2008-01-0995.

[30] Kocher, L., Koeberlein, E., Van Alstine, D. G., Stricker, K., and Shaver, G., 2012, "Physically based volumetric efficiency model for diesel engines utilizing variable intake valve actuation," Int. J. Engine Res., **13**(2), pp. 169–184.

[31] Jankovic, M., and Magner, S. W., 1999, "Air-charge estimation and prediction in spark ignition internal combustion engines," Proceedings of the 1999 American Control Conference (Cat. No. 99CH36251), IEEE, pp. 217–221.

[32] Rizzoni, G., and Utkin, V., 1998, "Automotive engine diagnosis and control via nonlinear estimation," IEEE Control Syst. Mag., **18**(5), pp. 84–99.

[33] Diop, S., Grizzle, J. W., Moraal, P. E., and Stefanopoulou, a., 1994, "Interpolation and numerical differentiation for observer design," Proc. 1994 Am. Control Conf. - ACC '94, **2**, pp. 1–22.

[34] Alexander Stotsky, and Stotsky, A. A., 2009, Automotive Engines, Springer Berlin

Heidelberg, Berlin, Heidelberg.

[35] Kolmanovsky, I., Sivergina, I., and Sun, J., 2006, "Simultaneous input and parameter estimation with input observers and set-membership parameter bounding: Theory and an automotive application," Int. J. Adapt. Control Signal Process., **20**(5), pp. 225–246.

[36] Liu, C., 2010, "Simultaneous Unknown State and Input Estimation With Application to Virtual Air Charge and EGR Sensors for Automotive Engines," ASME 2010 Dynamic Systems and Control Conference, Volume 1, ASME, pp. 727–734.

[37] Leroy, T., Chauvin, J., Petit, N. and Corde, G., 2007, "Motion planning control of the airpath of an S.I. engine with valve timing actuators," Fifth IFAC Symposium on Advances in Automotive Control, pp. 617–624.

[38] Dutka, a., Javaherian, H., and Grimble, M. J., 2006, "State-dependent Kalman filters for robust engine control," 2006 Am. Control Conf.

[39] Hendricks, E., 2001"Isothermal vs. adiabatic mean value SI engine models," Advances in Automotive Control 2001. Proceedings of the 3rd IFAC Workshop.

[40] Castillo, F., Witrant, E., Talon, V., and Dugard, L., 2013, "Simultaneous air fraction and low-pressure EGR mass flow rate estimation for diesel engines," IFAC Proc. Vol., pp. 731–736.

[41] Andersson, P., and Eriksson, L., 2004, "Cylinder Air Charge Estimator in Turbocharged SI-Engines," SAE Technical Paper 2004-01-1366.

[42] Andersson, P., 2002, Intake Air Dynamics on a Turbocharged SI-Engine with

Wastegate, Department of Electrical Engineering, Linköping University.

[43] Hendricks, E., Vesterholm, T., and Sorenson, S. C., 1992, "Nonlinear, Closed Loop, SI Engine Control Observers," SAE Technical Paper, p. 920237.

[44] Chevalier, A., Vigild, C. W., and Hendricks, E., 2000, "Predicting the Port Air Mass Flow of SI Engines in Air/Fuel Ratio Control Applications," SAE Technical.

[45] Polóni, T., Rohaľ-Ilkiv, B., and Arne Johansen, T., 2014, "Mass flow estimation with model bias correction for a turbocharged Diesel engine," Control Eng. Pract., **23**(1), pp. 22–31.

[46] Barbarisi, O., Gaeta, A., and Glielmo, L., 2002, "An Extended Kalman Observer for the In-Cylinder Air Mass Flow Estimation," Proc. MECA02 Int. Work. Diagnostics Automot. Engines Veh., pp. 1–14.

[47] Andersson, P., 2005, "Observer based feedforward air-fuel control of turbocharged SI-engines," P. Zítek, ed., pp. 1920–1920.

[48] Andersson, P., and Eriksson, L., 2001, "Air-to-Cylinder Observer on a Turbocharged SI-Engine with Wastegate," SAE Tech. Pap., pp. 2001-01–0262.

[49] Alberer, D., Hjalmarsson, H., and del Re, L., 2012, Identification for Automotive Systems, Springer Science & Business Media, London.

[50] Hassani Monir, V., Salehi, R., Salarieh, H., Alasty, A., and Vossoughi, G., 2015, "Real-time estimation of the volumetric efficiency in spark ignition engines using an adaptive sliding-mode observer," Proc. Inst. Mech. Eng. Part D J. Automob. Eng.

[51] Ahmed, Q., and Bhatti, a I., 2010, "Second order sliding mode observer for

estimation of SI engine Volumetric Efficiency amp; Throttle Discharge Coefficient," Var. Struct. Syst. (VSS), 2010 11th Int. Work., pp. 307–312.

[52] Storset, O. F., Stefanopoulou, A. G., and Smith, R., 2004, "Adaptive Air Charge Estimation for Turbocharged Diesel Engines Without Exhaust Gas Recirculation," J. Dyn. Syst. Meas. Control, **126**(3), p. 633.

[53] Stefanopoulou, A. G., Storset, O. F., and Smith, R., 2004, "Pressure and temperature-based adaptive observer of air charge for turbocharged diesel engines," Int. J. Robust Nonlinear Control, **14**(6), pp. 543–560.

[54] Tseng, T., and Cheng, W., 1999, "An Adaptive Air/Fuel Ratio Controller for SI Engine Throttle Transients," SAE Technical Papers, pp. 1999-01–0552.

[55] Stotsky, A., and Kolmanovsky, I., 2001, "Simple unknown input estimation techniques for automotive applications," Proceedings of the 2001 American Control Conference. (Cat. No.01CH37148), IEEE, pp. 3312–3317 vol.5.

[56] Stotsky, A., Kolmanovsky, I., and Eriksson, S., 2004, "Composite adaptive and input observer-based approaches to the cylinder flow estimation in spark ignition automotive engines," Int. J. Adapt. Control Signal Process., **18**(2), pp. 125–144.

[57] Qu, Z., Ma, M., and Zhao, F., 2012, "Estimation and Analysis of Crank-Angle-Resolved Gas Exchange Process of Spark-Ignition Engines," SAE Technical Paper, pp. 2012-01–0835.

[58] Xu, S., Wang, Z., Prucka, R., Filipi, Z., Prucka, M., and Dourra, H., 2016, "Physical Model for Real-Time Simultaneous Estimation of Intake Mass and Cylinder Pressure in an SI Engine," ASME 2016 Internal Combustion Engine Fall

Technical Conference, ASME, p. V001T05A007.

[59] Worm, J. J., 2005, "An Evaluation of Several Methods for Calculating Transient Trapped Air Mass with Emphasis on the ' Delta P ' Approach," SAE paper 2005-01-0990.

[60] Desantes, J. M., Galindo, J., Guardiola, C., and Dolz, V., 2010, "Air mass flow estimation in turbocharged diesel engines from in-cylinder pressure measurement," Exp. Therm. Fluid Sci., **34**(1), pp. 37–47.

[61] Colin, G., Giansetti, P., Chamaillard, Y., and Higelin, P., 2007, "In-Cylinder Mass Estimation Using Cylinder Pressure," SAE Technical Paper, pp. 2007-24–0049.

[62] Mladek, M., and Onder, C. H., 2000, "A Model for the Estimation of Inducted Air Mass and the Residual Gas Fraction using Cylinder Pressure Measurements," SAE Technical Papers, pp. 2000-01–0958.

[63] Sławomir, W., Rohal-Ilkiv, B., Šimončic, P., Honek, M., and Jozef, C., 2014, "in-Cylinder Mass Flow Estimation and Manifold Pressure Dynamics for State Prediction in Si Engines," Acta Polytech., **54**(3), pp. 240–247.

[64] Eriksson, L. and Nielsen, L., 2014. "Modeling and Control of Engines and Drivelines, " John Wiley & Sons.

[65] Probst, a., Magaña, M. E., and Sawodny, O., 2010, "Using a Kalman filter and a Padé approximation to estimate random time delays in a networked feedback control system," IET Control Theory Appl., **4**(11), p. 2263.

[66] Zope, R. A., Mohammadpour, J., Grigoriadis, K. M., and Franchek, M., 2009, "Air-Fuel Ratio Control of Spark Ignition Engines With TWC Using LPV

Techniques," ASME 2009 Dynamic Systems and Control Conference, Volume 1, ASME, pp. 897–903.

[67] Hendricks, E., and Luther, J. B., 2001, "Model and observer based control of internal combustion engines," Proc. Int. Work. Model. Emiss. Control Automot. Engines (MECA), Fisciano, Italy, pp. 9–21.

[68] Stefanopoulou, A. G., Freudenberg, J. S., and Grizzle, J. W., 2000, "Variable camshaft timing engine control," IEEE Trans. Control Syst. Technol., **8**(1), pp. 23–34.

[69] Chevalier, A., Müller, M., and Hendricks, E., 2000, "On the Validity of Mean Value Engine Models During Transient Operation," SAE International, pp. 1–24.

[70] Wang, J., 2007, "Air fraction estimation for multiple combustion mode diesel engines with dual-loop EGR systems," Proc. IEEE Conf. Decis. Control, **16**, pp. 2862–2867.

[71] Zhu, G.-S., Reitz, R. D., Xin, J., and Takabayashi, T., 2001, "Modelling characteristics of gasoline wall films in the intake port of port fuel injection engines," Int. J. Engine Res., **2**(4), pp. 231–248.

[72] Panse, P. A., and Suryanarayanan, S., 2005, "Dynamic Modeling and Control of Port Fuel Injection Engines," Departament of Mechanical Engineering. Indian Institute of Technology Bombay.

[73] Kyung-ho Ahn, Stefanopoulou, A. G., and Jankovic, M., 2009, "Fuel puddle model and AFR compensator for gasoline-ethanol blends in flex-fuel engines," 2009 IEEE Vehicle Power and Propulsion Conference, IEEE, pp. 1148–1155.

[74] Esse, P., 2001, “the Fuel Puddle Dynamics in the Spark ingition engine,” Journal of KONES, 8(1-2),, (1), pp. 27–34.

[75] Jankovic, M., Magner, S., Hagner, D., and Wang, Y., 2007, “Multi-input transient fuel control with auto-calibration,” Proc. Am. Control Conf., pp. 5100–5105.

[76] Ahn, K., Stefanopoulou, A. G., and Jankovic, M., 2010, “Puddle Dynamics and Air-to-Fuel Ratio Compensation for Gasoline-Ethanol Blends in Flex-Fuel Engines Greek :,” **18**(6), pp. 1241–1253.

[77] Aquino, C. F., 1981, “Transient A/F Control Characteristics of the 5 Liter Central Fuel Injection Engine.” SAE Technical Paper

[78] Eriksson, L., and Nielsen, L., 2014, Modeling and Control of Engines and Drivelines, John Wiley & Sons, Ltd, Chichester, UK.

[79] Turin, R. C., Casartelli, E. G. B., and Geering, H. P., 1994, “A New Model for Fuel Supply Dynamics in an SI Engine.”

[80] Curtis, E. W., Aquino, C. F., Trumpy, D. K., and Davis, G. C., 1996, “A New Port and Cylinder Wall Wetting Model to Predict Transient Air/Fuel Excursions in a Port Fuel Injected Engine.” SAE Technical Paper

[81] Locatelli, M., Onder, C. H., and Geering, H. P., 2004, “An Easily Tunable Wall-Wetting Model for PFI Engines,” SAE Technical Paper.

[82] Maloney, P. J., 1999, “An event-based transient fuel compensator with physically based parameters,” SAE Technical Paper.

[83] Locatelli, M. A., 2004, Modeling Compensation of of the Fuel Dynamics Spark Ignited Engine. SAE Technical Paper.

[84] Ahn, K. H., Stefanopoulou, A. G., and Jankovic, M., 2010, "Puddle dynamics and air-to-fuel ratio compensation for gasoline-ethanol blends in flex-fuel engines," IEEE Trans. Control Syst. Technol., **18**(6), pp. 1241–1253.

[85] Haluska, P., and Guzzella, L., 1998, "Control Oriented Modeling of Mixture Formation Phenomena in Multi-Port Injection SI Gasoline Engines." SAE Technical Paper.

[86] Bernard Friedland, 1986, Control System Design: An Introduction To State-Space Methods. Courier Corporation.

[87] Luenberger, D., 1971, "An introduction to observers," IEEE Trans. Automat. Contr., **16**(6).

[88] Luenberger, D. G., 1966, "Observers for Multivariable Systems," IEEE Trans. Automat. Contr., **11**(2), pp. 190–197.

[89] Luenberger, D. G., 1964, "Observing the State of a Linear System," IEEE Trans. Mil. Electron., **8**(2), pp. 74–80.

[90] Glenn, B. C., Upadhyay, D., Utkin, V. I., Washington, G. N., and Hopka, M. B., 2011, "Observer design of critical states for air path flow regulation in a variable geometry turbocharger exhaust gas recirculation diesel engine," Int. J. Engine Res., **12**(6), pp. 501–512.

[91] Vigild, C. W., Andersen, K. P. H., Hendricks, E., and Struwe, M., 1999, "Towards Robust H-infinity Control of an SI Engine1s Air / Fuel Ratio." SAE Technical Paper.

[92] Rawlings, J. B., and Bakshi, B. R., 2006, "Particle filtering and moving horizon

estimation," Comput. Chem. Eng., **30**(10–12), pp. 1529–1541.

[93] Kolmanovsky, I. V, and Winstead, V., 2006, "A receding horizon optimal control approach to active state and parameter estimation in automotive systems," 2006 IEEE Int. Conf. Control Appl. CCA 2006, Oct. 4, 2006 - Oct. 6, 2006, pp. 2796–2801.

[94] Kalman, R. E., and Bucy, R. S., 1961, "New Results in Linear Filtering and Prediction Theory," J. Basic Eng., **83**(1), p. 95.

[95] Zhang, Y., Zhao, Z., Lu, T., Yuan, L., Xu, W., and Zhu, J., 2009, "A comparative study of Luenberger observer, sliding mode observer and extended Kalman filter for sensorless vector control of induction motor drives," Energy Convers. Congr. Expo. 2009. ECCE 2009. IEEE , pp. 2466–2473.

[96] Boker, A. M., and Khalil, H. K., 2013, "Nonlinear observers comprising high-gain observers and extended Kalman filters," Automatica, **49**(12), pp. 3583–3590.

[97] Hermann, R., and Krener, A. J., 1977, "Nonlinear controllability and observability," IEEE Trans. Automat. Contr., **22**(5), pp. 728–740.

[98] Gauthier, J. P., and Kupka, I. A. K., 1994, "Observability and Observers for Nonlinear Systems," SIAM J. Control Optim., **32**(4), pp. 975–994.

[99] van der Schaft, A. J., 1982, "Observability and Controllability for Smooth Nonlinear Systems," SIAM J. Control Optim., **20**(3), pp. 338–354.

[100] Wen-Hua Chen, Ballance, D. J., Gawthrop, P. J., and O'Reilly, J., 2000, "A nonlinear disturbance observer for robotic manipulators," IEEE Trans. Ind. Electron., **47**(4), pp. 932–938.

[101] Chen, W.-H., 2004, "Disturbance Observer Based Control for Nonlinear Systems," IEEE/ASME Trans. Mechatronics, **9**(4), pp. 706–710.

[102] Kempf, C. J., and Kobayashi, S., 1999, "Disturbance observer and feedforward design for a high-speed direct-drive positioning table," IEEE Trans. Control Syst. Technol., **7**(5), pp. 513–526.

LIST OF ACRONYMS

AC	Alternating current
AFR	Air-to-fuel ratio
ANN	Artificial Neural Network
CAFE	Corporate average fuel economy
CARB	California Air Resources Board
EGR	Exhaust gas recirculation
EKF	Extended Kalman filter
EPA	U.S. Environmental Protection Agency
KF	Kalman filter
LDV	Light Duty Vehicle
MAF	Mass air flow sensor
MAP	Manifold absolute pressure sensor
MEVM	Mean value engine model
NHTSA	The National Highway Traffic Safety Administration
PW	Pulse width
SI	Spark-ignition
SISO	Single-input-single-output
TWC	Three way catalyst
VE	Volumetric efficiency
VVT	Variable valve timing